Transient Gratings, Four-Wave Mixing and Polariton Effects in Nonlinear Optics

Knoester, Jasper; Mukamel, Shaul

Published in:
Physics Reports

DOI:
10.1016/0370-1573(91)90051-M

Publication date:
1991

PHYSICS REPORTS (Review Section of Physics Letters) 205, No. 1 (1991) 1–58. North-Holland

TRANSIENT GRATINGS, FOUR-WAVE MIXING AND POLARITON EFFECTS IN NONLINEAR OPTICS

Jasper KNOESTER

University of Groningen, Department of Chemistry, Nijenborgh 16, 9747 AG Groningen, The Netherlands

and

Shaul MUKAMEL

University of Rochester, Department of Chemistry, River Campus, Rochester, New York 14627, USA

Editor: D.L. Mills Received December 1990

Contents:

1. Introduction 3
2. Model, Hamiltonian, and equations of motion 6
3. Nonlinear optical response of excitons 10
   3.1. Operator equations and linear optics 10
   3.2. The single-particle description: frequency-domain four-wave mixing 13
   3.3. The two-particle description: degenerate four-wave mixing 16
   3.4. Time-domain four-wave mixing: transient grating and exciton dynamics 22
   3.5. The Boltzmann and the diffusion equations for exciton transport 28
4. Nonlinear optical response of polaritons 31
   4.1. Canonical transformation and operator equations 31
   4.2. The polariton hierarchy in the two-particle description 36
   4.3. Polariton dynamics probed by transient grating spectroscopy 37
   4.4. Polariton effects in frequency-domain four-wave mixing 42
5. Concluding remarks 44
Appendix A. Elimination of phonon degrees of freedom 47
Appendix B. The two-particle Green function 51
Appendix C. The diffusive limit of the D4WM intensity 52
Appendix D. Effective polariton group velocity in the restricted Haken–Strobl model 53
References 55

Abstract:

Nonlinear optical susceptibilities provide a convenient means of relating macroscopic optical measurements to microscopic models. The susceptibilities are most useful when the radiation field and the material degrees of freedom are weakly coupled. In the opposite case, the dynamics is interpreted in terms of combined radiation–matter modes (polaritons) and susceptibilities are usually not used. In this review we analyze both situations from a unified dynamical framework based on equations of motion. The present formalism is also particularly suitable for the calculation of optical nonlinearities in nanostructures with restricted geometries. The transient grating and its frequency-domain analogue (degenerate four-wave mixing) are used to illustrate the formalism in both the strong and the weak radiation–matter coupling limit.

TRANSIENT GRATINGS, FOUR-WAVE MIXING AND POLARITON EFFECTS IN NONLINEAR OPTICS

Jasper KNOESTER

University of Groningen, Department of Chemistry, Nijenborgh 16, 9747 AG Groningen, The Netherlands

and

Shaul MUKAMEL

University of Rochester, Department of Chemistry, River Campus, Rochester, New York 14627, USA

NORTH-HOLLAND

1. Introduction

The transient grating (TG) technique is one of the most powerful means for the direct probe of dynamical processes in condensed phases [1–18]. It has been used to probe relaxation rates and transport phenomena in molecular crystals [2], ionic crystals [3–6], solutions of dye molecules [7, 8], conjugated polymers [9], semiconductors [10–14], surfaces [15] and proteins [16]. Laser gratings are important for holography and the elimination of beam distortions in random media (phase conjugation) [17, 18]. A simple phenomenological description of the TG can be obtained as follows: When two laser fields with wave vectors $\boldsymbol{k}_1$ and $\boldsymbol{k}_2$ simultaneously interact with the material system, they form an interference pattern with wave vector $\boldsymbol{k}_1 - \boldsymbol{k}_2$. Consequently some material property (e.g. excitons, electron–hole pairs, space charge, temperature, density, etc.) is created and modulated by the same wave vector. If the optical dielectric function depends on this property, it will be spatially modulated: $\Delta\varepsilon(\boldsymbol{r}) = A\cos[(\boldsymbol{k}_1 - \boldsymbol{k}_2)\cdot\boldsymbol{r}]$. When a third beam with wave vector $\boldsymbol{k}_3$ is now scattered by the sample, it will undergo diffraction resulting in a signal at wave vector $\boldsymbol{k}_s = \boldsymbol{k}_3 \pm (\boldsymbol{k}_1 - \boldsymbol{k}_2)$. By varying the delay between the initial and the probe beams we can follow the decay of the grating amplitude and, consequently, the underlying motions of the elementary excitations, on a controlled lengthscale determined by the grating wave vector $\boldsymbol{k}_g \equiv \boldsymbol{k}_1 - \boldsymbol{k}_2$ (fig. 1). For off-resonance conditions $\Delta\varepsilon$ is purely real (phase grating) whereas for resonant excitation it has an imaginary part (population grating). Phenomenological treatments of grating experiments have been developed and widely used for the interpretation of numerous experiments. These consist of identifying the nature of the relevant dynamical variables produced by the laser grating (excitation density, free charge carriers, temperature, mass density, etc.) and using macroscopic transport equations to describe their time evolution. An excellent review of this level of description is found in Eichler et al. [1].

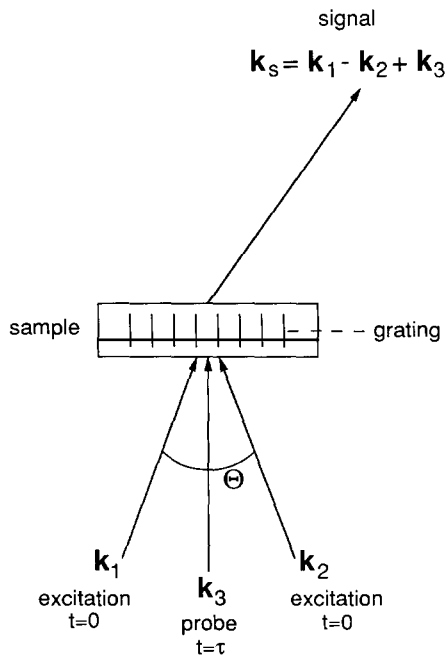

Fig. 1. Typical transient grating setup. Two excitation beams crossed under angle Θ create a grating in the sample with wave vector $\boldsymbol{k}_1 - \boldsymbol{k}_2$. After a variable delay τ, the grating is probed by a third pulse $\boldsymbol{k}_3$, resulting in a nonlinear ("diffracted") signal at $\boldsymbol{k}_s = \boldsymbol{k}_1 - \boldsymbol{k}_2 + \boldsymbol{k}_3$.

Alternatively, TG spectroscopy can be viewed as a particular technique of nonlinear optics which belongs to a broader family of processes known as *four-wave mixing* [1, 19–23]. Four-wave mixing is a technique in which three incoming beams with wave vectors $\boldsymbol{k}_1$, $\boldsymbol{k}_2$, $\boldsymbol{k}_3$ interact with a nonlinear medium and generate a coherent signal at a wave vector which is any combination of the wave vectors $\pm\boldsymbol{k}_1, \pm\boldsymbol{k}_2, \pm\boldsymbol{k}_3$. The four-wave mixing signal is usually calculated using the standard and well established systematic machinery of nonlinear optics. In this picture we expand the optical polarization in powers of the average electric field (the Maxwell field)

$$\boldsymbol{P} = \chi^{(1)}\boldsymbol{E} + \chi^{(2)}\boldsymbol{EE} + \chi^{(3)}\boldsymbol{EEE} + \cdots .$$

Four-wave mixing is related to the nonlinear susceptibility $\chi^{(3)}$. The four-wave mixing point of view allows us to put the TG technique in a broader context, and to explore its relationship to other spectroscopies (photon echo, pump-probe, CARS, etc.) [19–27]. For example, it has been shown that the information obtained from the TG experiment can in principle also be obtained using a frequency-domain technique, degenerate four-wave mixing (D4WM) [28–35]. In this variant, three *stationary* incident waves with wave vectors $\boldsymbol{k}_1$, $\boldsymbol{k}_2$ and $\boldsymbol{k}_3$ interact in the system and the scattered wave at $\boldsymbol{k}_s = \boldsymbol{k}_3 \pm (\boldsymbol{k}_1 - \boldsymbol{k}_2)$ is detected. It has been shown that resonances in the signal as a function of $\omega_1 - \omega_2$ are, under some very general conditions, equal to the Fourier transform of the TG signal [36]. The possibility of exciton localization [37–39], which is the analogue of the Anderson electron localization, could also be probed ideally by the grating technique [40].

In this review we develop a fully microscopic framework for the calculation of four-wave mixing processes in condensed phases, and use it to analyze TG spectroscopy in molecular crystals. Molecular crystals at low temperatures seem ideal systems for the application of the grating techniques. In these systems, optical excitation creates elementary excitations, Frenkel excitons [41–49] or charge transfer excitons [50], which are well understood. Such systems seem sufficiently simple to allow a rigorous microscopic treatment [50–56]. It was anticipated that the grating technique would directly probe the *exciton* motion. That motion is expected to be incoherent at high temperatures and to gradually become coherent as the temperature is lowered. Experiments performed on anthracene crystals [2b,c] showed however no evidence of coherent (nondiffusive) exciton motion. Instead they showed incoherent motion with a very large diffusion coefficient. These observations were interpreted by Agranovich et al. [51, 52] in terms of diffusion of *polaritons* [57–62], which are quasiparticles representing the correlated polarization and radiation field degrees of freedom. Other evidence related to polariton dynamics in organic crystals was obtained by Small and coworkers [60] who measured second harmonic generation and two-photon fluorescence in naphthalene. Their measurements strongly suggest the importance of polariton (rather than exciton) scattering, and cannot be accounted for using standard (nonretarded) expressions for the nonlinear susceptibilities. Polariton effects have also been measured by a variety of other nonlinear optical techniques [63–65].

The incorporation of polariton effects in the theory of nonlinear susceptibilities is not straightforward [51, 52, 66–69]. Traditionally the optical susceptibilities are viewed as purely material quantities, and calculated using summations over eigenstates of the molecular (unretarded) Hamiltonian. Consequently $\chi^{(3)}$ depends on exciton resonances and dipole matrix elements and does not depend on retarded interactions [21]. The calculation of any nonlinear optical signal is then conveniently divided into two steps: we first calculate susceptibilities in the absence of the radiation field and next, we use the susceptibilities in the Maxwell equations, thereby introducing the retarded interactions on a *macroscopic* level. This is the conventional formulation of nonlinear optics developed by Bloembergen

[19–23], which holds as long as the radiation and matter degrees of freedom are weakly coupled (e.g., for off-resonant processes or when exciton dephasing is large). Under these conditions the elementary excitations are excitons and photons, and it is possible to neglect correlations between the radiation field and the material polarization and to define susceptibilities. When the radiation and matter modes are strongly coupled, then retarded interactions need to be incorporated more microscopically and the optical response reflects the dynamics of polaritons [57–60]. It is then difficult to calculate susceptibilities. Instead, the signal is expanded directly in terms of the *external* field rather than the *Maxwell* field $\boldsymbol{E}$. It should be stressed that the linear susceptibility [68, 80] $\chi^{(1)}$ (and the dielectric function ε) can always be unambiguously defined, whether or not polariton effects are important. Optical nonlinearities require, however, a different approach in both situations.

One of the primary goals of the present review is to develop a systematic formulation in which polariton and exciton dynamics can be accounted for in a unified framework. In addition, we discuss several approximate schemes for the calculation of nonlinear optical response. The simplest is the anharmonic oscillator model for the polarization, proposed by Bloembergen [19]. Moreover, many-body effects are often handled using a mean-field theory (the local-field approximation) [70, 71]. Our general formalism reduces to these common procedures when specific approximations are made and therefore provides useful insight into their limitations.

The outline of this review is as follows. In section 2 we introduce the general model Hamiltonian for a molecular crystal which includes excitons, phonons, and photons and their coupling. The multipolar ($\boldsymbol{\mu} \cdot \boldsymbol{D}$) form of the exciton–photon coupling is adopted. The entire review is devoted to developing approximate schemes for calculating the dynamics described by this Hamiltonian and the Heisenberg equations (eqs. 2.9) for various limiting cases. In section 3 we focus on the material evolution alone (excitons and phonons) by factorizing out the electromagnetic field, treating it effectively as a classical c number. This is the usual framework in which linear and nonlinear optical susceptibilities are defined and calculated. In section 3.1 we present the operator equations and their solution to linear order in the electric field $\chi^{(1)}$. The material equations form a hierarchy whereby single-particle operators, such as the polarization, are coupled to operators involving successively more particles. To lowest order in the hierarchy we retain only single-particle operators and describe four-wave mixing and the nonlinear susceptibility $\chi^{(3)}$ within the local-field approximation (section 3.2). The incorporation of transport requires the next (two-particle) level of the hierarchy, which is addressed in section 3.3. The degenerate four-wave mixing signal, which is absent in the single-particle level, now shows up, and dephasing-induced resonances are obtained. In section 3.4 we discuss the transient grating, which is the time-domain analogue of degenerate four-wave mixing. This is only done within the two-particle description, as no transport exists on the single-particle level. In section 3.5 we show how the two-particle equations of the matter can be related to the Boltzmann and the diffusion equations. We further introduce the strong-collision and the Haken–Strobl models for exciton–phonon scattering. This concludes our discussion of exciton transport and dynamics.

In section 4 we turn to the more general and complex problem when the photon variables are strongly correlated with the material and cannot be factorized. In this case, we formulate nonlinear optics very differently, by using polaritons and avoiding the calculation of susceptibilities. In section 4.1 we introduce the polariton transformation which exactly solves the linear optics. In section 4.2 we develop equations of motion at the two-particle level (analogous to section 3.3). In sections 4.3 and 4.4 we apply these equations to the transient grating and its frequency-domain analogue (degenerate four-wave mixing), respectively. A detailed discussion of various limiting cases is given. Finally, in section 5 we present concluding remarks and summarize our results.

2. Model, Hamiltonian, and equations of motion

In this section we present our model system, the Hamiltonian, and the basic equations of motion that are used in sections 3 and 4 to calculate optical signals. We are interested in the nonlinear optical response of molecular crystals and restrict the model to a lattice of polarizable (nonpolar) two-level molecules with transition frequency Ω (one molecule per unit cell). The total number of molecules in the crystal is denoted by N. Even though optical experiments are usually carried out on thin crystal slabs, we will assume that the sample is still thick enough to invoke translational invariance in all lattice directions. For example, we will assume that the elementary excitations of the crystal (excitons or polaritons) are well-approximated by those for an infinite crystal. Refinements related to the treatment of multilevel molecules, the occurrence of more than one molecule per unit cell, or the explicit treatment of finite geometries, are possible, but not essential for the main objective of this paper and would obscure the physics by adding notational and algebraic complexity.

Any microscopic theory of (nonlinear) optical response should start with the choice of a Hamiltonian coupling the material system to the radiation field. The two best-known choices are the multipolar ($\boldsymbol{\mu}\cdot\boldsymbol{D}$) Hamiltonian and the minimal coupling ($\boldsymbol{p}\cdot\boldsymbol{A}$) Hamiltonian, which are related by a canonical transformation [72, 73]. Here, we will not elaborate on the controversial issue of the exact equivalence of both choices; an extensive literature exists which deals with this problem [74]. Suffice it to say that discrepancies between the results of both pictures are ultimately due to the fact that approximations (which are unavoidable in a practical calculation) affect them in a different way. We will use the multipolar Hamiltonian for the two following reasons: (i) This choice allows for a straightforward connection to the literature of the Bloch equations, which are used to describe nonlinear excited-state dynamics of isolated molecules [22, 75]. (ii) An easy connection to the popular local-field approach in condensed systems is possible within this Hamiltonian [76]. A drawback of the multipolar Hamiltonian is that it does not explicitly contain intermolecular interactions; these are instead carried by exchange of photons between the molecules [77]. The interactions can be recovered by elimination of the radiation field [78] or by a procedure presented previously by us, that keeps the radiation field as a degree of freedom [76]. The latter procedure will be used below.

In the dipole approximation, the explicit form of the multipolar Hamiltonian for our system reads [73]:

$$\hat{H} = \sum_m \hat{H}_m + \hat{H}_{\mathrm{rad}} - \int \hat{\boldsymbol{P}}(\boldsymbol{r})\cdot\hat{\boldsymbol{D}}^{\perp}(\boldsymbol{r})\,\mathrm{d}\boldsymbol{r} + 2\pi\sum_m \int |\hat{\boldsymbol{P}}_m^{\perp}(\boldsymbol{r})|^2\,\mathrm{d}\boldsymbol{r} + \hat{T} \tag{2.1}$$

[throughout this paper, operators are indicated by a caret ($\hat{O}$); the same symbol without caret denotes the expectation value $O(t)\equiv\langle\hat{O}(t)\rangle$]. In eq. (2.1) $\hat{H}_m$ is the Hamiltonian of the isolated molecule m and $\hat{H}_{\mathrm{rad}}$ is the contribution from the free radiation field. In second quantization, both can be expressed using creation and annihilation operators,

$$\hat{H}_m = \hbar\Omega\hat{B}_m^{\dagger}\hat{B}_m\,, \tag{2.2}$$

$$\hat{H}_{\mathrm{rad}} = \hbar\sum_{k\lambda} kc\hat{a}_{k\lambda}^{\dagger}\hat{a}_{k\lambda}\,. \tag{2.3}$$

Here, $\hat{B}_m^{\dagger}$ ($\hat{B}_m$) denotes the creation (annihilation) operator for an excitation on molecule m. These operators commute for different molecules, whereas for any single molecule they obey

$$[\hat{B}_m^{\dagger}, \hat{B}_m]_+ \equiv \hat{B}_m^{\dagger}\hat{B}_m + \hat{B}_m\hat{B}_m^{\dagger} = \hat{1}\,, \tag{2.4a}$$

$$[\hat{B}_m^\dagger, \hat{B}_m]_- \equiv \hat{B}_m^\dagger \hat{B}_m - \hat{B}_m \hat{B}_m^\dagger \equiv -\hat{1} + \hat{W}_m \,. \tag{2.4b}$$

The last equality defines the molecular population operator, which, combining eqs. (2.4a) and (2.4b), can also be written as

$$\hat{W}_m = 2\hat{B}_m^\dagger \hat{B}_m \,. \tag{2.4c}$$

Evidently, this operator has eigenvalue zero in the ground state and 2 in the excited state. For harmonic oscillators (bosons), eq. (2.4a) does not hold and $\hat{W}_m$ as defined in eq. (2.4b) vanishes identically. Therefore, neglecting this operator for two-level molecules is referred to as the Bose approximation [42, 58, 61]. In eq. (2.3), the operators $\hat{a}_{k\lambda}^\dagger$ and $\hat{a}_{k\lambda}$ create and annihilate a photon with wave vector $\boldsymbol{k}$ and transverse polarization λ ($\lambda = 1, 2$), respectively. They obey Bose commutation relations,

$$[\hat{a}_{k\lambda}, \hat{a}_{k'\lambda'}^\dagger]_- = \delta_{kk'}\delta_{\lambda\lambda'} \,, \qquad [\hat{a}_{k\lambda}, \hat{a}_{k'\lambda'}]_- = 0 \,, \tag{2.5}$$

and they commute with all material operators. Furthermore, $k \equiv |\boldsymbol{k}|$ and c is the velocity of light in vacuum.

The third term in eq. (2.1) gives the interaction between the radiation field and the molecules. $\hat{\boldsymbol{P}}(\boldsymbol{r})$ is the polarization field in the medium, which in the dipole approximation may be written as

$$\hat{\boldsymbol{P}}(\boldsymbol{r}) = \sum_m \hat{\boldsymbol{\mu}}_m \delta(\boldsymbol{r} - \boldsymbol{r}_m) \,. \tag{2.6a}$$

Here $\hat{\boldsymbol{\mu}}_m$ denotes the total dipole operator of molecule m (position $\boldsymbol{r}_m$), which can be written as

$$\hat{\boldsymbol{\mu}}_m = \boldsymbol{\mu}_m(\hat{B}_m + \hat{B}_m^\dagger) \,, \tag{2.6b}$$

with $\boldsymbol{\mu}_m$ the transition dipole matrix element of molecule m. $\hat{\boldsymbol{D}}^\perp(\boldsymbol{r})$ denotes the transverse part of the electric displacement field at position $\boldsymbol{r}$ and is related to the transverse part of the Maxwell electric-field operator $\hat{\boldsymbol{E}}(\boldsymbol{r})$ by

$$\hat{\boldsymbol{D}}^\perp(\boldsymbol{r}) = \hat{\boldsymbol{E}}^\perp(\boldsymbol{r}) + 4\pi\hat{\boldsymbol{P}}^\perp(\boldsymbol{r}) \,. \tag{2.7}$$

We stress that in the multipolar Hamiltonian, the displacement field $\hat{\boldsymbol{D}}^\perp(\boldsymbol{r})$ (and not the Maxwell field $\hat{\boldsymbol{E}}^\perp$) is the conjugate momentum of the vector potential $\hat{\boldsymbol{A}}(\boldsymbol{r})$, so that in second quantization $\hat{\boldsymbol{D}}^\perp(\boldsymbol{r})$ is totally expressed in terms of *radiation* creation and annihilation operators only. Explicitly, we have [73]

$$\hat{\boldsymbol{A}}^\perp(\boldsymbol{r}) = \sum_{k\lambda} \left(\frac{2\pi\hbar c}{Vk}\right)^{1/2} [\hat{a}_{k\lambda} \exp(\mathrm{i}\boldsymbol{k}\cdot\boldsymbol{r}) + \hat{a}_{k\lambda}^\dagger \exp(-\mathrm{i}\boldsymbol{k}\cdot\boldsymbol{r})]\boldsymbol{e}_{k\lambda} \,, \tag{2.8a}$$

$$\hat{\boldsymbol{D}}^\perp(\boldsymbol{r}) = \mathrm{i}\sum_{k\lambda} \left(\frac{2\pi\hbar kc}{V}\right)^{1/2} [\hat{a}_{k\lambda} \exp(\mathrm{i}\boldsymbol{k}\cdot\boldsymbol{r}) - \hat{a}_{k\lambda}^\dagger \exp(-\mathrm{i}\boldsymbol{k}\cdot\boldsymbol{r})]\boldsymbol{e}_{k\lambda} \,, \tag{2.8b}$$

with V the quantization volume, taken equal to the crystal volume in all calculations, and $\boldsymbol{e}_{k\lambda}$ ($\lambda = 1, 2$) the transverse unit polarization vectors belonging to the wave vector $\boldsymbol{k}$. We work in the Coulomb gauge, so that the longitudinal part of the vector potential vanishes. Of course, the longitudinal part of the displacement field also vanishes, because there are no free charges in our system. The transverse electric field in second quantization is now defined by eq. (2.7), in combination with eqs. (2.6) and

(2.8b). In general, the longitudinal part of the electric field, $\hat{\boldsymbol{E}}^{\parallel}$, does not vanish, but is fully determined by the polarization field through the relation $\hat{\boldsymbol{E}}^{\parallel} = -4\pi\hat{\boldsymbol{P}}^{\parallel}$.

The fourth term in eq. (2.1) is a self-energy, in which $\hat{\boldsymbol{P}}_m^{\perp}(\boldsymbol{r})$ is the transverse polarization field caused by molecule m only. For two-level molecules this term is an infinite *constant* which does not contribute to the evolution, so that it is often omitted completely from the Hamiltonian. Finally, the last term in eq. (2.1), $\hat{T}$, represents the kinetic energy related to the nuclear motion (phonons).

To calculate optical response, coupled equations of motion for the expectation values of dynamical variables (e.g., the polarization field) are ideal. Such equations can be obtained from the expectation values of Heisenberg equations of motion, supplemented with some factorization approximation to truncate the coupling to increasingly more complicated variables (sections 3 and 4). A great advantage of an equation-of-motion approach is that, unlike the density-matrix approach in the Schrödinger picture [19–23], it does not involve the tedious calculation of the eigenstates of the total system. Instead, we focus directly on the relevant dynamical variables which carry the information necessary for a given measurement. The complete dynamical information as given by the eigenstates is usually too complex and not required for most applications involving complex systems in condensed phases.

We have shown earlier [76] that the Heisenberg equations of motion for material operators within the multipolar Hamiltonian, can be written in a form which explicitly contains the instantaneous Coulomb interactions between the molecules, and the interactions between the molecular dipoles and the transverse Maxwell field $\hat{\boldsymbol{E}}^{\perp}$ (instead of $\hat{\boldsymbol{D}}^{\perp}$). It is essential that in the derivation of these equations, we split the (transverse) displacement field according to eq. (2.7), i.e., in terms of the *transverse* electric and polarization fields. An alternative approach that uses $\hat{\boldsymbol{D}}^{\perp} = \hat{\boldsymbol{D}} = \hat{\boldsymbol{E}} + 4\pi\hat{\boldsymbol{P}}$, leads to equations of a very different form, in which the instantaneous interactions are not readily recognized. It is straightforward to extend the derivation of ref. [76] to the present situation where also nuclear motion is possible. For an arbitrary operator $\hat{Q}$ (material, radiation, or mixed), we find (all operators taken at time t)

$$(1/\mathrm{i})\,\mathrm{d}\hat{Q}/\mathrm{d}t = L\hat{Q}\,, \tag{2.9a}$$

$$\hbar L\hat{Q} = [\hat{H}_{\mathrm{mat}} + \hat{H}_{\mathrm{rad}}, \hat{Q}]_- - \frac{1}{2}\sum_m \{[\hat{\boldsymbol{\mu}}_m, \hat{Q}]_- \cdot \hat{\boldsymbol{E}}^{\perp}(\boldsymbol{r}_m) + \hat{\boldsymbol{E}}^{\perp}(\boldsymbol{r}_m)\cdot[\hat{\boldsymbol{\mu}}_m, \hat{Q}]_-\}$$
$$- \frac{1}{2}\sum_m \{\boldsymbol{\mu}_m \cdot [\hat{\boldsymbol{D}}^{\perp}(\boldsymbol{r}_m), \hat{Q}]_- + [\hat{\boldsymbol{D}}^{\perp}(\boldsymbol{r}_m), \hat{Q}]_- \cdot \hat{\boldsymbol{\mu}}_m\}\,. \tag{2.9b}$$

Here, $\hat{H}_{\mathrm{mat}}$ denotes a material Hamiltonian which consists of three well-known parts,

$$\hat{H}_{\mathrm{mat}} = \hat{H}_{\mathrm{ex}} + \hat{H}_{\mathrm{ph}} + \hat{H}_{\mathrm{ep}}\,. \tag{2.10}$$

$\hat{H}_{\mathrm{ex}}$ is the usual Frenkel exciton Hamiltonian [42]

$$\hat{H}_{\mathrm{ex}} = \hbar\Omega\sum_m \hat{B}_m^{\dagger}\hat{B}_m + \frac{\hbar}{2}{\sum_{m,n}}' J(\boldsymbol{r}_{mn})(\hat{B}_m^{\dagger} + \hat{B}_m)(\hat{B}_n^{\dagger} + \hat{B}_n)\,, \tag{2.11}$$

where the second term accounts for the instantaneous dipole–dipole interactions between the molecules in their equilibrium positions and orientations (the prime excludes terms with $m = n$ from the summation). We have defined $\boldsymbol{r}_{mn} \equiv \boldsymbol{r}_m - \boldsymbol{r}_n$, where, from now on, $\boldsymbol{r}_m$ denotes the equilibrium position of molecule m. The explicit form of the interaction reads

$$\hbar J(\boldsymbol{r}) = \boldsymbol{\mu}\cdot(1/r^3 - 3\boldsymbol{r}\boldsymbol{r}/r^5)\cdot\boldsymbol{\mu}\,, \tag{2.12}$$

with $\boldsymbol{\mu}$ the molecular transition dipole in the equilibrium configuration (equal for all molecules on the lattice). Of course, short-range interactions (e.g., exchange), which have been omitted from the Hamiltonian from the very start (eq. 2.1), can be added heuristically to $J(\boldsymbol{r})$. The second term in eq. (2.10) is the energy of the phonons, which are treated within the harmonic approximation [42, 79],

$$\hat{H}_{\mathrm{ph}} = \hbar \sum_{\boldsymbol{q},s} \bar{\Omega}_{\boldsymbol{q}s} \hat{b}^{\dagger}_{\boldsymbol{q}s} \hat{b}_{\boldsymbol{q}s} \,. \tag{2.13}$$

Here, $\hat{b}^{\dagger}_{\boldsymbol{q}s}$ ($\hat{b}_{\boldsymbol{q}s}$) is the creation (annihilation) operator for a phonon with wave vector $\boldsymbol{q}$ in branch s and $\hbar\bar{\Omega}_{\boldsymbol{q}s}$ is its energy. $\hat{b}^{\dagger}_{\boldsymbol{q}s}$ and $\hat{b}_{\boldsymbol{q}s}$ obey Bose commutation relations [cf. eq. (2.5)].

Finally, the last contribution to $\hat{H}_{\mathrm{mat}}$ is the exciton–phonon interaction, which arises from the dependence of the intermolecular interactions and the Van der Waals shifts on the displacements of the nuclear coordinates from their equilibrium values. To lowest (linear) order in these displacements, we can write [42, 60a]

$$\hat{H}_{\mathrm{ep}} = \frac{1}{\sqrt{N}} \sum_{\boldsymbol{k},\boldsymbol{q},s} [F_s(\boldsymbol{k},\boldsymbol{q}) + \chi_s(\boldsymbol{q})] \hat{B}^{\dagger}_{\boldsymbol{k}+\boldsymbol{q}} \hat{B}_{\boldsymbol{k}} (\hat{b}_{\boldsymbol{q}s} + \hat{b}^{\dagger}_{-\boldsymbol{q}s}) \,, \tag{2.14}$$

where $\hat{B}_{\boldsymbol{k}}$ and $\hat{B}^{\dagger}_{\boldsymbol{k}}$ are the exciton annihilation and creation operators in momentum representation, respectively,

$$\hat{B}_{\boldsymbol{k}} \equiv \frac{1}{\sqrt{N}} \sum_{m} \hat{B}_m \exp(-\mathrm{i}\boldsymbol{k}\cdot\boldsymbol{r}_m) \,, \qquad \hat{B}^{\dagger}_{\boldsymbol{k}} \equiv \frac{1}{\sqrt{N}} \sum_{m} \hat{B}^{\dagger}_m \exp(\mathrm{i}\boldsymbol{k}\cdot\boldsymbol{r}_m) \,. \tag{2.15a, b}$$

Of course, these operators are periodic on the reciprocal lattice and the inverse transformations read

$$\hat{B}_m = \frac{1}{\sqrt{N}} \sum_{\substack{\boldsymbol{k} \\ 1\mathrm{BZ}}} \hat{B}_{\boldsymbol{k}} \exp(\mathrm{i}\boldsymbol{k}\cdot\boldsymbol{r}_m) \,, \qquad \hat{B}^{\dagger}_m = \frac{1}{\sqrt{N}} \sum_{\substack{\boldsymbol{k} \\ 1\mathrm{BZ}}} \hat{B}^{\dagger}_{\boldsymbol{k}} \exp(-\mathrm{i}\boldsymbol{k}\cdot\boldsymbol{r}_m) \,, \tag{2.15c, d}$$

where the $\boldsymbol{k}$ summations extend over the first Brillouin zone only. $F_s(\boldsymbol{k},\boldsymbol{q})$ and $\chi_s(\boldsymbol{q})$ are complex coupling constants that can be expressed in the first derivatives of the intermolecular interactions and the Van der Waals shifts, respectively, with respect to the nuclear displacements [42]. They obey the symmetry relations $F_s(\boldsymbol{k},\boldsymbol{q}) = F^*_s(\boldsymbol{k}+\boldsymbol{q},-\boldsymbol{q})$ and $\chi_s(\boldsymbol{q}) = \chi^*_s(-\boldsymbol{q})$ (the asterisk denotes the complex conjugate), which guarantees that $\hat{H}_{\mathrm{ep}}$ is Hermitian. It is noteworthy that in the delocalized representation of eq. (2.14), $F_s(\boldsymbol{k},\boldsymbol{q})$ and $\chi_s(\boldsymbol{q})$ multiply the same operators, so that their sum may be replaced by a single total coupling constant, which we will write $\tilde{F}_s(\boldsymbol{k},\boldsymbol{q})$. In the standard reference [42] for $\hat{H}_{\mathrm{ep}}$, this is not the case, as a result of improper use of translational symmetry. This completes the discussion of $\hat{H}_{\mathrm{mat}}$ in eq. (2.9b).

All other contributions to this equation speak for themselves. In the last two r.h.s. terms, the equilibrium positions and orientations for the molecules are implied, in agreement with the common neglect of direct photon–phonon interactions [60, 80]. Clearly, for a purely material operator $\hat{Q}$, eq. (2.9) reduces to eq. (12) of ref. [76], with additional contributions due to exciton–phonon interactions. Equation (2.9) is the basis for all equations of motion that are used in this paper. In general, eq. (2.9) will result in an infinite hierarchy of coupled dynamical equations whereby single-body operators are successively coupled to more complex quantities. Fortunately, the optical response to electromagnetic fields that are not too strong, requires the explicit introduction of only few-particle states. This allows us

to truncate the hierarchy at a very early stage. We shall demonstrate in the coming sections how a truncation at the two-particle or even the single-particle level is adequate for the calculation of a variety of optical measurements. This situation is formally very similar to the zero-temperature many-body theory where a few quasiparticles dominate the dynamical behavior [44, 81].

We conclude this section by giving the definition for the spatial and temporal Fourier transforms of an arbitrary function $f(\boldsymbol{r}, t)$,

$$f(\boldsymbol{k}, \omega) = \int_V \mathrm{d}\boldsymbol{r} \int_{-\infty}^{+\infty} \mathrm{d}t\, f(\boldsymbol{r}, t) \exp(-\mathrm{i}\boldsymbol{k}\cdot\boldsymbol{r} + \mathrm{i}\omega t)\,. \tag{2.16a}$$

The inverse transform then reads

$$f(\boldsymbol{r}, t) = \frac{1}{2\pi V} \sum_{\boldsymbol{k}} \int_{-\infty}^{+\infty} \mathrm{d}\omega\, f(\boldsymbol{k}, \omega) \exp(\mathrm{i}\boldsymbol{k}\cdot\boldsymbol{r} - \mathrm{i}\omega t)\,, \tag{2.16b}$$

where the $\boldsymbol{k}$ summation extends over all Brillouin zones.

3. Nonlinear optical response of excitons

3.1. Operator equations and linear optics

In this section, we consider the exciton theory of nonlinear optical response. This is the conventional approach, in which the electric field $\hat{\boldsymbol{E}}^{\perp}$ is treated as an external c-number. Equivalently, in equations of motion, the expectation value $\langle \hat{Q}\hat{\boldsymbol{E}}^{\perp}\rangle$, with $\hat{Q}$ an arbitrary material operator, is always factored into $\langle \hat{Q}\rangle\langle \hat{\boldsymbol{E}}^{\perp}\rangle$. All material variables can then be expanded in powers of $\langle \hat{\boldsymbol{E}}^{\perp}\rangle$. For the polarization field, the expansion coefficients define the susceptibilities or response functions [19–22]. In combination with the Maxwell equations, the susceptibilities suffice to calculate the optical signal. In this approach, the susceptibilities are completely determined by the evolution of the isolated material system with *instantaneous* intermolecular interactions, i.e., by the eigenstates of $\hat{H}_{\mathrm{mat}}$, which are the Coulomb excitons. This approach does not, therefore, account for the fact that in low-temperature crystals strongly mixed coherent combinations of photons and excitons (polaritons [57, 58]) occur as eigenmodes; polariton effects will be studied in section 4.

The first step in the exciton theory consists of deriving equations of motion for the exciton operators $\hat{B}_{\boldsymbol{k}}$ and $\hat{B}^{\dagger}_{-\boldsymbol{k}}$ (with $\boldsymbol{k}$ in the first Brillouin zone) from eq. (2.9). Throughout this paper, we neglect Umklapp contributions to $\boldsymbol{E}^{\perp}$, i.e., we neglect Fourier components $\boldsymbol{E}^{\perp}(\boldsymbol{k}, t)$ with $\boldsymbol{k}$ outside the first Brillouin zone. This approximation is customary (see, e.g., ref. [57]) and has in the context of the multipolar Hamiltonian been discussed in ref. [76]. Using the commutation relation (2.4b), the following compact form for the equations of motion can now be obtained (all operators taken at time t):

$$\frac{1}{\mathrm{i}}\frac{\mathrm{d}}{\mathrm{d}t}\begin{pmatrix}\hat{B}_{\boldsymbol{k}}\\ \hat{B}^{\dagger}_{-\boldsymbol{k}}\end{pmatrix} = \begin{pmatrix}-\Omega - J(\boldsymbol{k}) - \Sigma(\boldsymbol{k}) & -J(\boldsymbol{k})\\ J(\boldsymbol{k}) & \Omega + J(\boldsymbol{k}) + \Sigma^{*}(\boldsymbol{k})\end{pmatrix}\begin{pmatrix}\hat{B}_{\boldsymbol{k}}\\ \hat{B}^{\dagger}_{-\boldsymbol{k}}\end{pmatrix} + \frac{1}{2\Omega\sqrt{N}}\left[2\Omega\rho\hbar^{-1}\boldsymbol{\mu}\cdot\hat{\boldsymbol{E}}^{\perp}(\boldsymbol{k}) + \hat{\mathcal{M}}(\boldsymbol{k})\right]\begin{pmatrix}1\\ -1\end{pmatrix}. \tag{3.1}$$

Here, $J(\boldsymbol{k})$ is the lattice Fourier transform of the intermolecular interaction

$$J(\boldsymbol{k}) = \sum_{m \neq 0} J(\boldsymbol{r}_m) \exp(-\mathrm{i}\boldsymbol{k} \cdot \boldsymbol{r}_m) . \tag{3.2}$$

Because the lattice model described in section 2 is centrosymmetric, we have $J(\boldsymbol{k}) = J(-\boldsymbol{k})$. Furthermore, $\Sigma(\boldsymbol{k})$ $[= \Sigma(-\boldsymbol{k})]$ is the complex exciton self-energy which accounts for the effect of phonon scattering on the electronic evolution. In appendix A we discuss a procedure to calculate $\Sigma(\boldsymbol{k})$ and obtain, to second order in the exciton–phonon interaction, the well-known expressions [42]

$$\Sigma(\boldsymbol{k}) \equiv \Delta(\boldsymbol{k}) - \mathrm{i}\Gamma(\boldsymbol{k}) , \tag{3.3a}$$

$$\Delta(\boldsymbol{k}) = -\frac{1}{\hbar^2 N} \mathrm{P} \sum_{qs} |\tilde{F}_s(\boldsymbol{k}, \boldsymbol{q})|^2 \left(\frac{\langle n_{qs} \rangle_{\mathrm{T}}}{\Omega_{k+q} - \Omega_k - \bar{\Omega}_{qs}} + \frac{\langle n_{-qs} + 1 \rangle_{\mathrm{T}}}{\Omega_{k+q} - \Omega_k + \bar{\Omega}_{-qs}} \right) , \tag{3.3b}$$

$$\Gamma(\boldsymbol{k}) = \frac{\pi}{\hbar^2 N} \sum_{q,s} |\tilde{F}_s(\boldsymbol{k}, \boldsymbol{q})|^2 [\langle n_{qs} \rangle_{\mathrm{T}} \delta(\Omega_{k+q} - \Omega_k - \bar{\Omega}_{qs}) + \langle n_{-qs} + 1 \rangle_{\mathrm{T}} \delta(\Omega_{k+q} - \Omega_k - \bar{\Omega}_{-qs})] . \tag{3.3c}$$

Here, Ω_k is the frequency of the Coulomb exciton with wave vector $\boldsymbol{k}$ (eq. 3.6), $\langle n_{qs} \rangle_{\mathrm{T}}$ denotes the thermal (Bose–Einstein) occupation number of phonons with wave vector $\boldsymbol{q}$ in branch s, and P stands for the principal part. $\Gamma(\boldsymbol{k})$ is the damping rate of the exciton induced by the phonon bath; $\Delta(\boldsymbol{k})$ is the phonon induced frequency shift, which will henceforth be neglected. $\Gamma(\boldsymbol{k})$ plays a crucial role in the occurrence of polariton effects (section 4.1).

Returning to eq. (3.1), $\rho \equiv N/V$ denotes the average molecular density in the crystal and, finally,

$$\hat{\mathcal{M}}(\boldsymbol{k}) \equiv \Omega \sum_{k'} [J(\boldsymbol{k}')\sqrt{N}(\hat{B}_{k'} + \hat{B}^{\dagger}_{-k'}) - \rho\hbar^{-1}\boldsymbol{\mu} \cdot \hat{\boldsymbol{E}}^{\perp}(\boldsymbol{k}'), \hat{W}(\boldsymbol{k} - \boldsymbol{k}')]_+ . \tag{3.4}$$

Here, the $\boldsymbol{k}'$ summation (as from now on all wave vector sums in this paper) extends over the first Brillouin zone only, and $\hat{W}(\boldsymbol{k} - \boldsymbol{k}')$ is the lattice Fourier transform of the population operator,

$$\hat{W}(\boldsymbol{k} - \boldsymbol{k}') \equiv \frac{1}{N} \sum_m \hat{W}_m \exp[-\mathrm{i}(\boldsymbol{k} - \boldsymbol{k}') \cdot \boldsymbol{r}_m] = \frac{2}{N} \sum_{k''} \hat{B}^{\dagger}_{k'+k''} \hat{B}_{k+k''} . \tag{3.5}$$

Let us first consider eq. (3.1) without the inhomogeneous source terms multiplying the vector $\binom{1}{-1}$. This defines an eigenvalue problem whose solutions are the annihilation operator for the Coulomb exciton at wave vector $\boldsymbol{k}$ and the creation operator for the Coulomb exciton at $-\boldsymbol{k}$, in terms of $\hat{B}_k$ and $\hat{B}^{\dagger}_{-k}$ [42]. The Coulomb exciton frequency is determined by the secular equation of the problem and easily found to be $\Omega_k - \mathrm{i}\Gamma(\boldsymbol{k})$, with

$$\Omega_k = \{\Omega[\Omega + 2J(\boldsymbol{k})]\}^{1/2} . \tag{3.6}$$

For $|J(\boldsymbol{k})| \ll \Omega$, which is almost by definition the case in molecular crystals [42, 48], this yields $\Omega_k \approx \Omega + J(\boldsymbol{k})$. This is known as the Heitler–London approximation and is obtained directly if one does not use second quantization. In this approximation, the Coulomb excitons are simply created (annihilated) by $\hat{B}^{\dagger}_k$ ($\hat{B}_k$) [42]. The excitons respond to the source term in eq. (3.1), which contains a linear ($\sim \hat{\boldsymbol{E}}^{\perp}$) and a nonlinear ($\sim \hat{\mathcal{M}}$) contribution. The latter is the source of nonlinear optical response and vanishes identically for harmonic oscillators [$\hat{W}(\boldsymbol{k}) \equiv 0$]. We note that in the present paper $\hat{W}(\boldsymbol{k})$ is the only source of nonlinearities. In systems with multilevel (and *polar* two-level) molecules, other sources

arise from intermolecular interaction terms that are cubic and quartic in the molecular exciton creation and annihilation operators [47, 59]. Such terms even give rise to nonlinearities if a Bose approximation is applied, which is usually done in the literature considering this kind of nonlinearities. In reality, both types of nonlinearities will occur.

It proves useful to rewrite eq. (3.1) by introducing the variables

$$\hat{P}(\boldsymbol{k}) \equiv \sqrt{N}(\hat{B}_{\boldsymbol{k}} + \hat{B}^{\dagger}_{-\boldsymbol{k}}) , \qquad \hat{V}(\boldsymbol{k}) \equiv \sqrt{N}(\hat{B}_{\boldsymbol{k}} - \hat{B}^{\dagger}_{-\boldsymbol{k}}) . \tag{3.7a, b}$$

$\hat{P}(\boldsymbol{k})$ equals, up to a factor $\boldsymbol{\mu}$, the material polarization field. Adding and subtracting the temporal Fourier transforms of the two equations contained in eq. (3.1) and eliminating $\hat{V}(\boldsymbol{k}, \omega)$, we obtain

$$\{-[\omega + \mathrm{i}\Gamma(\boldsymbol{k})]^2 + \Omega_{\boldsymbol{k}}^2\}\hat{P}(\boldsymbol{k}, \omega) = 2\Omega\rho\hbar^{-1}\boldsymbol{\mu}\cdot\hat{\boldsymbol{E}}^{\perp}(\boldsymbol{k}, \omega) + \hat{\mathcal{M}}(\boldsymbol{k}, \omega) , \tag{3.8a}$$

$$\hat{\mathcal{M}}(\boldsymbol{k}, \omega) = \frac{\Omega}{2\pi}\int \mathrm{d}\omega' \sum_{\boldsymbol{k}'} [J(\boldsymbol{k}')\hat{P}(\boldsymbol{k}', \omega') - \rho\hbar^{-1}\boldsymbol{\mu}\cdot\hat{\boldsymbol{E}}^{\perp}(\boldsymbol{k}', \omega'), \hat{W}(\boldsymbol{k} - \boldsymbol{k}', \omega - \omega')]_+ . \tag{3.8b}$$

Alternatively, we can write

$$\hat{\mathcal{M}}(\boldsymbol{k}, \omega) = \frac{(2\Omega)^{-1}}{(2\pi N)^2}\int \mathrm{d}\omega' \int \mathrm{d}\omega'' \sum_{\boldsymbol{k}'}\sum_{\boldsymbol{k}''} [\Omega - \omega'' - \mathrm{i}\Gamma(\boldsymbol{k}'')][\Omega + \omega - \omega' - \omega'' + \mathrm{i}\Gamma(\boldsymbol{k} - \boldsymbol{k}' - \boldsymbol{k}'')]$$
$$\times [J(\boldsymbol{k}')\hat{P}(\boldsymbol{k}', \omega') - (\rho/\hbar)\boldsymbol{\mu}\cdot\hat{\boldsymbol{E}}^{\perp}(\boldsymbol{k}', \omega'), \hat{P}(\boldsymbol{k}'', \omega'')\hat{P}(\boldsymbol{k} - \boldsymbol{k}' - \boldsymbol{k}'', \omega - \omega' - \omega'')]_+ , \tag{3.8c}$$

where $\hat{W}(\boldsymbol{k}, \omega)$ has been reexpressed using eq. (3.5) and the exact relations

$$\hat{B}_{\boldsymbol{k}}(\omega) = [\Omega + \omega + \mathrm{i}\Gamma(\boldsymbol{k})]\hat{P}(\boldsymbol{k}, \omega)/(2\Omega\sqrt{N}) , \tag{3.9a}$$

$$\hat{B}^{\dagger}_{-\boldsymbol{k}}(\omega) = [\Omega - \omega - \mathrm{i}\Gamma(\boldsymbol{k})]\hat{P}(\boldsymbol{k}, \omega)/(2\Omega\sqrt{N}) . \tag{3.9b}$$

Here, $\hat{B}^{\dagger}_{\boldsymbol{k}}(\omega)$ denotes the temporal Fourier transform of $\hat{B}^{\dagger}_{\boldsymbol{k}}(t)$, and *not* the Hermitian conjugate $[\hat{B}_{\boldsymbol{k}}(\omega)]^{\dagger}$ of $\hat{B}_{\boldsymbol{k}}(\omega)$. Of course, we have $\hat{B}^{\dagger}_{\boldsymbol{k}}(\omega) = [\hat{B}_{\boldsymbol{k}}(-\omega)]^{\dagger}$. Relations (3.9) follow easily from eqs. (3.1) and (3.7). Transforming eq. (3.8a) back to the time domain, it becomes clear that we have replaced two first-order (in time) differential equations by a single second-order equation.

To conclude this subsection, we discuss the simple case of linear optics, governed by the first-order susceptibility. We first note that, in practice, susceptibilities are defined using discrete Fourier decompositions for the expectation values of the fields, instead of the Fourier transforms eq. (2.16) [19, 22, 68, 82]. The electric field is then written in the form

$$\boldsymbol{E}^{\perp}(\boldsymbol{r}, t) = \sum_j [\boldsymbol{E}_j^{+} \exp(\mathrm{i}\boldsymbol{k}_j\cdot\boldsymbol{r} - \mathrm{i}\omega_j t) + \text{c.c.}] , \tag{3.10}$$

where j labels a few modes which are essential in the experiment. $\omega_j\,(>0)$ and $\boldsymbol{k}_j$ are related by the dispersion relation of the crystal. The Fourier transform eq. (2.16) for this field reads

$$\boldsymbol{E}^{\perp}(\boldsymbol{k}, \omega) = 2\pi V \sum_j [\boldsymbol{E}_j^{+}\delta_{\boldsymbol{k},\boldsymbol{k}_j}\delta(\omega - \omega_j) + \boldsymbol{E}_j^{-*}\delta_{\boldsymbol{k},-\boldsymbol{k}_j}\delta(\omega + \omega_j)] . \tag{3.11}$$

Similar decompositions are possible for, e.g., the polarization field $\boldsymbol{P}$. The coefficients appearing in the expansion of the amplitudes $\boldsymbol{P}_j$ in terms of powers of the electric-field amplitudes $\boldsymbol{E}_j^{\perp}$, are now the susceptibilities [19, 22, 68, 82]. The first-order susceptibility is easily obtained from eq. (3.8a). Namely, the part of the polarization that is linear in the electric field is found by neglecting the nonlinearity $\hat{\mathcal{M}}(\boldsymbol{k})$. After taking expectation values and substituting eq. (3.11) and its analogue for the polarization, we obtain

$$\boldsymbol{P}_j^{(1)} = \boldsymbol{\mu} P_j^{(1)} \equiv \overleftrightarrow{\chi}^{(1)}(\boldsymbol{k}_j, \omega_j) \cdot \boldsymbol{E}_j^{\perp} , \tag{3.12a}$$

with the linear susceptibility tensor

$$\overleftrightarrow{\chi}^{(1)}(\boldsymbol{k}, \omega) \equiv \frac{\overleftrightarrow{\varepsilon}(\boldsymbol{k}, \omega) - 1}{4\pi} = \frac{2\Omega\rho\hbar^{-1}\boldsymbol{\mu}\boldsymbol{\mu}}{-[\omega + \mathrm{i}\Gamma(\boldsymbol{k})]^2 + \Omega_{\boldsymbol{k}}^2} . \tag{3.12b}$$

Here, and throughout the paper, superscripts in parentheses indicate the order in the electric field amplitudes. $\overleftrightarrow{\varepsilon}(\boldsymbol{k}, \omega)$ is the frequency and wave-vector dependent dielectric tensor. Equation (3.12b) is a standard result (see, e.g., ref. [42]); for crystals containing molecules with more than two well-separated levels, eq. (3.12) gives the contribution of each level to the linear susceptibility. In the remainder of this section, we will address the nonlinear optical response of the crystal by including the effect of $\mathcal{M}(\boldsymbol{k})$ in various approximate ways.

3.2. *The single-particle description: frequency-domain four-wave mixing*

The first nonlinear optical technique that we discuss is frequency-domain four-wave mixing. We consider a situation with three fundamental fields [$j = 1, 2, 3$ in eq. (3.10)] and are interested in the signal at $(\boldsymbol{k}_s, \omega_s) \equiv (\boldsymbol{k}_1 - \boldsymbol{k}_2 + \boldsymbol{k}_3, \omega_1 - \omega_2 + \omega_3)$. To lowest order in the field amplitudes $\boldsymbol{E}_j^{\perp}$, this is determined by the third-order susceptibility, which is defined through

$$\boldsymbol{P}_s^{(3)} = \boldsymbol{\mu} P_s^{(3)} \equiv \overleftrightarrow{\chi}^{(3)}(-\boldsymbol{k}_s - \omega_s; \boldsymbol{k}_1\omega_1, -\boldsymbol{k}_2 - \omega_2, \boldsymbol{k}_3\omega_3) \vdots \boldsymbol{E}_1^{\perp}\boldsymbol{E}_2^{\perp *}\boldsymbol{E}_3^{\perp} , \tag{3.13}$$

where $\boldsymbol{P}_s^{(3)}$ is the discrete Fourier coefficient of the polarization field with wave vector $\boldsymbol{k}_s$ and frequency ω_s to third order in the electric field amplitudes. We note that $\overleftrightarrow{\chi}^{(3)}$ is the lowest nonlinearity allowed by the present model, since $\overleftrightarrow{\chi}^{(2)}$ vanishes for a centrosymmetric medium [21].

To evaluate $\overleftrightarrow{\chi}^{(3)}$, we take the expectation value of eq. (3.8a) with $(\boldsymbol{k}, \omega) = (\boldsymbol{k}_s, \omega_s)$. The nonlinear source term for the third-order polarization is $\langle \hat{\mathcal{M}}(\boldsymbol{k}_s, \omega_s) \rangle^{(3)}$, which involves the expectation values of products of two and three "single-particle" operators [$\langle \hat{E}^{\perp} \rangle \langle \hat{P}\hat{P} \rangle$ and $\langle \hat{P}\hat{P}\hat{P} \rangle$ in eq. (3.8c)]. For these products, new equations of motion must be derived, which will involve yet higher-order products of operators, etc. In order to truncate the thus generated hierarchy of equations of motion [61], a factorization approximation must be invoked that breaks apart expectation values of products of operators into products of expectation values. It is natural to start with the simplest possible truncation, which consists of factoring $\langle \hat{\mathcal{M}} \rangle$ completely into single-particle expectation values. A typical contribution to $\mathcal{M}^{(3)}(\boldsymbol{k}_s, \omega_s)$ then reads

$$\mathcal{M}^{(3)}(\boldsymbol{k}_s, \omega_s) \propto (J(\boldsymbol{k}_1)P_1^{(1)} - \rho\hbar^{-1}\boldsymbol{\mu} \cdot \boldsymbol{E}_1^{\perp})P_2^{(1)*}P_3^{(1)} .$$

The first-order polarizations in this expression are obtained from the linear approximation to eq. (3.8a)

and straightforward algebra leads to

$$\overleftrightarrow{\chi}^{(3)}(-\boldsymbol{k}_s-\omega_s;\boldsymbol{k}_1\omega_1,-\boldsymbol{k}_2-\omega_2,\boldsymbol{k}_3\omega_3)=4\Omega\rho\,\frac{\boldsymbol{\mu\mu\mu\mu}}{\hbar^3}\,\frac{[\Omega+\omega_2-\mathrm{i}\Gamma(\boldsymbol{k}_2)][\Omega+\omega_1+\mathrm{i}\Gamma(\boldsymbol{k}_1)]}{\Delta(\boldsymbol{k}_s,\omega_s)\,\Delta(\boldsymbol{k}_1,\omega_1)\,\Delta(-\boldsymbol{k}_2,-\omega_2)}$$
$$\left(\frac{2\Omega J(\boldsymbol{k}_3)}{\Delta(\boldsymbol{k}_3,\omega_3)}-1\right)+\text{permutations of } j=1,2,3\,, \tag{3.14a}$$

$$\Delta(\boldsymbol{k},\omega)\equiv-[\omega+\mathrm{i}\Gamma(\boldsymbol{k})]^2+\Omega_{\boldsymbol{k}}^2\,. \tag{3.14b}$$

The permutations of $(\boldsymbol{k}_1,\omega_1)$, $(-\boldsymbol{k}_2,-\omega_2)$, and $(\boldsymbol{k}_3,\omega_3)$ account for the different time orderings with which the electric fields can interact with the sample [23]. Expression (3.14a) can be simplified if the three following conditions hold: (i) $|J(\boldsymbol{k})|\ll\Omega$ for all $\boldsymbol{k}$, which is generally the case; (ii) $|\omega_j-\Omega_{\boldsymbol{k}_j}|\gg|J(\boldsymbol{k}_j)|$ (off-resonance fundamental waves); (iii) $|\omega_s-\Omega_{\boldsymbol{k}_s}|\gg\Omega$, so that the rotating wave approximation (RWA) [75] can be applied to the signal wave. We then obtain

$$\begin{aligned}&\overleftrightarrow{\chi}^{(3)}(-\boldsymbol{k}_s-\omega_s;\boldsymbol{k}_1\omega_1,-\boldsymbol{k}_2-\omega_2,\boldsymbol{k}_3\omega_3)\\&\quad=2\rho(\boldsymbol{\mu\mu\mu\mu}/\hbar^3)[\omega_s-\Omega_{\boldsymbol{k}_s}+\mathrm{i}\Gamma(\boldsymbol{k}_s)]^{-1}[\omega_1-\Omega_{\boldsymbol{k}_1}+\mathrm{i}\Gamma(\boldsymbol{k}_1)]^{-1}[\omega_2-\Omega_{\boldsymbol{k}_2}-\mathrm{i}\Gamma(\boldsymbol{k}_2)]^{-1}\\&\qquad+\text{permutations of } j=1,2,3\,.\end{aligned} \tag{3.15}$$

We note that contributions which are anti-rotating with respect to the fundamental frequencies are still contained in this expression. They are hidden in the permutations; for example, interchanging $(\boldsymbol{k}_1,\omega_1)$ and $(-\boldsymbol{k}_2,-\omega_2)$ results in two anti-rotating denominators.

It is instructive at this point to make a connection to the (damped) anharmonic oscillator picture, which is a popular way to think about nonlinear response [19, 22]. If we take the expectation value of eq. (3.8) in the single-particle factorization and transform back to the time domain, we find [neglecting $\Gamma(\boldsymbol{k})^2$ with respect to Ω_k^2]

$$\ddot{P}(\boldsymbol{k},t)+2\Gamma(\boldsymbol{k})\dot{P}(\boldsymbol{k},t)+\Omega_{\boldsymbol{k}}^2P(\boldsymbol{k},t)=2\Omega\rho\hbar^{-1}\boldsymbol{\mu}\cdot\boldsymbol{E}^{\perp}(\boldsymbol{k},t)+\mathcal{M}(\boldsymbol{k},t)\,, \tag{3.16a}$$

$$\begin{aligned}\mathcal{M}(\boldsymbol{k},t)=&-\frac{1}{N^2\Omega}\sum_{\boldsymbol{k}'}\sum_{\boldsymbol{k}''}[\rho\hbar^{-1}\boldsymbol{\mu}\cdot\boldsymbol{E}^{\perp}(\boldsymbol{k}',t)-J(\boldsymbol{k}')P(\boldsymbol{k}',t)]\{[\Omega-\mathrm{i}\Gamma(\boldsymbol{k}'')]P(\boldsymbol{k}'',t)-\mathrm{i}\dot{P}(\boldsymbol{k}'',t)\}\\&\times\{[\Omega+\mathrm{i}\Gamma(\boldsymbol{k}-\boldsymbol{k}'-\boldsymbol{k}'')]P(\boldsymbol{k}-\boldsymbol{k}'-\boldsymbol{k}'',t)+\mathrm{i}\dot{P}(\boldsymbol{k}-\boldsymbol{k}'-\boldsymbol{k}'',t)\}\,.\end{aligned} \tag{3.16b}$$

Equation (3.16a) represents a set of damped harmonic oscillators, coupled by anharmonic driving terms. The oscillator picture can be pushed even further, if we realize that all intermolecular interactions can be eliminated from eqs. (3.16) by introducing the local electric field through

$$\boldsymbol{\mu}\cdot\boldsymbol{E}_{\mathrm{L}}(\boldsymbol{k},t)\equiv\boldsymbol{\mu}\cdot\boldsymbol{E}^{\perp}(\boldsymbol{k},t)-(\hbar/\rho)J(\boldsymbol{k})P(\boldsymbol{k},t)\,. \tag{3.17a}$$

For dipolar interactions in the continuum ($\boldsymbol{k}\to0$) limit, this coincides with the Lorentz local field [19, 22, 83]

$$\boldsymbol{E}_{\mathrm{L}}(\boldsymbol{k},t)\equiv\boldsymbol{E}(\boldsymbol{k},t)+\tfrac{4}{3}\pi\boldsymbol{P}(\boldsymbol{k},t)\,. \tag{3.17b}$$

Here we used $J(\boldsymbol{k}) = 4\pi\rho\hbar^{-1}\boldsymbol{\mu}\cdot(\boldsymbol{k}\boldsymbol{k}/k^2 - \overleftrightarrow{1}/3)\cdot\boldsymbol{\mu}$ for the dipole sum [84–86] and $\boldsymbol{E}^{\parallel} = -4\pi\boldsymbol{P}^{\parallel}$ as there are no free charges in the system ($\operatorname{div}\boldsymbol{D} = 0$). The equation of motion (3.16a) can now be rewritten

$$\ddot{P}(\boldsymbol{k}, t) + 2\Gamma(\boldsymbol{k})\dot{P}(\boldsymbol{k}, t) + \Omega^2 P(\boldsymbol{k}, t) = 2\Omega\rho\hbar^{-1}\boldsymbol{\mu}\cdot\boldsymbol{E}_{\mathrm{L}}(\boldsymbol{k}, t) + \mathcal{M}(\boldsymbol{k}, t)\,. \tag{3.18}$$

In $\boldsymbol{r}$-space, this equation takes the compact form

$$\ddot{P}(\boldsymbol{r}, t) + 2\Gamma\dot{P}(\boldsymbol{r}, t) + \Omega^2 P(\boldsymbol{r}, t) = 2\Omega\rho\hbar^{-1}\boldsymbol{\mu}\cdot\boldsymbol{E}_{\mathrm{L}}(\boldsymbol{r}, t) + \mathcal{M}(\boldsymbol{r}, t)\,, \tag{3.19a}$$

with $\boldsymbol{r}$ an arbitrary lattice site and

$$\mathcal{M}(\boldsymbol{r}, t) = -(\rho\boldsymbol{\mu}/\hbar\Omega)\cdot\boldsymbol{E}_{\mathrm{L}}(\boldsymbol{r}, t)[(\Omega - \mathrm{i}\Gamma)P(\boldsymbol{r}, t) - \mathrm{i}\dot{P}(\boldsymbol{r}, t)][(\Omega + \mathrm{i}\Gamma)P(\boldsymbol{r}, t) + \mathrm{i}\dot{P}(\boldsymbol{r}, t)]\,. \tag{3.19b}$$

Here, the $\boldsymbol{k}$ dependence of the damping is neglected; otherwise, a local picture is, of course, impossible. The polarization at every site behaves like an oscillator driven by the local electric field and by anharmonic (nonlinear) "forces". It is noteworthy that the anharmonicity is a function of both the "position" (P) and the "velocity" ($\dot{P}$) of the oscillator; in heuristic anharmonic oscillator models, one usually assumes an anharmonicity in the position only [19, 22].

The fact that the single-particle factorization used here leads to a local-field description, is not surprising and agrees with the more general conclusion that any theory that uses a factorization of single-molecule variables is equivalent to the local-field approximation [76]. Consequently, it must be possible to write the susceptibility eq. (3.14a) as the third-order molecular polarizability $\overleftrightarrow{\gamma}(-\omega_s; \omega_1, -\omega_2, \omega_3)$ multiplied by appropriate local-field correction factors [19, 22]. We check this explicitly. $\overleftrightarrow{\gamma}$ is easily obtained from eq. (3.14a) by setting $J(\boldsymbol{k}) = 0$ and $\rho = 1$. We then find

$$\begin{aligned}&\overleftrightarrow{\chi}^{(3)}(-\boldsymbol{k}_s - \omega_s; \boldsymbol{k}_1\omega_1, -\boldsymbol{k}_2 - \omega_2, \boldsymbol{k}_3\omega_3)\\ &\quad = \rho\,\frac{\cancel{\tilde{\Delta}(\omega_s)}}{\Delta(\boldsymbol{k}_s, \omega_s)}\,\frac{\cancel{\tilde{\Delta}(\omega_1)}}{\Delta(\boldsymbol{k}_1, \omega_1)}\,\frac{\cancel{\tilde{\Delta}(-\omega_2)}}{\Delta(-\boldsymbol{k}_2, -\omega_2)}\,\frac{\tilde{\Delta}(\omega_3)}{\Delta(\boldsymbol{k}_3, \omega_3)}\,\overleftrightarrow{\gamma}(-\omega_s; \omega_1, -\omega_2, \omega_3)\,,\end{aligned} \tag{3.20a}$$

$$\tilde{\Delta}(\omega) \equiv -(\omega + \mathrm{i}\Gamma)^2 + \Omega^2\,. \tag{3.20b}$$

The first three numerators in eq. (3.20a) simply cancel the molecular resonances in $\overleftrightarrow{\gamma}$. We now restrict our treatment for simplicity to the case that all wave vectors are perpendicular to the dipoles. Then, for optical wave vectors and dipolar interactions [84–86],

$$J(\boldsymbol{k}) = -(4\pi/3\hbar)\rho\mu^2\,. \tag{3.21}$$

Combining this with eq. (3.12b), it is easily found that

$$\tilde{\Delta}(\omega)/\Delta(\boldsymbol{k}, \omega) = \tfrac{1}{3}[\varepsilon(\boldsymbol{k}, \omega) + 2]\,, \tag{3.22}$$

so that eq. (3.20a) is indeed of the familiar local-field form [19, 22]. We finally note that cascading contributions to $\overleftrightarrow{\chi}^{(3)}$, which are usually found in a local-field approach [21, 82, 87], are absent here, because the second-order polarizability vanishes for nonpolar two-level molecules.

3.3. The two-particle description: degenerate four-wave mixing

In this section, we extend our study of frequency-domain four-wave mixing by relaxing the single-particle factorization. Instead of factorizing $\langle \hat{\mathcal{M}}(\boldsymbol{k}, \omega)\rangle$ in the expectation value of eq. (3.8a) [or eq. (3.1)] completely, we only factor the population $W(\boldsymbol{k}-\boldsymbol{k}')$ from it. We thus do not break up the population into single-particle variables, as we did in section 3.2. We then obtain from eq. (3.1) [with $B_{\boldsymbol{k}}(t) \equiv \langle \hat{B}_{\boldsymbol{k}}(t)\rangle$]

$$(1/\mathrm{i})\,\mathrm{d}B_{\boldsymbol{k}}(t)/\mathrm{d}t = -[\Omega + J(\boldsymbol{k}) - \mathrm{i}\Gamma(\boldsymbol{k})]B_{\boldsymbol{k}}(t) - J(\boldsymbol{k})B^{*}_{-\boldsymbol{k}}(t) + \frac{1}{\sqrt{N}}\,\rho\hbar^{-1}\boldsymbol{\mu}\cdot\boldsymbol{E}^{\perp}(\boldsymbol{k}, t)$$
$$+ \frac{1}{\sqrt{N}}\sum_{\boldsymbol{k}'}[J(\boldsymbol{k}')P(\boldsymbol{k}', t) - \rho\hbar^{-1}\boldsymbol{\mu}\cdot\boldsymbol{E}^{\perp}(\boldsymbol{k}', t)]W(\boldsymbol{k}-\boldsymbol{k}', t)\,, \tag{3.23}$$

and a similar equation for $B^{*}_{-\boldsymbol{k}}(t) = \langle \hat{B}^{\dagger}_{-\boldsymbol{k}}(t)\rangle$.

$W(\boldsymbol{k}-\boldsymbol{k}', t)$ now appears as a new variable. However, instead of pursuing the hierarchy by deriving an equation for the population itself, it proves more useful to introduce the two-particle variables

$$Q(\boldsymbol{k}, \boldsymbol{p}, t) \equiv \langle \hat{B}^{\dagger}_{\boldsymbol{p}-\boldsymbol{k}/2}(t)\hat{B}_{\boldsymbol{p}+\boldsymbol{k}/2}(t)\rangle$$
$$= \frac{1}{N}\sum_{m,n}\langle \hat{B}^{\dagger}_{m}(t)\hat{B}_{n}(t)\rangle \exp[-\mathrm{i}\boldsymbol{k}\cdot(\boldsymbol{r}_m + \boldsymbol{r}_n)/2 + \mathrm{i}\boldsymbol{p}\cdot(\boldsymbol{r}_m - \boldsymbol{r}_n)]\,, \tag{3.24a}$$

which are the diagonal elements ($\boldsymbol{k}=\boldsymbol{0}$) and coherences ($\boldsymbol{k}\neq\boldsymbol{0}$) of the exciton density matrix in the momentum representation. From the last form of eq. (3.24a), it is clear that $\boldsymbol{k}$ is conjugate to the exciton center of mass; $\boldsymbol{p}$ is related to the classical exciton momentum. The significance of the $\boldsymbol{k}$ and $\boldsymbol{p}$ variables may be clarified by switching to the Wigner representation for the exciton density matrix. This is done in section 3.5, where we also make the connection to common transport equations such as the Boltzmann equation. The exciton population can now be written [cf. eq. (3.5)],

$$W(\boldsymbol{k}, t) = \frac{2}{N}\sum_{\boldsymbol{p}} Q(\boldsymbol{k}, \boldsymbol{p}, t)\,. \tag{3.24b}$$

As next step in the hierarchy we now consider the equation of motion for $Q(\boldsymbol{k}, \boldsymbol{p}, t)$. We first concentrate on the *electronic* (coherent) part of this equation, i.e., without accounting for phonons. This is obtained from ($\boldsymbol{k}_1 \equiv \boldsymbol{p} - \boldsymbol{k}/2$; $\boldsymbol{k}_2 \equiv \boldsymbol{p} + \boldsymbol{k}/2$)

$$\langle \mathrm{d}[\hat{B}^{\dagger}_{\boldsymbol{k}_1}(t)\hat{B}_{\boldsymbol{k}_2}(t)]/\mathrm{d}t\rangle = \langle [\mathrm{d}\hat{B}^{\dagger}_{\boldsymbol{k}_1}(t)/\mathrm{d}t]\hat{B}_{\boldsymbol{k}_2}(t)\rangle + \langle \hat{B}^{\dagger}_{\boldsymbol{k}_1}(t)\,\mathrm{d}\hat{B}_{\boldsymbol{k}_2}(t)/\mathrm{d}t\rangle\,,$$

and eq. (3.1) without the self-energy terms. In the final result the following approximations are made: (i) $\langle \hat{\boldsymbol{E}}^{\perp}\rangle$ is factored from all other variables (exciton theory!); (ii) we neglect terms coupling to variables of the form $\langle \hat{B}^{\dagger}_{\boldsymbol{k}_1}(t)\hat{B}^{\dagger}_{-\boldsymbol{k}_2}(t)\rangle$ and $\langle \hat{B}_{-\boldsymbol{k}_1}(t)\hat{B}_{\boldsymbol{k}_2}(t)\rangle$, which is equivalent to invoking the Heitler–London approximation on this level of the hierarchy; (iii) we neglect all variables which are higher than bilinear in the exciton variables (such as $\langle \hat{W}\hat{B}\rangle$), as they eventually result in contributions to the polarization that are of order four and higher in the electric field amplitudes. The leading order for four-wave mixing processes is three. The *phonon* (incoherent) contribution to $\dot{Q}(\boldsymbol{k}, \boldsymbol{p}, t)$ is, to second order in the exciton–phonon interaction, derived in appendix A. The total equation of motion

then reads,

$$\frac{1}{\mathrm{i}}\frac{\mathrm{d}}{\mathrm{d}t}Q(\boldsymbol{k},\boldsymbol{p},t)=[J(\boldsymbol{p}-\boldsymbol{k}/2)-J(\boldsymbol{p}+\boldsymbol{k}/2)]Q(\boldsymbol{k},\boldsymbol{p},t)-\sum_{p'}\Sigma(\boldsymbol{k};\boldsymbol{p},\boldsymbol{p}')Q(\boldsymbol{k},\boldsymbol{p}',t)$$
$$-(\sqrt{N}/\hbar V)[B_{p+k/2}(t)\boldsymbol{\mu}\cdot\boldsymbol{E}^{\perp}(-\boldsymbol{p}+\boldsymbol{k}/2,t)-B^{*}_{p-k/2}(t)\boldsymbol{\mu}\cdot\boldsymbol{E}^{\perp}(\boldsymbol{p}+\boldsymbol{k}/2,t)]\,. \tag{3.25}$$

The first r.h.s. term describes the free-exciton motion and the last term represents a source for two-particle coherences created by electric fields in a sample in which a polarization already exists. The second r.h.s. term in eq. (3.25) is due to the phonon bath, where the complex self-energy matrix has the form

$$\Sigma(\boldsymbol{k};\boldsymbol{p},\boldsymbol{p}')=[\Sigma(\boldsymbol{p}+\boldsymbol{k}/2)-\Sigma^{*}(\boldsymbol{p}-\boldsymbol{k}/2)]\delta_{pp'}$$
$$+\tilde{\Sigma}(\boldsymbol{p}+\boldsymbol{k}/2,\boldsymbol{p}-\boldsymbol{k}/2,\boldsymbol{p}'-\boldsymbol{p})-\tilde{\Sigma}^{*}(\boldsymbol{p}-\boldsymbol{k}/2,\boldsymbol{p}+\boldsymbol{k}/2,\boldsymbol{p}'-\boldsymbol{p})\,. \tag{3.26}$$

Here, $\Sigma(\boldsymbol{k})$ has been defined in eq. (3.3) and $\tilde{\Sigma}(\boldsymbol{k}_1,\boldsymbol{k}_2,\boldsymbol{k}_3)$ is given in eq. (A.13). Note that $\Sigma(\boldsymbol{k};\boldsymbol{p},\boldsymbol{p}')$ consists of the independent sum of the self-energies of the excitons $\hat{B}^{\dagger}_{p-k/2}$ and $\hat{B}_{p+k/2}$ that make up the coherence $Q(\boldsymbol{k},\boldsymbol{p},t)$ (T_1-processes) [22, 75] and additional contributions ($\tilde{\Sigma}$) due to the correlated dynamics of these excitons (T_2^{*}- or pure dephasing processes [22, 75]). Due to the pure dephasing contributions, the single-particle factorization in section 3.2 breaks down; this will be seen explicitly in the result eq. (3.33). It is important to observe that the phonon bath only induces coupling (scattering) between coherences with different $\boldsymbol{p}$ values. The variable $\boldsymbol{k}$ is conserved in eq. (3.25), which is a consequence of the system's translational symmetry and the thermal average performed over the phonon bath in appendix A. We also note from eq. (3.26) that for $\boldsymbol{k}=\boldsymbol{0}$ the self-energy is purely imaginary. The physical explanation for this is that a diagonal density matrix element has no frequency associated with it, and hence no frequency shifts either. Equations (3.23)–(3.25) form a closed set and govern our two-particle description of excited state dynamics.

To study frequency-domain response, we apply temporal Fourier transforms and introduce the variable $\hat{P}$ defined in eq. (3.7) to obtain

$$\{-[\omega+\mathrm{i}\Gamma(\boldsymbol{k})]^2+\Omega_k^2\}P(\boldsymbol{k},\omega)=2\Omega\rho\hbar^{-1}\boldsymbol{\mu}\cdot\boldsymbol{E}^{\perp}(\boldsymbol{k},\omega)$$
$$+\frac{2\Omega}{2\pi}\int\mathrm{d}\omega'\sum_{k'}[J(\boldsymbol{k}')P(\boldsymbol{k}',\omega')-\rho\hbar^{-1}\boldsymbol{\mu}\cdot\boldsymbol{E}^{\perp}(\boldsymbol{k}',\omega')]\frac{2}{N}\sum_{p}Q(\boldsymbol{k}-\boldsymbol{k}',\boldsymbol{p},\omega-\omega')\,, \tag{3.27a}$$

and, using eqs. (3.9),

$$-\omega Q(\boldsymbol{k},\boldsymbol{p},\omega)=[J(\boldsymbol{p}-\boldsymbol{k}/2)-J(\boldsymbol{p}+\boldsymbol{k}/2)]Q(\boldsymbol{k},\boldsymbol{p},\omega)-\sum_{p'}\Sigma(\boldsymbol{k};\boldsymbol{p},\boldsymbol{p}')Q(\boldsymbol{k},\boldsymbol{p}',\omega)$$
$$-\frac{(2\hbar\Omega)^{-1}}{2\pi V}\int\mathrm{d}\omega'\{[\Omega+\omega'+\mathrm{i}\Gamma(\boldsymbol{p}+\boldsymbol{k}/2)]P(\boldsymbol{p}+\boldsymbol{k}/2,\omega')\boldsymbol{\mu}\cdot\boldsymbol{E}^{\perp}(-\boldsymbol{p}+\boldsymbol{k}/2,\omega-\omega')$$
$$-[\Omega-\omega'-\mathrm{i}\Gamma(-\boldsymbol{p}+\boldsymbol{k}/2)]P(-\boldsymbol{p}+\boldsymbol{k}/2,\omega')\boldsymbol{\mu}\cdot\boldsymbol{E}^{\perp}(\boldsymbol{p}+\boldsymbol{k}/2,\omega-\omega')\}\,. \tag{3.27b}$$

These equations have to be iterated in order to obtain the third-order susceptibility.

Instead of treating the general case, however, we will direct our attention to the degenerate four-wave mixing (D4WM) experiment [28–35]. In this experiment, two fundamental fields exist, $(\boldsymbol{k}_1, \omega_1)$ and $(\boldsymbol{k}_2, \omega_2)$ and the nonlinear signal at $\boldsymbol{k}_s = 2\boldsymbol{k}_1 - \boldsymbol{k}_2$, $\omega_s = 2\omega_1 - \omega_2$ is observed while the frequency difference $\omega_1 - \omega_2$ is tuned through zero. We will assume that ω_1, ω_2, and $2\omega_1 - \omega_2$ are all far from the material resonance and we solely concentrate on contributions to the third-order polarization that have possible resonances at $\omega_1 - \omega_2$. Furthermore, we restrict our study to the Haken–Strobl model for the phonon-induced self-energies [54, 88]. Within this simple model, the basic equations are

$$[\mathrm{d}\langle \hat{B}_m(t)\rangle / \mathrm{d}t]_{\mathrm{ph}} = -\tfrac{1}{2}(\hat{\Gamma} + \gamma)\langle \hat{B}_m(t)\rangle \,, \tag{3.28a}$$

$$[\mathrm{d}\langle \hat{B}^{\dagger}_m(t)\hat{B}_n(t)\rangle / \mathrm{d}t]_{\mathrm{ph}} = -[\hat{\Gamma}(1 - \delta_{nm}) + \gamma]\langle \hat{B}^{\dagger}_m(t)\hat{B}_n(t)\rangle \,, \tag{3.28b}$$

where $[\cdots]_{\mathrm{ph}}$ denotes the phonon contribution. These equations imply for the self-energies

$$\Sigma(\boldsymbol{k}) \equiv -\mathrm{i}\Gamma(\boldsymbol{k}) = -\mathrm{i}(\hat{\Gamma} + \gamma)/2 \,, \qquad \Sigma(\boldsymbol{k};\, \boldsymbol{p},\, \boldsymbol{p}') = -\mathrm{i}(\hat{\Gamma} + \gamma)\delta_{\boldsymbol{p}\boldsymbol{p}'} + \mathrm{i}\hat{\Gamma}/N \,. \tag{3.28c, d}$$

The parameters $\hat{\Gamma}$ and γ are usually taken real, so that only imaginary self-energy contributions are included. $\hat{\Gamma}$ is the pure dephasing rate and γ represents the population relaxation rate. The main motivation to use this model is that it allows for analytical results, while still preserving the essential physical aspects related to pure dephasing. Previous studies of D4WM (using response theory [36]) and of transient gratings [40, 55] in crystals have also used the Haken–Strobl model.

Given our microscopic expressions for the self-energies derived in appendix A, we can in principle improve the theory. Yet alternative (Markovian and non-Markovian) exciton self-energy models have been proposed within the theory of optical absorption in molecular crystals [89–91]. However, both the evaluation of more realistic self-energies and the subsequent solution of the equations of motion will involve extensive numerical calculations. Other, probably more practical improvements over the Haken-Strobl model lie in the connection between the equation of motion (3.25) and the Boltzmann equation (section 3.5). This connection enables us to utilize the well-developed methods for solving the Boltzmann equation within transport theory.

We now calculate the third-order susceptibility for the D4WM setup. Define $\boldsymbol{k}_{\mathrm{g}} \equiv \boldsymbol{k}_1 - \boldsymbol{k}_2$, $\boldsymbol{p}_{\mathrm{g}} \equiv (\boldsymbol{k}_1 + \boldsymbol{k}_2)/2$ (g stands for "grating") and let $Q_{\mathrm{g}}(\boldsymbol{p})$ denote the component at wave vector $\boldsymbol{k}_{\mathrm{g}}$ and frequency $\omega_1 - \omega_2$ in the *discrete* Fourier decomposition of the two-particle coherences. From eq. (3.27a) we then obtain for the third-order polarization at the signal wave vector and frequency and with a possible resonance at $\omega_1 - \omega_2$,

$$P_s^{(3)} = \frac{4\Omega\rho^{-1}}{\Delta(\boldsymbol{k}_s, \omega_s)} [J(\boldsymbol{k}_1)P_1^{(1)} - \rho\hbar^{-1}\boldsymbol{\mu}\cdot\boldsymbol{E}_1^{\perp}] \sum_{\boldsymbol{p}} Q_{\mathrm{g}}^{(2)}(\boldsymbol{p}) \,. \tag{3.29}$$

$P_1^{(1)}$ has already been solved in section 3.1 and from eq. (3.27b) it follows that the $Q_{\mathrm{g}}^{(2)}(\boldsymbol{p})$ for different $\boldsymbol{p}$ values obey the coupled equations

$$\begin{aligned} -(\omega_1 - \omega_2)Q_{\mathrm{g}}^{(2)}(\boldsymbol{p}) = {} & [J(\boldsymbol{p} - \boldsymbol{k}_{\mathrm{g}}/2) - J(\boldsymbol{p} + \boldsymbol{k}_{\mathrm{g}}/2) + \mathrm{i}(\hat{\Gamma} + \gamma)]Q_{\mathrm{g}}^{(2)}(\boldsymbol{p}) \\ & - \mathrm{i}\frac{\hat{\Gamma}}{N}\sum_{\boldsymbol{p}'} Q_{\mathrm{g}}^{(2)}(\boldsymbol{p}') + \sigma_{\mathrm{R}}\delta_{\boldsymbol{p}\boldsymbol{p}_{\mathrm{g}}} + \sigma_{\mathrm{A}}\delta_{\boldsymbol{p},-\boldsymbol{p}_{\mathrm{g}}} \,. \end{aligned} \tag{3.30}$$

Here, $\sigma_R \delta_{pp_g}$ and $\sigma_A \delta_{p,-p_g}$ are "source terms" that originate from the last r.h.s. term of eq. (3.27b). Using eq. (3.12b) for the first-order polarizations, we find

$$\sigma_R = -\rho\hbar^{-2}\left(\frac{\Omega+\omega_1+i(\hat{\Gamma}+\gamma)/2}{\Delta(k_1,\omega_1)} - \frac{\Omega+\omega_2-i(\hat{\Gamma}+\gamma)/2}{\Delta(-k_2,-\omega_2)}\right)\boldsymbol{\mu}\cdot\boldsymbol{E}_1^{\perp}\boldsymbol{\mu}\cdot\boldsymbol{E}_2^{\perp *}$$

$$\approx \rho\hbar^{-2}\{[\omega_1-\Omega_{k_1}+i(\hat{\Gamma}+\gamma)/2]^{-1}-[\omega_2-\Omega_{k_2}-i(\hat{\Gamma}+\gamma)/2]^{-1}\}\boldsymbol{\mu}\cdot\boldsymbol{E}_1^{\perp}\boldsymbol{\mu}\cdot\boldsymbol{E}_2^{\perp *}, \tag{3.31a}$$

$$\sigma_A = \rho\hbar^{-2}\left(\frac{\Omega-\omega_1-i(\hat{\Gamma}+\gamma)/2}{\Delta(k_1,\omega_1)} - \frac{\Omega-\omega_2+i(\hat{\Gamma}+\gamma)/2}{\Delta(-k_2,-\omega_2)}\right)\boldsymbol{\mu}\cdot\boldsymbol{E}_1^{\perp}\boldsymbol{\mu}\cdot\boldsymbol{E}_2^{\perp *}$$

$$\approx \rho\hbar^{-2}\{[\omega_1+\Omega_{k_1}+i(\hat{\Gamma}+\gamma)/2]^{-1}-[\omega_2+\Omega_{k_2}-i(\hat{\Gamma}+\gamma)/2]^{-1}\}\boldsymbol{\mu}\cdot\boldsymbol{E}_1^{\perp}\boldsymbol{\mu}\cdot\boldsymbol{E}_2^{\perp *}, \tag{3.31b}$$

where the approximations hold if $|J(k_1)|, |J(k_2)| \ll \Omega$. Obviously, $\sigma_R\delta_{pp_g}$ and $\sigma_A\delta_{p,-p_g}$ are the rotating and anti-rotating sources for the two-particle coherences, respectively, and they transform into each other if (k_1, ω_1) and $(-k_2, -\omega_2)$ are interchanged. In section 3.2 the same interchange of rotating and anti-rotating terms under permutation of the fundamental fields was observed (eq. 3.15).

Equation (3.30) is solved in appendix B and yields

$$\sum_p Q_g^{(2)}(p) = \left(\frac{i\sigma_R}{-i\omega_{12}-i[J(k_2)-J(k_1)]+(\hat{\Gamma}+\gamma)} + \frac{i\sigma_A}{-i\omega_{12}-i[J(k_1)-J(k_2)]+(\hat{\Gamma}+\gamma)}\right)$$
$$\times\left(1-\frac{\hat{\Gamma}}{N}\sum_p[-i\omega_{12}-iJ(p-k_g/2)+iJ(p+k_g/2)+\hat{\Gamma}+\gamma]^{-1}\right)^{-1}, \tag{3.32}$$

where $\omega_{12} \equiv \omega_1 - \omega_2$. Combining eqs. (3.29), (3.12b), (3.31), and (3.32), the third-order susceptibility is easily found. To simplify the result, we apply the RWA with respect to the fundamental fields ($\sigma_A \approx 0$) as well as the signal field. Furthermore, we use $|\omega_1 - \Omega_{k_1}| \gg |J(k_1)|$ (ω_1 is off-resonance), so that $J(k_1)P_1^{(1)}$ in eq. (3.29) is negligible relative to $\rho\hbar^{-1}\boldsymbol{\mu}\cdot\boldsymbol{E}_1^{\perp}$. Finally, we use the approximate identity

$$\frac{\omega_{12}+\Omega_{k_2}-\Omega_{k_1}+i(\hat{\Gamma}+\gamma)}{\omega_{12}+J(k_2)-J(k_1)+i(\hat{\Gamma}+\gamma)} \approx 1.$$

This relation becomes an exact identity within the Heitler–London approximation (HLA) $\Omega_k = \Omega + J(k)$. Here, we do not obtain an exact identity, because the HLA has not been invoked in eq. (3.29) for the polarization, whereas it *is* used in the equation for the two-particle variables. We finally obtain

$$\overleftrightarrow{\chi}^{(3)}(-k_s,-\omega_s;k_1\omega_1,-k_2-\omega_2,k_1\omega_1)$$
$$= 2\rho(\boldsymbol{\mu}\boldsymbol{\mu}\boldsymbol{\mu}\boldsymbol{\mu}/\hbar^3)[\omega_s-\Omega_{k_s}+i(\hat{\Gamma}+\gamma)/2]^{-1}[\omega_1-\Omega_{k_1}+i(\hat{\Gamma}+\gamma)/2]^{-1}[\omega_2-\Omega_{k_2}-i(\hat{\Gamma}+\gamma)/2]^{-1}$$
$$\times\left(1-\frac{\hat{\Gamma}}{N}\sum_p[-i\omega_{12}-iJ(p-k_g/2)+iJ(p+k_g/2)+\hat{\Gamma}+\gamma]^{-1}\right)^{-1}. \tag{3.33}$$

We immediately observe that this result is the product of the rotating part of eq. (3.15), which was

obtained in the single-particle factorization, and a dephasing-induced factor which is unity if $\hat{\Gamma} = 0$. In other words, in the presence of pure dephasing, the single-particle description breaks down.

Loring and Mukamel [36] were the first to calculate the D4WM susceptibility for a molecular crystal, within the Haken–Strobl model for dephasing and using Liouville-space Green-function techniques. Specific application was made for a one-dimensional system with nearest-neighbor interactions, for which the sum over the momenta $\boldsymbol{p}$ in eq. (3.33) can be evaluated. Their analysis of the D4WM signal for various limiting cases is also possible from our general expression (3.33). The signal intensity $S(\boldsymbol{k}_s, \omega_s)$ is, within the slowly varying amplitude approximation, proportional to $|\overleftrightarrow{\chi}^{(3)}(-\boldsymbol{k}_s - \omega_s; \boldsymbol{k}_1\omega_1, -\boldsymbol{k}_2 - \omega_2, \boldsymbol{k}_1\omega_1)|^2$. Any frequency dependences deriving from the first three denominators in eq. (3.33) may be neglected, as we assumed that ω_1, ω_2 and ω_s are off-resonance. The only frequency dependence in $S(\boldsymbol{k}_s, \omega_s)$ then emerges from the last factor in eq. (3.33).

Three limiting cases are now of special interest [36]. First, we consider non-interacting molecules $[J(\boldsymbol{k}) = 0]$ and find

$$S(\boldsymbol{k}_s, \omega_s) \propto 1 + \hat{\Gamma}(\hat{\Gamma} + 2\gamma)/(\omega_{12}^2 + \gamma^2)\,. \tag{3.34}$$

This signal has a Lorentzian resonance at $\omega_{12} = 0$, whose width is the inverse of the excited-state lifetime. The resonance vanishes in the absence of dephasing. These dephasing-induced resonances have been observed by Bloembergen et al. [31] in the gas phase and have been denoted PIER4 (pressure-induced extra resonances in four-wave mixing). In fig. 2 we show the variation of such a

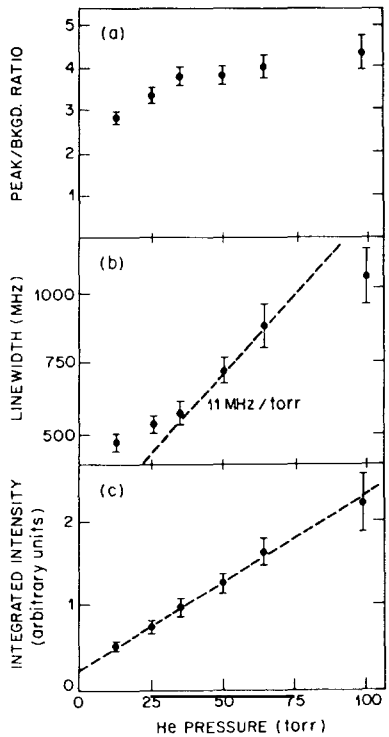

Fig. 2. PIER4 signal characteristics in Na as a function of buffer gas pressure [31b]. (a) Ratio of peak height to nonresonant signal; (b) resonance full width; (c) integrated intensity of resonant signal.

resonance in Na induced by the buffer gas He. (The dephasing rate $\hat{\Gamma}$ is in this case proportional to the He gas pressure.) In molecular crystals similar resonances have been observed by Hochstrasser et al. [32] and have been denoted DICE (dephasing-induced coherent emission). An example is displayed in fig. 3a and 3b. This resonance is similar to the one discussed here, except that it occurs at ω_{12} equal to some vibrational frequency rather than $\omega_{12} = 0$. This is a Raman transition which is totally analogous to the D4WM resonance. In Hochstrasser's experiment, $\omega_{12} = -747\,\mathrm{cm}^{-1}$ represents a vibrational mode and in Bloembergen's case $\omega_{12} = 17\,\mathrm{cm}^{-1}$ is the splitting of the Na D lines. The unique and surprising aspect of these resonances is that usually dephasing results in loss of coherence and line broadening, whereas here, it induces new sharp resonances as ω_{12} is varied. The reason is a delicate interference of various terms contributing to $\chi^{(3)}$ which exactly cancel in the absence of dephasing. The addition of dephasing eliminates this cancellation and results in the new resonance [34, 23].

As a second special case, we consider molecules with arbitrary interactions in the absence of dephasing. For $\hat{\Gamma} = 0$, the Haken–Strobl model describes coherent exciton motion on the lattice, and from eq. (3.33) it is clear that the D4WM signal exhibits no resonance as a function of ω_{12} in this limit.

We finally discuss the case of finite interactions in the strong dephasing (incoherent or diffusive) limit, defined by $\hat{\Gamma} \gg |J(\boldsymbol{p} - \boldsymbol{k}_g/2) - J(\boldsymbol{p} + \boldsymbol{k}_g/2)|$ (for all $\boldsymbol{p}$) and $\hat{\Gamma} \gg \gamma$. In this limit, the Haken–Strobl

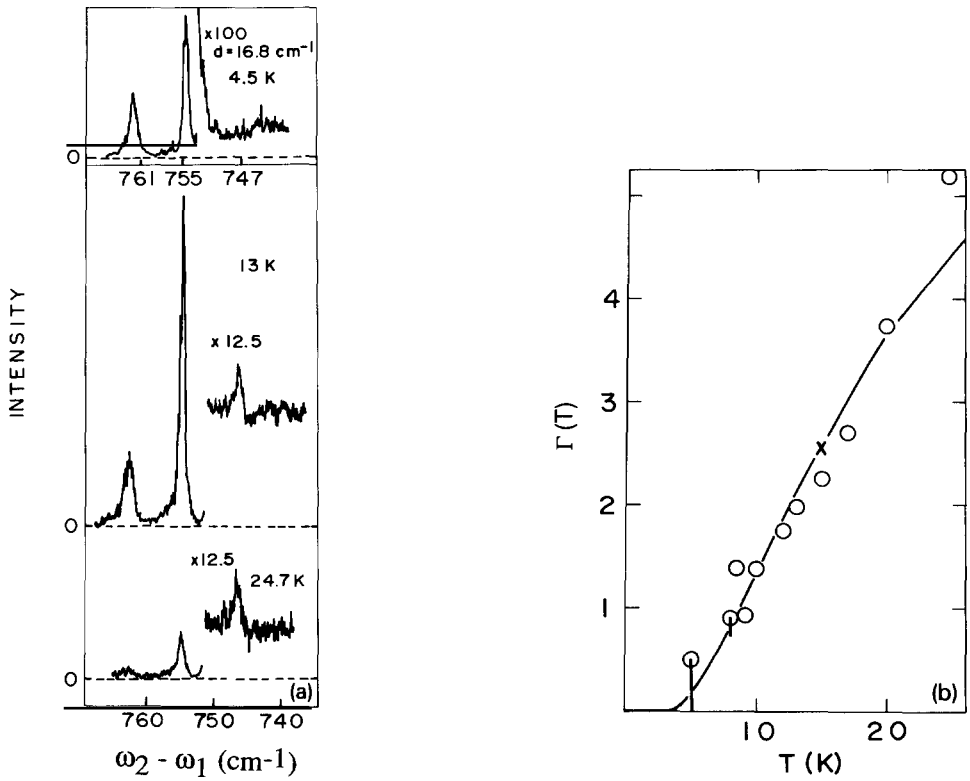

Fig. 3(a). Stationary four-wave mixing (coherent Raman) spectrum of a doped crystal (pentacene in benzoic acid) as a function of temperature [32b]. The portion of the spectrum near $\omega_{21} = 747\,\mathrm{cm}^{-1}$ is shown on an expanded vertical scale. Note that the dephasing-induced band at $\omega_{21} = 747\,\mathrm{cm}^{-1}$ grows relative to the peak at $\omega_{21} = 755\,\mathrm{cm}^{-1}$ with increasing temperature. (b) Growth of the pure dephasing rate $\Gamma(T)$ as a function of temperature [32b], as derived from experimental measurements of the intensity of the dephasing-induced band at $\omega_{21} = 747\,\mathrm{cm}^{-1}$. The solid line is a fit to an Arrhenius form.

model describes diffusive exciton motion. In appendix C it is shown that for arbitrary interactions and dimensionality we now have

$$S(\boldsymbol{k}_s, \omega_s) \propto 1 + \frac{\hat{\Gamma}(\hat{\Gamma} + 2\gamma)}{\omega_{12}^2 + [\gamma + (\boldsymbol{k}_1 - \boldsymbol{k}_2)^2 D_e]^2}, \tag{3.35}$$

with the exciton diffusion constant (tensor) defined by

$$D_e \equiv \frac{1}{|\boldsymbol{k}_g|^2} \frac{1}{\hat{\Gamma} N} \sum_{\boldsymbol{p}} [J(\boldsymbol{p} - \boldsymbol{k}_g/2) - J(\boldsymbol{p} + \boldsymbol{k}_g/2)]^2 = \frac{4}{|\boldsymbol{k}_1 - \boldsymbol{k}_2|^2} \frac{1}{\hat{\Gamma}} \sum_m J^2(\boldsymbol{r}_m) \sin^2[\tfrac{1}{2}(\boldsymbol{k}_1 - \boldsymbol{k}_2) \cdot \boldsymbol{r}_m]. \tag{3.36}$$

In the last step of eq. (3.36) we have used eq. (3.2). In the incoherent limit, the D4WM signal shows a Lorentzian resonance with a width that is the sum of the inverse excited-state lifetime (γ) and a contribution from exciton motion ($D_e k_g^2$). The same result has been obtained for a disordered medium [82]. In general, D_e is a tensor depending on the magnitude and the direction of $\boldsymbol{k}_g$; if, however, the range of interactions is small compared to the characteristic length scale $|\boldsymbol{k}_g|^{-1}$ of the experiment, eq. (3.36) reduces for an isotropic d-dimensional system to

$$D_e = \frac{1}{d\hat{\Gamma}} \sum_m J^2(r_m) r_m^2. \tag{3.37}$$

Alternatively, eq. (3.36) may be written as

$$D_e \approx \frac{1}{|\boldsymbol{k}_g|^2} \frac{1}{\hat{\Gamma} N} \sum_{\boldsymbol{p}} [\boldsymbol{k}_g \cdot \boldsymbol{v}_e(\boldsymbol{p})]^2, \tag{3.38a}$$

with $\boldsymbol{v}_e(\boldsymbol{p}) \equiv \nabla_{\boldsymbol{p}} J(\boldsymbol{p})$, the exciton group velocity at wave vector $\boldsymbol{p}$. For an isotropic d-dimensional system, this yields

$$D_e = \frac{1}{d\hat{\Gamma}} \frac{1}{N} \sum_{\boldsymbol{p}} v_e^2(\boldsymbol{p}) \equiv \frac{1}{d\hat{\Gamma}} \bar{v}_e^2, \tag{3.38b}$$

with $\bar{v}_e$ an effective exciton group velocity.

3.4. *Time-domain four-wave mixing: transient grating and exciton dynamics*

We now turn to the study of transient grating (TG) experiments within the exciton theory. The following typical setup is considered (fig. 1). At time $t = 0$, two short excitation pulses, $(\boldsymbol{k}_1, \omega_1)$ and $(\boldsymbol{k}_2, \omega_2)$, crossed under an angle Θ interfere in the sample and create an excitonic grating. The decay of the grating as a result of dephasing and population relaxation is monitored by applying a probe pulse, $(\boldsymbol{k}_3, \omega_3)$, at $t = \tau$. The observable is the time-integrated intensity of the nonlinear ("diffracted") signal with wave vector $\boldsymbol{k}_s = \boldsymbol{k}_1 - \boldsymbol{k}_2 + \boldsymbol{k}_3$ and frequency $\omega_s = \omega_1 - \omega_2 + \omega_3$ as a function of the pump-probe delay τ. The electric fields now take the form of eq. (3.10), except that $\boldsymbol{E}_j^{\perp}$ $(j = 1, 2, 3)$ is replaced by the pulse envelope $\boldsymbol{E}_j^{\perp}(t)$. For simplicity, we will consider square pulses with polarization parallel to the molecular transition dipoles, with amplitudes E_j, and with duration τ_j. All pulses are long compared to an optical cycle ($\omega_j \tau_j \gg 1$), but short (delta pulses) on the dynamical time scales in the sample.

To describe this experiment microscopically, we use our equations of motion in the two-particle factorization [eqs. (3.23)–(3.25)]. Working with the polarization as variable, eq. (3.23) takes the same form as eq. (3.16a), but now with

$$\mathcal{M}(\boldsymbol{k}, t) = 2\Omega \sum_{\boldsymbol{k}'} [J(\boldsymbol{k}')P(\boldsymbol{k}', t) - \rho\hbar^{-1}\boldsymbol{\mu} \cdot \boldsymbol{E}^{\perp}(\boldsymbol{k}', t)]W(\boldsymbol{k} - \boldsymbol{k}', t) . \tag{3.39}$$

To lowest (third) order in the pulse amplitudes, the observed polarization $P(\boldsymbol{k}_s, t)$ is sourced by $\mathcal{M}^{(3)}(\boldsymbol{k}_s, t)$ in eq. (3.16a), and the only important contribution to $\mathcal{M}^{(3)}(\boldsymbol{k}_s, t)$ in eq. (3.39) arises from the term $\boldsymbol{k}' = \boldsymbol{k}_3$. (In principle, third-order contributions are also obtained from $\boldsymbol{k}' = \boldsymbol{k}_1$ or $\boldsymbol{k}' = -\boldsymbol{k}_2$, but these are very small due to negligible temporal overlap of pump and probe pulses.) We assume an off-resonance probe pulse ($|\omega_3 - \Omega|\tau_3 \gg 1$), so that the polarization envelope associated with it instantaneously follows the electric field [92],

$$\boldsymbol{P}_3^{(1)}(t) = \overleftrightarrow{\chi}^{(1)}(\boldsymbol{k}_3, \omega_3) \cdot \boldsymbol{E}_3^{\perp}(t) . \tag{3.40a}$$

The envelope of the nonlinear source term then obeys

$$\mathcal{M}_s^{(3)}(t) \propto \boldsymbol{E}_3^{\perp}(t) W^{(2)}(\boldsymbol{k}_1 - \boldsymbol{k}_2, t) . \tag{3.40b}$$

Within the slowly varying envelope approximation [22], the observable now reads

$$S(\tau) \propto \int_{\tau}^{\infty} \mathrm{d}t \, |P_s^{(3)}(t)|^2 \propto |\vartheta_3|^2 |W^{(2)}(\boldsymbol{k}_1 - \boldsymbol{k}_2, \tau)|^2 , \tag{3.41a}$$

with ϑ_3 the probe pulse area defined by

$$\vartheta_3 \equiv \mu E_3 \tau_3 / \hbar . \tag{3.41b}$$

In eq. (3.41a) we used the fact that $\boldsymbol{E}_3^{\perp}(t)$ is a delta function on the dynamical time scale, so that $W(\boldsymbol{k}_1 - \boldsymbol{k}_2, t)$ does not vary appreciably during the pulse. According to eq. (3.41), the TG is determined by the Fourier component of the exciton population at the grating wave vector $\boldsymbol{k}_g \equiv \boldsymbol{k}_1 - \boldsymbol{k}_2$ and at time $t = \tau$. This result agrees with the usual diffraction picture [1, 2a, 55, 93] and was first derived microscopically by Loring and Mukamel [56], using response theory. These authors also pointed out limitations of the diffraction picture by showing that in general the temporal profile of the signal does not follow that of the probe pulse.

The evolution of the population can be found from eqs. (3.24) and (3.25). During the pump-probe delay, the last term in eq. (3.25), containing the electric field amplitudes, is, of course, absent. As in the previous section, we restrict ourselves to the Haken–Strobl model for the phonon-induced self-energies. If we define the Laplace transform of a time-dependent function $f(t)$ by

$$f(s) = \int_0^{\infty} \mathrm{d}t \, f(t) \exp(-st) , \tag{3.42}$$

then eq. (3.25) translates into

$$sQ^{(2)}(\boldsymbol{k}_g, \boldsymbol{p}, s) = [iJ(\boldsymbol{p} - \boldsymbol{k}_g/2) - iJ(\boldsymbol{p} + \boldsymbol{k}_g/2) - (\hat{\Gamma} + \gamma)]Q^{(2)}(\boldsymbol{k}_g, \boldsymbol{p}, s)$$

$$+ \frac{\hat{\Gamma}}{N} \sum_{\boldsymbol{p}'} Q^{(2)}(\boldsymbol{k}_g, \boldsymbol{p}', s) + Q^{(2)}(\boldsymbol{k}_g, \boldsymbol{p}, t = 0) . \tag{3.43}$$

This equation has the same form as eq. (3.30) governing the D4WM experiment, except that $-i\omega$ is replaced by s and the source term is now determined by the grating's initial condition $Q^{(2)}(\boldsymbol{k}_g, \boldsymbol{p}, t = 0)$ right after the pump pulses.

Before solving eq. (3.43), we first determine these initial conditions. As the pump pulses are short on the dynamical time scale, the phonon bath has no time to establish correlations between the ket and bra sides of the exciton density matrix (the crystal state is still a pure state), so that immediately following the pump pulses we may use the factorization

$$Q^{(2)}(\boldsymbol{k}_g, \boldsymbol{p}, t = 0) = \langle \hat{B}^{\dagger}_{\boldsymbol{p} - \boldsymbol{k}_g/2}(0) \rangle^{(1)} \langle \hat{B}_{\boldsymbol{p} + \boldsymbol{k}_g/2}(0) \rangle^{(1)} . \tag{3.44a}$$

The first-order exciton amplitudes can be obtained by integrating the linear part of eq. (3.23) during the pump pulses. In the RWA, assuming $|\omega_j - \Omega|\tau_j \ll 1$ ($j = 1, 2$), and neglecting intermolecular interactions during the pulses, we find [56]

$$\langle \hat{B}_{\boldsymbol{k}}(0) \rangle^{(1)} = i\sqrt{\rho V}(\vartheta_1 \delta_{\boldsymbol{k}\boldsymbol{k}_1} + \vartheta_2 \delta_{\boldsymbol{k}\boldsymbol{k}_2}) , \tag{3.44b}$$

and $\langle B^{\dagger}_{\boldsymbol{k}}(0) \rangle^{(1)} = [\langle \hat{B}_{\boldsymbol{k}}(0) \rangle^{(1)}]^*$. Here the ϑ_j ($j = 1, 2$) denote the pump pulse areas defined in analogy with eq. (3.41b). Thus

$$Q^{(2)}(\boldsymbol{k}_g, \boldsymbol{p}, t = 0) = \rho V \vartheta_1 \vartheta_2^* \delta_{\boldsymbol{p}\boldsymbol{p}_g} , \tag{3.44c}$$

with $\boldsymbol{p}_g \equiv (\boldsymbol{k}_1 + \boldsymbol{k}_2)/2$, as before. As most theories for the TG signal work within the site representation, it is useful to mention that, using eq. (2.15), the present initial condition (a coherence of excitons at wave vectors $\boldsymbol{k}_1$ and $\boldsymbol{k}_2$) translates into

$$\langle \hat{B}^{\dagger}_m(0) \hat{B}_n(0) \rangle = |\vartheta|^2 \cos(\boldsymbol{k}_g \cdot \boldsymbol{r}_m/2) \cos(\boldsymbol{k}_g \cdot \boldsymbol{r}_n/2) . \tag{3.45a}$$

Here we made the common assumptions that $\vartheta_1 = \vartheta_2 = \vartheta$ and that the system is quasi one-dimensional with $\boldsymbol{k}_1 + \boldsymbol{k}_2$ perpendicular to the lattice vector [55, 56]. Equation (3.45a) is known as the *coherent* initial condition, which contains site populations ($m = n$) as well as intersite coherences ($m \neq n$). It is expected to be most relevant in the case of resonant pumping. Wong and Kenkre [93] have also introduced the *diagonal* initial condition

$$\langle \hat{B}^{\dagger}_m(0) \hat{B}_n(0) \rangle = |\vartheta|^2 \cos^2(\boldsymbol{k}_g \cdot \boldsymbol{r}_m/2) \delta_{mn} , \tag{3.45b}$$

which only contains populations. This condition is important in the case of off-resonance excitation followed by ultrafast vibrational relaxation [4].

We will restrict our treatment to the case of coherent excitation. Combining eqs. (3.43), (3.44c), (3.24b), and using appendix B, we eventually arrive at the Laplace transform of the population

$$W(\boldsymbol{k}_1 - \boldsymbol{k}_2, s) = 2\vartheta_1 \vartheta_2^* \{s - \mathrm{i}[J(\boldsymbol{k}_2) - J(\boldsymbol{k}_1)] + \hat{\Gamma} + \gamma\}^{-1} \times \left(1 - \frac{\hat{\Gamma}}{N} \sum_{\boldsymbol{p}} [s - \mathrm{i}J(\boldsymbol{p} - \boldsymbol{k}_g/2) + \mathrm{i}J(\boldsymbol{p} + \boldsymbol{k}_g/2) + \hat{\Gamma} + \gamma]^{-1}\right)^{-1} . \tag{3.46a}$$

This can be rewritten as

$$W(\boldsymbol{k}_1 - \boldsymbol{k}_2, s) = 2\vartheta_1 \vartheta_2^* \left(s - \mathrm{i}\mathcal{J}(\boldsymbol{p}_g) + \gamma - \frac{\hat{\Gamma}}{N} \sum_{\boldsymbol{p}} \frac{\mathrm{i}[\mathcal{J}(\boldsymbol{p}) - \mathcal{J}(\boldsymbol{p}_g)]}{s - \mathrm{i}\mathcal{J}(\boldsymbol{p}) + \hat{\Gamma} + \gamma}\right)^{-1} , \tag{3.46b}$$

$$\mathcal{J}(\boldsymbol{p}) \equiv J(\boldsymbol{p} - \boldsymbol{k}_g/2) - J(\boldsymbol{p} + \boldsymbol{k}_g/2) , \tag{3.46c}$$

where the $\boldsymbol{k}_g$-dependence of $\mathcal{J}(\boldsymbol{p})$ is suppressed for compactness.

One interesting exact result follows directly from eq. (3.46): in the absence of exciton dispersion [$J(\boldsymbol{k}) = \text{constant}$], or, in particular, in the absence of interactions, the population $W(\boldsymbol{k}_1 - \boldsymbol{k}_2, t)$ only decays with the trivial rate γ, independently of the scattering strength $\hat{\Gamma}$. The TG signal thus decays with rate 2γ (eq. 3.41a). The physical explanation is that all coherences $Q(\boldsymbol{k}, \boldsymbol{p}, t)$ now have the same frequency (zero), so that they do not dephase with respect to each other and keep adding up coherently to the population (eq. 3.24b) at all times, irrespective of the scattering rates between them. This result is, of course, not restricted to the Haken–Strobl model.

In the case of general interactions, it is hard to transform eq. (3.46b) back to the time domain and we will therefore restrict ourselves from now on to a study of the long-time behavior of the grating signal. Analytical results valid for all times, have been derived by Garrity and Skinner for a one-dimensional system with nearest-neighbor interactions [55]. Their important conclusions concerning the limits of coherent and incoherent motion on the experimental length scale, however, can also be reached from our expression. We first note that the long-time limit, $|\hat{\Gamma} + \gamma - \mathrm{i}\mathcal{J}(p)|t \gg 1$, is governed by the small s region ($|s| \ll |\hat{\Gamma} + \gamma - \mathrm{i}\mathcal{J}(\boldsymbol{p})|$) in the Laplace domain. Equation (3.46b) then yields

$$W(\boldsymbol{k}_1 - \boldsymbol{k}_2, t) = 2\vartheta_1 \vartheta_2^* \exp(\alpha t) , \qquad \alpha = \mathrm{i}\mathcal{J}(\boldsymbol{p}_g) - \gamma + \frac{\hat{\Gamma}}{N} \sum_{\boldsymbol{p}} \frac{\mathrm{i}[\mathcal{J}(\boldsymbol{p}) - \mathcal{J}(\boldsymbol{p}_g)]}{\hat{\Gamma} + \gamma - \mathrm{i}\mathcal{J}(\boldsymbol{p})} . \tag{3.47a, b}$$

In the remainder of this section, we will assume that $\mathcal{J}(\boldsymbol{p}_g) = J(\boldsymbol{k}_2) - J(\boldsymbol{k}_1) = 0$, which holds under very general symmetry conditions with respect to the experimental set-up. We further note that $\mathcal{J}(\boldsymbol{p}) \approx -\boldsymbol{k}_g \cdot \boldsymbol{v}_e(\boldsymbol{p})$, with $\boldsymbol{v}_e(\boldsymbol{p})$ the exciton group velocity defined under eq. (3.38a). Let us first concentrate on the limit of weak scattering: $\mathcal{J}(\boldsymbol{p}) \gg \hat{\Gamma} + \gamma$ for most $\boldsymbol{p}$ in the first Brillouin zone. This is the *coherent* limit, as the exciton scattering length $v_e(\boldsymbol{p})/\hat{\Gamma}$ is now much larger than the experimental length scale $|\boldsymbol{k}_g|^{-1}$. We then obtain

$$\alpha = -\gamma - \hat{\Gamma} , \tag{3.48a}$$

so that, using eq. (3.41a), we find for the intensity of the TG signal normalized to its initial value

$$S(\tau) = \exp[-2(\gamma + \hat{\Gamma})\tau] . \tag{3.48b}$$

This result has also been found by Garrity and Skinner [55]. In the extreme case of $\hat{\Gamma} = 0$, no grating

decay is observed, apart from the trivial population decay $\exp(-2\gamma t)$. This result is rigorous for all times, as is directly seen from eq. (3.46b), and is easily understood: for $\hat{\Gamma} = 0$ the coherent initial condition is an exact eigenstate of the system. By contrast, the diagonal initial condition is a superposition of eigenstates and leads, even in the case $\hat{\Gamma} = 0$, to a nontrivial decay of the grating on a time scale $(k_g v_e)^{-1}$ with v_e a typical exciton group velocity (ballistic motion) [55, 93].

We now turn to the opposite limit of strong scattering, $\hat{\Gamma} \gg \gamma$ *and* $\hat{\Gamma} \gg \mathscr{J}(\boldsymbol{p})$ (all $\boldsymbol{p}$), where the exciton scattering length is much smaller than the grating length scale (*diffusive* or *incoherent* motion). Equation (3.47b) then reduces to

$$\alpha = -\gamma - D_e|\boldsymbol{k}_1 - \boldsymbol{k}_2|^2 , \tag{3.49a}$$

with D_e the exciton diffusion constant as defined in eq. (3.36). In the derivation of eq. (3.49a), we used that $\Sigma_{\boldsymbol{p}} \mathscr{J}(\boldsymbol{p}) = 0$, as is explained in appendix C. We now obtain for the signal intensity [55]

$$S(\tau) = \exp[-2(\gamma + D_e|\boldsymbol{k}_1 - \boldsymbol{k}_2|^2)\tau] . \tag{3.49b}$$

We can get an idea how well this long-time expression describes the actual decay by using in eq. (3.46b)

$$\sum_{\boldsymbol{p}} \frac{\mathrm{i}\mathscr{J}(\boldsymbol{p})}{s - \mathrm{i}\mathscr{J}(\boldsymbol{p}) + \hat{\Gamma} + \gamma} \approx -\frac{1}{(s + \hat{\Gamma} + \gamma)^2} \sum_{\boldsymbol{p}} [\mathscr{J}(\boldsymbol{p})]^2 .$$

(Equation (3.49) agrees with taking $s = 0$ in the r.h.s. of this expression.) The thus obtained approximation to $W(\boldsymbol{k}_1 - \boldsymbol{k}_2, s)$ can be Laplace-inverted analytically and leads to an additive correction in eq. (3.49b). This correction term has a relative magnitude $(D_e \boldsymbol{k}_g^2/\hat{\Gamma})^{1/2}$, which is much smaller than unity, and decays on a time scale $\hat{\Gamma}^{-1}$, which is very fast compared to the decay in eq. (3.49b). This suggests that eq. (3.49b) is a good approximation to the actual signal over the entire observable decay. Furthermore, we note that the present result is not affected by the exact initial condition and is also found for diagonal excitation of the system [55, 93]. The reason is that in the incoherent limit, intersite coherences anyhow relax very fast compared to the grating decay [cf. eq. (3.28b)].

We will now discuss the result eq. (3.49) in more detail. The signal decay rate consists of a trivial contribution due to population relaxation (2γ) and a contribution from the exciton motion, which is proportional to $|\boldsymbol{k}_1 - \boldsymbol{k}_2|^2$. This is characteristic for diffusive motion [1, 2a, 55, 93] and leads, for small cross angles Θ between the two pump pulses (fig. 1), to a linear relation between the observed decay rate and Θ^2. This relation allows us to distinguish experimentally between diffusive and coherent exciton motion on the scale $|\boldsymbol{k}_1 - \boldsymbol{k}_2|^{-1}$. In fig. 4 we display the TG signal showing incoherent (diffusive) motion and its dependence on the fringe spacing through the variation of Θ. In fig. 4a, the TG probes exciton motion in disodium fluorescein in ethanol [8], whereas in fig. 4b it probes carrier motion in a semiconductor (GaAs). In both cases the TG decay becomes slower as Θ is reduced. In fig. 5 we show the Θ^2 variation of the TG decay rate in anthracene at two temperatures (10 K and 20 K) [2b]. Note the diffusive character, even at these low temperatures. In spite of an active search, coherent motion has never been directly observed in transient grating experiments.

In the incoherent limit, an interesting relation exists between the D4WM and TG signals. Namely, the amplitude of the D4WM signal (eq. C.4) can be obtained by evaluating the Fourier transform of the amplitude of the TG signal [$\exp(\alpha\tau)$] at the frequency ω_{12}. This single-Fourier-transform relation

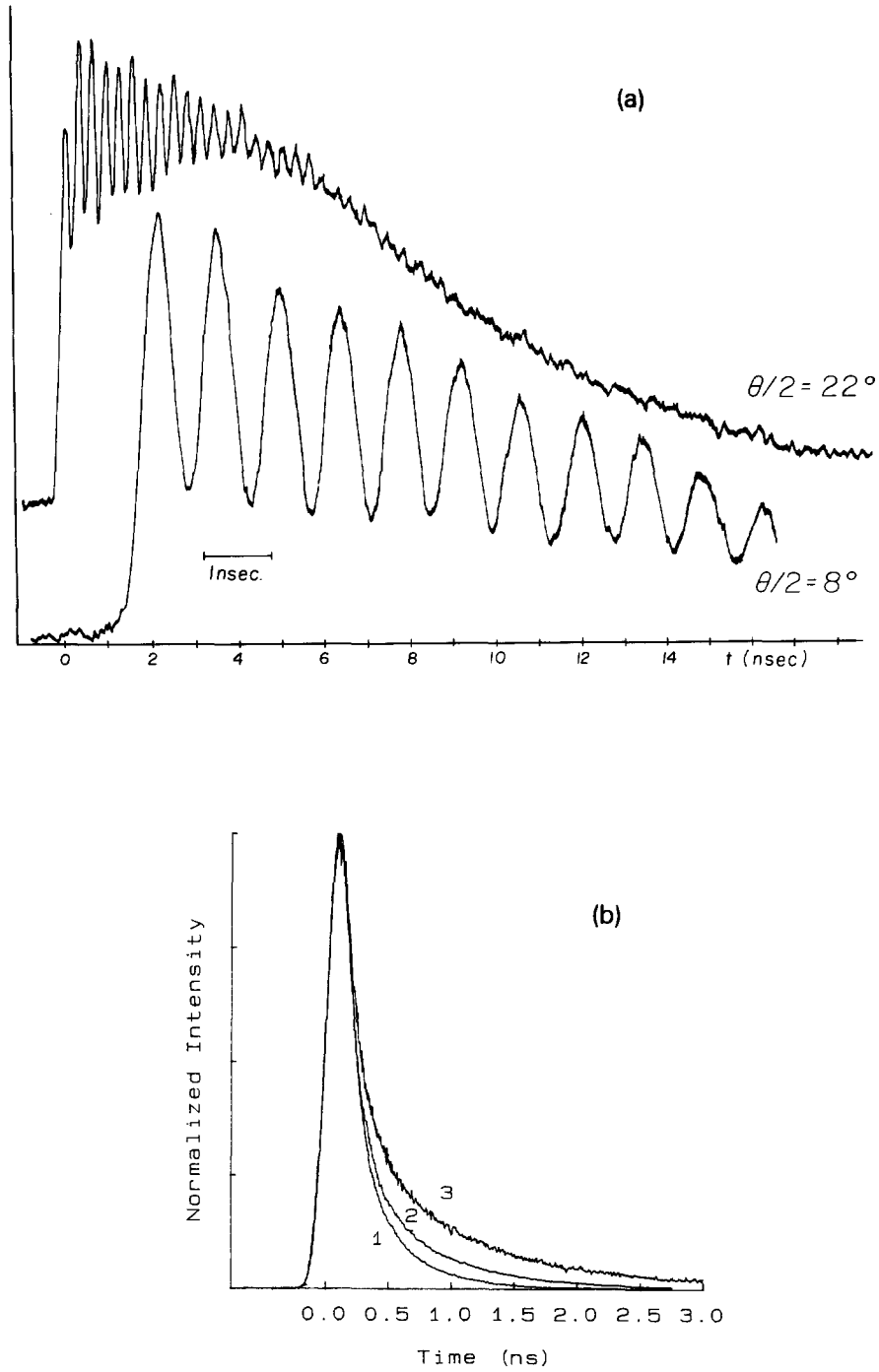

Fig. 4. (a) Fringe spacing dependence of the TG signal probing excited-state energy transport in disodium fluorescein in ethanol, for $\Theta/2 = 8°$ and 22° (excitation wavelength 266 nm) [8]. For the smaller angle, the signal is dominated by acoustic effects (note: time scale is different for $\Theta/2 = 8°$). At $\Theta/2 = 22°$, the acoustic-signal contribution damps out due to acoustic attenuation. (b) Fringe spacing dependence of the TG signal probing carrier density diffusion in GaAs. $N_{eh} = 2 \times 10^{19}$ photocarriers/cm^3. The measured ambipolar diffusion constant is in good agreement with the known value for high purity GaAs ($D_{ex} \cong 8\,\text{cm}^2/\text{sec}$). Curve 1: $\Theta = 4.9°$, curve 2: $\Theta = 3°$, curve 3: $\Theta = 1.1°$ (see ref. [117]).

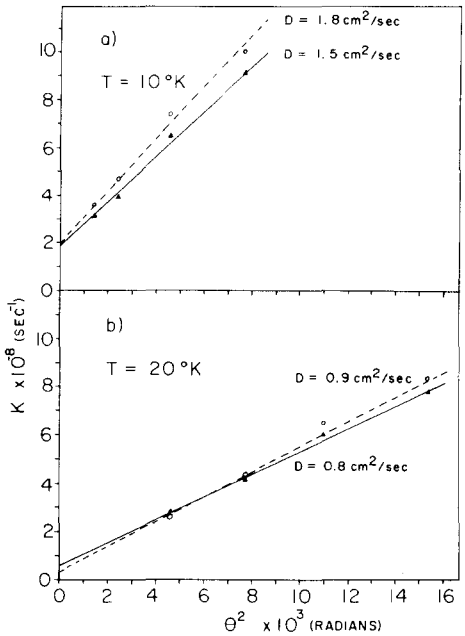

Fig. 5. (a) The decay rate of the transient grating signal versus θ^2 for two anthracene crystals at 10 K, along the a axis [2b]. The magnitude of the slope equals $8\pi^2 D_e/\lambda^2$, with λ the wavelength of the pump pulses, and thus yields directly the exciton diffusion constant D_e. The value of the intercept equals 2γ, where γ is the population relaxation rate. (b) The decay rate of the transient grating signal for the same two crystals at 20 K. The difference in slopes is due to the temperature dependence of the exciton diffusion constant. As the temperature increases, a decrease in the diffusion constant is observed. The average diffusion constant obtained from these measurements is roughly 10 times larger than the expected value for incoherent exciton diffusion [51].

between *nonlinear* frequency-domain and time-resolved techniques is not trivial and was first established by Loring and Mukamel [36]. In concluding this section, we mention that the TG signal for cases intermediate between the coherent and incoherent limits has been studied by Garrity and Skinner (using the Haken–Strobl model) [55] and by Wong and Kenkre (using a generalized master equation approach) [93]. Finally, we remark that we only studied the TG within the two-particle description. The single-particle (local-field) description would lead to the exponential decay eq. (3.48b), independently of the magnitude of $\hat{\Gamma}$. Diffusive exciton transfer cannot be incorporated at this level of description, which is intimately related to the fact that in the single-particle factorization no resonance with respect to ω_{12} is found in the D4WM signal. This illustrates the limitations of the local-field approach.

3.5. *The Boltzmann and the diffusion equations for exciton transport*

Further physical insight into the equation of motion (3.25) for the two-particle coherences $Q(\boldsymbol{k}, \boldsymbol{p}, t)$ can be obtained by making the connection to macroscopic transport equations, such as the Boltzmann equation and the diffusion equation. To this end, we define the Wigner phase-space distribution function $\phi(\boldsymbol{r}, \boldsymbol{p}, t)$ by [94, 95]

$$\phi(\boldsymbol{r}, \boldsymbol{p}, t) \equiv \frac{1}{\sqrt{N}} \sum_{k} Q(\boldsymbol{k}, \boldsymbol{p}, t) \exp(\mathrm{i}\boldsymbol{k} \cdot \boldsymbol{r}) . \tag{3.50}$$

Here, $\boldsymbol{r}$ and $\boldsymbol{p}$ play the role of the classical position and momentum, respectively, of the particle that is described by the Wigner distribution. Comparing with eq. (3.24a), it is clear that $\boldsymbol{r}$ is the position of the exciton "center-of-mass". That $\boldsymbol{p}$ indeed corresponds to the exciton momentum, becomes evident if we consider the pure state for a completely delocalized exciton with momentum $\boldsymbol{p}_0$; then, namely, $Q(\boldsymbol{k}, \boldsymbol{p}, t) = \delta_{\boldsymbol{p}\boldsymbol{p}_0}\delta_{\boldsymbol{k}\boldsymbol{0}}$. The Wigner distribution function carries the full quantum behavior, yet it has a well defined classical analogue: as $\hbar \to 0$ it reduces to the classical density matrix of the particle (exciton in our case), and it is therefore very useful in providing a semiclassical insight in quantum dynamics [94].

In this section we will only be interested in the homogeneous equation of motion for the two-particle variables, i.e., we ignore the last term in eq. (3.25), which couples to the electric field. Also, we will only consider a purely imaginary self-energy matrix $\Sigma(\boldsymbol{k}; \boldsymbol{p}, \boldsymbol{p}') \equiv -\mathrm{i}\Gamma(\boldsymbol{k}; \boldsymbol{p}, \boldsymbol{p}')$. The Wigner distribution then obeys the equation

$$\frac{\mathrm{d}}{\mathrm{d}t}\phi(\boldsymbol{r}, \boldsymbol{p}, t) = 2\sum_{\boldsymbol{a}} J(\boldsymbol{a}) \sin(\boldsymbol{p}\cdot\boldsymbol{a})\phi(\boldsymbol{r} + \boldsymbol{a}/2, \boldsymbol{p}, t) - \sum_{\boldsymbol{a}}\sum_{\boldsymbol{p}'} \tilde{\Gamma}(\boldsymbol{a}; \boldsymbol{p}, \boldsymbol{p}')\phi(\boldsymbol{r} + \boldsymbol{a}/2, \boldsymbol{p}', t)\,, \tag{3.51a}$$

$$\tilde{\Gamma}(\boldsymbol{a}; \boldsymbol{p}, \boldsymbol{p}') \equiv \frac{1}{N}\sum_{\boldsymbol{k}} \Gamma(\boldsymbol{k}; \boldsymbol{p}, \boldsymbol{p}') \exp(-\mathrm{i}\boldsymbol{k}\cdot\boldsymbol{a}/2)\,. \tag{3.51b}$$

The first term in eq. (3.51a) describes coherent exciton motion on the lattice [we used $J(\boldsymbol{r}) = J(-\boldsymbol{r})$]; the second term is due to (phonon) scattering. For scattering kernels that do not depend on $\boldsymbol{k}$, $\Gamma(\boldsymbol{k}; \boldsymbol{p}, \boldsymbol{p}') = g(\boldsymbol{p}, \boldsymbol{p}')$, we have

$$\tilde{\Gamma}(\boldsymbol{a}; \boldsymbol{p}, \boldsymbol{p}') = \delta_{\boldsymbol{a},\boldsymbol{0}} g(\boldsymbol{p}, \boldsymbol{p}')\,. \tag{3.52}$$

This implies that the position is not affected, whereas the momentum is scattered as in a discretized Boltzmann equation with collision kernel $g(\boldsymbol{p}, \boldsymbol{p}')$. An interesting class of collision kernels is found by further restriction to

$$g(\boldsymbol{p}, \boldsymbol{p}') = (\hat{\Gamma} + \gamma)\delta_{\boldsymbol{p}\boldsymbol{p}'} - \hat{\Gamma} g(\boldsymbol{p})\,, \tag{3.53}$$

with $\Sigma_{\boldsymbol{p}}\, g(\boldsymbol{p}) = 1$ (sum over the first Brillouin zone). The Haken–Strobl model, eq. (3.28), is contained within this class, with $g(\boldsymbol{p}) \equiv 1/N$. For a general $g(\boldsymbol{p})$, the equation of motion now reads

$$\begin{aligned}\frac{\mathrm{d}}{\mathrm{d}t}\phi(\boldsymbol{r}, \boldsymbol{p}, t) = {} & 2\sum_{\boldsymbol{a}} J(\boldsymbol{a}) \sin(\boldsymbol{p}\cdot\boldsymbol{a})\phi(\boldsymbol{r} + \boldsymbol{a}/2, \boldsymbol{p}, t) \\ & - \hat{\Gamma}\sum_{\boldsymbol{p}'} [g(\boldsymbol{p}')\phi(\boldsymbol{r}, \boldsymbol{p}, t) - g(\boldsymbol{p})\phi(\boldsymbol{r}, \boldsymbol{p}', t)] - \gamma\phi(\boldsymbol{r}, \boldsymbol{p}, t)\,.\end{aligned} \tag{3.54}$$

The second term in this equation has the form of the BGK strong collision operator in the Boltzmann equation [96, 97], in which collisions occur with rate $\hat{\Gamma}$ and the momentum after each collision is distributed according to $g(\boldsymbol{p})$. In this model, $g(\boldsymbol{p})$ is the equilibrium momentum distribution. This implies in particular that the Haken–Strobl model is a high-temperature model, as the equilibrium distribution is then uniform over all momenta. The strong collision operator conserves the number of particles (population); a population loss with rate γ is described by the last term in eq. (3.54). This is also nicely illustrated in yet another representation for the two-particle variables, which is found by Fourier transforming $\phi(\boldsymbol{r}, \boldsymbol{p}, t)$ with respect to $\boldsymbol{p}$ [95],

$$\bar{\phi}(\boldsymbol{r}, s, t) = \frac{1}{\sqrt{N}} \sum_{\boldsymbol{p}} \phi(\boldsymbol{r}, \boldsymbol{p}, t) \exp(-\mathrm{i}\boldsymbol{p} \cdot \boldsymbol{s}) . \tag{3.55}$$

Comparison with eq. (3.24a) shows that s plays the role of a relative coordinate and $\phi(\boldsymbol{r}, s = \boldsymbol{0}, t)$ represents the exciton population at site $\boldsymbol{r}$.

Equation (3.54) now translates into [95]

$$\frac{\mathrm{d}}{\mathrm{d}t} \bar{\phi}(\boldsymbol{r}, s, t) = -\mathrm{i} \sum_{\boldsymbol{a}} J(\boldsymbol{a}) [\bar{\phi}(\boldsymbol{r} + \boldsymbol{a}/2, s - \boldsymbol{a}, t) - \bar{\phi}(\boldsymbol{r} + \boldsymbol{a}/2, s + \boldsymbol{a}, t)] - (\hat{\Gamma} + \gamma) \bar{\phi}(\boldsymbol{r}, s, t) + \hat{\Gamma} \bar{g}(s) \bar{\phi}(\boldsymbol{r}, \boldsymbol{0}, t) , \tag{3.56a}$$

$$\bar{g}(s) \equiv \sum_{\boldsymbol{p}} g(\boldsymbol{p}) \exp(-\mathrm{i}\boldsymbol{p} \cdot \boldsymbol{s}) . \tag{3.56b}$$

As a consequence of the normalization of $g(\boldsymbol{p})$, we have $g(s = \boldsymbol{0}) = 1$, so that the last two terms of eq. (3.56a) indeed describe a net loss of population with rate γ.

We return to the equation of motion (3.54) for the Wigner distribution and direct our attention to the coherent term. We will assume that the interaction is symmetric [$J(\boldsymbol{r}) = J(-\boldsymbol{r})$] and has a short range R. Furthermore, we assume that $g(\boldsymbol{p})$ is centered at optical momenta $\boldsymbol{p}$, for which $|\boldsymbol{p}|R \ll 1$. In the continuum approximation, eq. (3.54) then becomes [95]

$$\frac{\partial}{\partial t} \phi(\boldsymbol{r}, \boldsymbol{p}, t) = \frac{\boldsymbol{p}}{m^*} \cdot \boldsymbol{\nabla}_{\boldsymbol{r}} \phi(\boldsymbol{r}, \boldsymbol{p}, t) - \hat{\Gamma} \int \mathrm{d}\boldsymbol{p}' [\tilde{g}(\boldsymbol{p}') \phi(\boldsymbol{r}, \boldsymbol{p}, t) - \tilde{g}(\boldsymbol{p}) \phi(\boldsymbol{r}, \boldsymbol{p}', t)] - \gamma \phi(\boldsymbol{r}, \boldsymbol{p}, t) , \tag{3.57a}$$

where, for an isotropic d-dimensional system,

$$(m^*)^{-1} = (1/d) \sum_{n} J(r_n) r_n^2 . \tag{3.57b}$$

Here, n runs over the original lattice and $r_n \equiv |\boldsymbol{r}_n|$. Furthermore, $\tilde{g}(\boldsymbol{p})$ is defined in analogy with $g(\boldsymbol{p})$, but has continuum normalization $\int \tilde{g}(\boldsymbol{p}) \, \mathrm{d}\boldsymbol{p} = 1$. Equation (3.57a) clearly has the form of the Boltzmann equation for a classical particle of mass m^*. It can now be shown quite generally that in the limit of high friction, $\hat{\Gamma}$, eq. (3.57a) reduces to a diffusion equation for the particle position distribution function defined by

$$\phi(\boldsymbol{r}, t) \equiv \int \mathrm{d}\boldsymbol{p} \, \phi(\boldsymbol{r}, \boldsymbol{p}, t) . \tag{3.58}$$

Explicitly, one finds (see ref. [97], chapter 10 and appendix 2):

$$(\partial/\partial t) \phi(\boldsymbol{r}, t) = D \nabla^2 \phi(\boldsymbol{r}, t) - \gamma \phi(\boldsymbol{r}, t) , \tag{3.59a}$$

with the diffusion constant defined by

$$D \equiv \frac{1}{\hat{\Gamma}} \langle (\boldsymbol{p}/m^*)^2 \rangle_{\tilde{g}} = \frac{1}{\hat{\Gamma}} \left(\frac{1}{d} \sum_{n} J(r_n) r_n^2 \right)^2 \langle \boldsymbol{p}^2 \rangle_{\tilde{g}} . \tag{3.59b}$$

where $\langle \cdots \rangle_{\tilde{g}}$ takes the average over the equilibrium distribution $\tilde{g}(\boldsymbol{p})$.

The direct solution of the equation of motion for $Q(\boldsymbol{k}, \boldsymbol{p}, t)$ within the Haken–Strobl model also leads to a diffusion constant (eq. 3.37),

$$D_e = (1/d\hat{\Gamma}) \sum_n J^2(r_n) r_n^2 . \tag{3.60}$$

It is clear that in general D does not coincide with D_e, even if we take $\tilde{g}(\boldsymbol{p}) = (a/2\pi)^d$, which is the equilibrium distribution in the Haken–Strobl model (a is the lattice spacing). The quantitative difference between the two above diffusion constants can be illustrated by giving their values in the case of nearest-neighbor interactions (J) on a lattice with spacing a,

$$D_e = (2/\hat{\Gamma}) J^2 a^2 , \qquad D = (4\pi^2 d/3\hat{\Gamma}) J^2 a^2 . \tag{3.61a, b}$$

The solution to this apparent discrepancy is that for the Haken–Strobl model, strictly speaking, the Boltzmann equation cannot be derived through the above method, because the equilibrium distribution $g(\boldsymbol{p})$ is uniform instead of centered at optical wave vectors. Consequently, eq. (3.59b) cannot be derived within the Haken–Strobl model. Alternatively, for a very broad equilibrium distribution $g(\boldsymbol{p})$, the classical picture of a momentum-independent effective mass m^* is an oversimplification.

That it is possible, however, to derive in a rigorous way a diffusion equation for the exciton motion within the incoherent limit of the Haken–Strobl model is clear from the discussion following eq. (C.5). A very elegant derivation has been put forward by Reineker and Kühne [54, 98, 99]. These authors first derive the Pauli master equation for the site exciton populations W_n in the strong scattering limit. In our notation, this equation reads [54, 98]

$$\frac{dW_n}{dt} = \sum_{n'} w_{nn'}(W_{n'} - W_n) - \gamma W_n , \quad w_{nn'} \equiv 2|J(\boldsymbol{r}_{nn'})|^2/\hat{\Gamma} . \tag{3.62a, b}$$

Equation (3.62a) has been extensively studied within the field of incoherent energy transfer [100]; $w_{nn'}$ is the well-known Förster rate of energy transfer between the molecules n and n' [41, 101]. For dipolar interactions, $w_{nn'}$ has the characteristic $1/r_{nn'}^6$ dependence. In the continuum approximation, the diffusion equation for the exciton population density is now easily derived from eq. (3.62a), by expanding W_n around the lattice point $\boldsymbol{r}_n$ [54, 99]. For an isotropic system the diffusion constant obtained in this way indeed coincides with eq. (3.60).

4. Nonlinear optical response of polaritons

4.1. Canonical transformation and operator equations

In this section we develop a polariton theory of nonlinear optical response for the case that the radiation and the matter degrees of freedom are strongly coupled and the TG and D4WM experiments are dominated by polariton dynamics. Polaritons are the combined radiation–electronic eigenmodes of the crystal, which have a dispersion diagram that can differ profoundly from that for excitons (see fig. 6) [57, 58]. Of course, the optical response of a crystal is in general determined by its proper elementary excitations, so that optical signals must exhibit resonances and broadenings determined by the energetics and dynamics of polaritons instead of excitons. The theory of section 3 cannot account for those effects: the calculation of response functions and susceptibilities was based on a factorization of

the electric field, thus treating it effectively as an external c-number and neglecting part of the correlations between the material (excitons) and the radiation fields. Such a scheme leads to signals characterized by the exciton dispersion and dynamics. Although it is in principle possible to define and calculate susceptibilities without factorization, this does not lead to a very practical scheme [66, 67]. Here, we rather follow an approach in which a hierarchy of nonlinear equations of motion for polariton variables inside the crystal is built, which directly leads to the optical signal (polariton hierarchy) [76]. This method is described in more detail in the next section.

As in the exciton theory, our approach starts by deriving a basic set of operator equations. Now, however, we also consider equations for the photon operators, as the radiation field is treated as an explicit degree of freedom. We use eq. (2.9) as starting point and neglect Umklapp contributions to $\hat{\boldsymbol{E}}^{\perp}$. Furthermore, we note that, at every wave vector $\boldsymbol{k}$, we only need to consider photons with polarization in the plane spanned by $\boldsymbol{k}$ and the molecular transition dipole $\boldsymbol{\mu}$; photons polarized perpendicular to this plane do not couple to the crystal and form no new eigenmodes with the excitons. We, thus, drop the polarization labels λ on the photon creation and annihilation operators and arrive at (all operators taken at time t)

$$\frac{1}{\mathrm{i}}\frac{\mathrm{d}}{\mathrm{d}t}\begin{pmatrix}\hat{a}_k\\ \hat{B}_k\\ \hat{a}^{\dagger}_{-k}\\ \hat{B}^{\dagger}_{-k}\end{pmatrix}=\begin{pmatrix}-kc & -\mathrm{i}C_k & 0 & -\mathrm{i}C_k\\ \mathrm{i}C_k & -\Omega - D_k + \mathrm{i}\Gamma(k) & -\mathrm{i}C_k & -D_k\\ 0 & -\mathrm{i}C_k & kc & -\mathrm{i}C_k\\ -\mathrm{i}C_k & D_k & \mathrm{i}C_k & \Omega + D_k + \mathrm{i}\Gamma(k)\end{pmatrix}\begin{pmatrix}\hat{a}_k\\ \hat{B}_k\\ \hat{a}^{\dagger}_{-k}\\ \hat{B}^{\dagger}_{-k}\end{pmatrix}+\hat{\mathcal{N}}(\boldsymbol{k})\begin{pmatrix}0\\1\\0\\-1\end{pmatrix}, \tag{4.1a}$$

$$\hat{\mathcal{N}}(\boldsymbol{k})=\frac{1}{2}\sum_{k'}[D_{k'}(\hat{B}_{k'}+\hat{B}^{\dagger}_{-k'})-\mathrm{i}C_{k'}(\hat{a}_{k'}-\hat{a}^{\dagger}_{-k'}),\hat{W}(\boldsymbol{k}-\boldsymbol{k}')]_{+}\,, \tag{4.1b}$$

$$C_k=(2\pi kc\rho\hbar^{-1}\mu_{\perp}^2)^{1/2}\,, \tag{4.2a}$$

$$D_k=J(k)+4\pi\rho\hbar^{-1}\mu_{\perp}^2\,,\qquad \mu_{\perp}^2=\mu^2-(\boldsymbol{\mu}\cdot\boldsymbol{k})^2/k^2\,. \tag{4.2b, c}$$

In the derivation of eq. (4.1) we used eqs. (2.6)–(2.8) to express $\hat{\boldsymbol{E}}^{-}$ in terms of photon and exciton creation and annihilation operators. Of course, the equations for $\hat{B}_k$ and $\hat{B}^{\dagger}_{-k}$ are equivalent to eq. (3.1). The inclusion of $\Gamma(\boldsymbol{k})$, the phonon-induced exciton damping, is not fully consistent here, as it was calculated without accounting for polaritons. We will come back to this further on in this section. From eq. (4.1) one easily derives the Maxwell equations in the electric dipole approximation [71, 76]

$$\hat{\boldsymbol{E}}^{\perp}(\boldsymbol{k},t)=-\frac{1}{c}\frac{\partial}{\partial t}\hat{\boldsymbol{A}}^{\perp}(\boldsymbol{k},t)\,,\qquad \left(k^2+\frac{1}{c^2}\frac{\partial^2}{\partial t^2}\right)\hat{\boldsymbol{E}}^{\perp}(\boldsymbol{k},t)=-\frac{4\pi}{c^2}\frac{\partial^2}{\partial t^2}\hat{\boldsymbol{P}}^{\perp}(\boldsymbol{k},t)\,. \tag{4.3a, b}$$

These equations are not affected by the nonlinear term $\sim\hat{\mathcal{N}}(\boldsymbol{k})$ in eq. (4.1).

We now consider eq. (4.1) in the Bose approximation $\hat{\mathcal{N}}(\boldsymbol{k})=0$. It is then a closed 4×4 matrix equation that completely describes the linear propagation of electromagnetic waves. The eigenmodes of this problem are the polaritons, which are related to the photons and excitons by a canonical transformation [57, 58, 61]. We follow Hopfield's notation and search for a transformation [57]

$$\hat{\xi}_{k\nu} = w_{k\nu}\hat{a}_k + x_{k\nu}\hat{B}_k + y_{k\nu}\hat{a}^{\dagger}_{-k} + z_{k\nu}\hat{B}^{\dagger}_{-k}\,, \tag{4.4}$$

such that

$$(\mathrm{d}/\mathrm{d}t)\hat{\xi}_{k\nu} = -\mathrm{i}\omega_{k\nu}\hat{\xi}_{k\nu} \quad \text{(Bose approximation)}\,. \tag{4.5}$$

Here $\hat{\xi}_{k\nu}$ denotes the annihilation operator for a polariton with wave vector $\boldsymbol{k}$ in branch ν, and $\omega_{k\nu}$ is the frequency of this polariton. In combination with eq. (4.1) this defines an eigenvalue problem whose secular equation gives the polariton dispersion relation,

$$\frac{(kc)^2}{\omega_{k\nu}^2} = 1 + \frac{f^2}{-[\omega_{k\nu} + \mathrm{i}\Gamma(\boldsymbol{k})]^2 + \Omega_k^2}\,, \quad f = (8\pi\rho\mu_{\perp}^2\Omega/\hbar)^{1/2}\,, \tag{4.6a, b}$$

where Ω_k is the exciton dispersion eq. (3.6). As the polariton dispersion is by definition equivalent to the one for electromagnetic waves in the crystal, $(kc/\omega_{k\nu})^2$ must also define the transverse dielectric function $\varepsilon^{\perp}(\boldsymbol{k}, \omega_{k\nu})$. Comparison with eq. (3.12b) shows that the thus obtained transverse dielectric function is identical to the one found through exciton response. *The linear response of the crystal, apart from a possible change of the damping constant $\Gamma(\boldsymbol{k})$ [see below], is not affected by the introduction of the polariton concept* [57, 58, 80].

We now first analyze the polariton dispersion and transformation in more detail for the important case $\Gamma(\boldsymbol{k}) = 0$, i.e., totally neglecting the phonon bath. This is the standard case considered in the literature. Equation (4.6) then gives the usual dispersion diagram (cf. fig. 6) with two branches separated by the polariton stopgap: the frequency interval where no real wave-vector solutions to the dispersion relation exist, so that no waves with those frequencies can propagate in the crystal. In an atomic crystal, the stopgap ranges from the transverse ($\omega_{\perp}$) to the longitudinal ($\omega_{\parallel}$) exciton frequency [43, 57, 58]. For our crystal of two-level molecules, these boundaries depend on the direction of

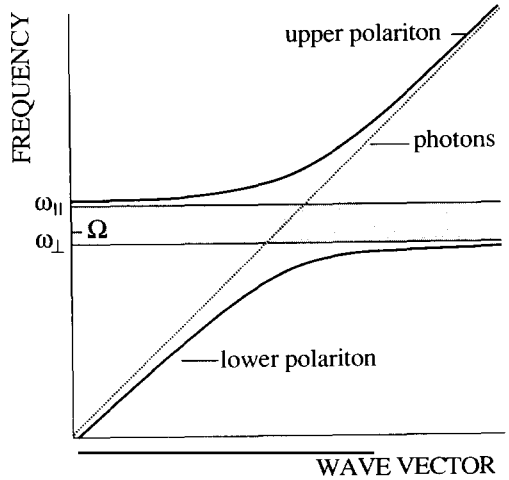

Fig. 6. Typical polariton dispersion curves in the optical region for an atomic crystal (thick solid curves). The diagonal line represents the pure photon dispersion curve ($\omega_k = kc$). The shaded region between the transverse ($\omega_{\perp}$) and longitudinal ($\omega_{\parallel}$) crystal exciton frequencies is the stopgap, where no polariton modes exist. Ω indicates the atomic transition frequency. For a crystal of two-level molecules, the stopgap position depends on the direction of propagation (see text).

propagation and are replaced by Ω_0 and $(\Omega_0^2 + f^2)^{1/2}$, respectively, with $\Omega_0 \equiv \lim_{k\to 0} \Omega_k$ and f as defined in eq. (4.6). (Exciton dispersion is neglected when considering the stopgap.)

The strongest mixture between excitons and photons occurs in the photon- and exciton-band crossing region $kc \approx \Omega_0 \approx \Omega$. In that region the frequency difference between the two branches reaches its minimum value, which, to a good approximation, is given by f [60b]. From eq. (4.6), we observe that f is a measure for the density of oscillator strength in the crystal and in combination with eq. (4.2a), it is also seen that $f/2$ is the coupling C_k between the exciton and the radiation field in the band-crossing region. For molecular crystals, we usually have $f \ll \Omega$. For example, for the lowest singlet a-exciton in naphthalene, we have $f \approx 45\ \mathrm{cm}^{-1}$ and $\Omega_0 \approx \Omega \approx 31\,500\ \mathrm{cm}^{-1}$ [60b]; for the same exciton in anthracene, we find $f \approx 1000\ \mathrm{cm}^{-1}$ and $\Omega_0 \approx 25\,000\ \mathrm{cm}^{-1}$ [60a]. (Both f values account for the crystal's background index of refraction.)

The polariton transformation coefficients, which are determined by the eigenvectors of the diagonalization procedure, also nicely demonstrate the mixed character of the polaritons. In the case $\Gamma(\boldsymbol{k}) = 0$, the coefficients are found to be

$$w_{k\nu} = \mathrm{e}^{\mathrm{i}\varphi} \frac{(\omega + kc)(\omega^2 - \Omega_k^2 - f^2)}{2(\omega kc)^{1/2}[(\omega^2 - \Omega_k^2 - f^2)^2 + f^2 k^2 c^2]^{1/2}} , \tag{4.7a}$$

$$x_{k\nu} = \mathrm{i}\,\mathrm{e}^{\mathrm{i}\varphi} \frac{fkc(\omega + \Omega)}{2(\omega\Omega)^{1/2}[(\omega^2 - \Omega_k^2 - f^2)^2 + f^2 k^2 c^2]^{1/2}} , \tag{4.7b}$$

$$y_{k\nu} = \frac{kc - \omega}{kc + \omega} w_{k\nu} , \qquad z_{k\nu} = \frac{\omega - \Omega}{\omega + \Omega} x_{k\nu} , \tag{4.7c, d}$$

where φ is an arbitrary phase and ω stands for $\omega_{k\nu}$. These coefficients have been normalized according to [57, 58, 61]

$$|w_{k\nu}|^2 + |x_{k\nu}|^2 - |y_{k\nu}|^2 - |z_{k\nu}|^2 = 1 . \tag{4.8}$$

In spite of the complexity of eqs. (4.7), several general and instructive conclusions can be drawn. First, the coefficients $y_{k\nu}$ and $z_{k\nu}$ usually have absolute values small compared to unity (see, e.g., ref. [68]). Second, the limits for small and large wave vectors are easily studied. In the limit $|\boldsymbol{k}| \to 0$, we find for the upper branch $|x| = 1$, $|w| = |y| = |z| = 0$ (up to order f/Ω), so that the polariton is a pure exciton there. For $|\boldsymbol{k}| \to \infty$, the same branch represents a pure photon ($|w| = 1$, $|x| = |y| = |z| = 0$). This could, of course, have been already guessed from the dispersion diagram (fig. 6). Equally natural results are found for the lower branch. For intermediate wave vectors the polaritons smoothly change character from exciton-like to photon-like (or vice versa). Third, at the band crossing ($kc \approx \Omega$), we find $|w|^2 = |x|^2 = \frac{1}{2}$ for both branches, confirming that the strongest photon–exciton mixture occurs there.

We note that the coefficients (4.7) do not exactly coincide with the ones obtained within the minimal coupling Hamiltonian [57, 58], but their basic features are not affected by this. The dispersion relation (4.6), which is an "observable", is of course independent of the choice of the Hamiltonian. The present polariton transformation *does* coincide with the one derived in ref. [102], if in the latter we ignore the coefficients coupling to the higher Brillouin zones (Umklapp contributions) and neglect the retardation in the effective interatomic interaction. Finally, we will need the inverse polariton transformation, which can, quite generally, be shown to read [61]

$$\hat{a}_k = \sum_\nu (w^*_{k\nu}\hat{\xi}_{k\nu} - y_{k\nu}\hat{\xi}^\dagger_{-k\nu}), \qquad \hat{B}_k = \sum_\nu (x^*_{k\nu}\hat{\xi}_{k\nu} - z_{k\nu}\hat{\xi}^\dagger_{-k\nu}). \tag{4.9a, b}$$

We now return to the general polariton transformation with $\Gamma(\boldsymbol{k}) \neq 0$. The two branches found above are then no longer the correct eigenmodes. For $f/\Gamma(\boldsymbol{k}) \ll 1$, the maximum amount of mixing between photons and excitons is of the order $f/\Gamma(\boldsymbol{k})$, so that the polaritons are to a good approximation just the photons and (damped) excitons [60, 68]. In other words, if the exciton–radiation coupling, f, is small compared to the coupling of excitons to phonons (or any other perturbing degree of freedom [103]), measured by $\Gamma(\boldsymbol{k})$, no strongly mixed radiation–matter eigenmodes exist. We then expect the exciton description of optical response to be accurate. We note that in this case of strong exciton damping, the elimination of the phonon bath [leading to $\Gamma(\boldsymbol{k})$] *before* considering the coupled exciton–photon system is fully justified.

Conversely, the condition $f/\Gamma(\boldsymbol{k}) \gg 1$, which is typically met in low-temperature pure crystals, marks the region of strong polariton effects in optical response. It is then inconsistent to account for phonons (or other bath variables) by including the exciton damping $\Gamma(\boldsymbol{k})$ in eq. (4.1). Instead, we should first diagonalize the bare exciton–photon system [$\Gamma(\boldsymbol{k}) = 0$] and then account for other degrees of freedom by considering their perturbation to the thus found polariton eigenmodes (polariton self-energies) [60b, 68]. In the remainder of this review we will assume that the limit of strong polariton effects applies, so that from now on the polariton dispersion and transformation coefficients refer to the case $\Gamma(\boldsymbol{k}) = 0$. The polariton self-energies are addressed in appendix A and incorporated in the equations of motion in section 4.2. For completeness we note that the theoretical treatment of the intermediate region where the exciton–photon coupling roughly equals the exciton–phonon coupling, is very complicated, because it is then impossible to indicate a simple set of eigenmodes that are weakly perturbed by the phonon bath.

So far we only considered polaritons in the Bose approximation, which results in a purely linear optical response. However, using the above-obtained polariton transformation, the full equation of motion (4.1) yields

$$\mathrm{d}\hat{\xi}_{k\nu}/\mathrm{d}t = -\mathrm{i}\omega_{k\nu}\hat{\xi}_{k\nu} + \mathrm{i}(x_{k\nu} - z_{k\nu})\hat{\mathcal{N}}(\boldsymbol{k}), \tag{4.10}$$

and its hermitian conjugate for the polariton creation operator $\hat{\xi}^\dagger_{k\nu}$. Equation (4.10) is, apart from the omission of the phonon-induced self-energy, exact and fully accounts for nonlinear behavior. The linear part of the equation is, of course, equivalent to eq. (4.5); the nonlinear part is determined by eq. (4.1b) and may be translated into polariton creation and annihilation operators by using the inverse polariton transformation (4.9). A typical term in $\hat{\mathcal{N}}(\boldsymbol{k})$ reads

$$\sum_{\boldsymbol{k}'\boldsymbol{k}''} \sum_{\nu'\nu''\nu'''} \alpha(\boldsymbol{k}\boldsymbol{k}'\boldsymbol{k}'', \nu'\nu''\nu''')\hat{\xi}_{\boldsymbol{k}'\nu'}\hat{\xi}^\dagger_{\boldsymbol{k}'+\boldsymbol{k}''\nu''}\hat{\xi}_{\boldsymbol{k}+\boldsymbol{k}''\nu'''}, \tag{4.11}$$

with $\alpha(\boldsymbol{k}\boldsymbol{k}'\boldsymbol{k}'', \nu\nu''\nu''')$ a complicated function of wave vectors and branches. Finally, as the exciton population operator plays a crucial role in the nonlinearity, it is useful to give its full expression in terms of polariton operators. Using eqs. (3.5) and (4.9) we arrive at

$$\begin{aligned}\hat{W}(\boldsymbol{k}-\boldsymbol{k}') = \frac{2}{N}\sum_{\boldsymbol{k}''}\sum_{\nu\nu'} (&x_{\boldsymbol{k}'+\boldsymbol{k}''\nu'}x^*_{\boldsymbol{k}+\boldsymbol{k}''\nu}\hat{\xi}^\dagger_{\boldsymbol{k}'+\boldsymbol{k}''\nu'}\hat{\xi}_{\boldsymbol{k}+\boldsymbol{k}''\nu} + z^*_{\boldsymbol{k}'+\boldsymbol{k}''\nu'}z_{\boldsymbol{k}+\boldsymbol{k}''\nu}\hat{\xi}_{-\boldsymbol{k}'-\boldsymbol{k}''\nu'}\hat{\xi}^\dagger_{-\boldsymbol{k}-\boldsymbol{k}''\nu} \\ &- x_{\boldsymbol{k}'+\boldsymbol{k}''\nu'}z_{\boldsymbol{k}+\boldsymbol{k}''\nu}\hat{\xi}^\dagger_{\boldsymbol{k}'+\boldsymbol{k}''\nu'}\hat{\xi}^\dagger_{-\boldsymbol{k}-\boldsymbol{k}''\nu} - z^*_{\boldsymbol{k}'+\boldsymbol{k}''\nu'}x^*_{\boldsymbol{k}+\boldsymbol{k}''\nu}\hat{\xi}_{-\boldsymbol{k}-\boldsymbol{k}''\nu'}\hat{\xi}_{\boldsymbol{k}+\boldsymbol{k}''\nu}).\end{aligned} \tag{4.12}$$

4.2. The polariton hierarchy in the two-particle description

Before turning to the treatment of the TG and the D4WM experiments in the limit of strong polariton effects, we first discuss the general approach, the polariton hierarchy [76]. Consider a finite crystal that is still large enough, however, so that its eigenmodes are to a good approximation the polaritons discussed in section 4.1. The nonlinear evolution of the isolated polariton system is in principle fully described by eq. (4.10), but this equation does not yet describe the generation of polaritons by the external laser fields. It is important that this generation is not caused by a direct interaction term between electromagnetic fields and polaritons in the Hamiltonian [69], because the electromagnetic field itself is, inside the crystal, fully contained within the polaritons. Instead, the coupling occurs through the boundary conditions at the surface of the crystal. If an external electric field with wave vector $\boldsymbol{k}'_j$ and frequency ω_j ($\omega_j = |\boldsymbol{k}'_j|c$) is incident on the crystal, it launches a polariton which is specified by matching the boundary conditions for the expectation values of its electromagnetic field components to the external field (accounting for reflection). Thus, the polariton will also have frequency ω_j; its wave vector $\boldsymbol{k}_j$ is determined by the component parallel to the crystal's surface ($\boldsymbol{k}_{j,\parallel} = \boldsymbol{k}'_{j,\parallel}$) and by its magnitude, $|\boldsymbol{k}_j|$, which is fixed through ω_j and the polariton dispersion relation (i.e. the crystal's dielectric function) [69]. This agrees with Snell's law. Finally, the amplitude of the polariton, $\langle \hat{\xi}_{\boldsymbol{k}_j\nu_j}(t)\rangle$, is (in the frame rotating with frequency ω_j) proportional to the external field amplitude E^{e}_j.

The complete solution to the boundary value problem is, in particular if spatial dispersion is taken into account, a complicated problem [43, 104–107]. Instead of rigorously solving this problem, we will incorporate the above well accepted ideas about the generation of polaritons by adding simple source terms to our equations of motion (see below). In the absence of the nonlinear term in eq. (4.10), the thus generated "first-order" polaritons constitute the only response of the crystal to exciting fields. Clearly, however, the nonlinear term causes fusion of first-order polaritons to higher-order ones at new (not fundamental) wave vectors and frequencies. Such a higher-order polariton generates an observable nonlinear signal outside the crystal which is, again, found by matching boundary conditions. In particular, the signal amplitude will be proportional to the amplitude $\langle \hat{\xi}_{\boldsymbol{k}_s\nu_s}(t)\rangle$ of the higher-order polariton. The problem of calculating the optical response of the crystal now boils down to calculating the amplitude $\langle \hat{\xi}_{\boldsymbol{k}_s\nu_s}\rangle$, which can be done using a truncated hierarchy of equations of motion for polariton expectation values based on eq. (4.10).

To apply this scheme to the TG and D4WM experiments, we use the truncation that also proved useful in the exciton theory, namely, we factorize the exciton population in the expectation value of $\mathcal{N}(\boldsymbol{k})$ (two-particle description). From eq. (4.10), we then obtain [$\xi_{\boldsymbol{k}\nu}(t) \equiv \langle \hat{\xi}_{\boldsymbol{k}\nu}(t)\rangle$]

$$\begin{aligned}\frac{\mathrm{d}}{\mathrm{d}t}\,\xi_{\boldsymbol{k}\nu}(t) = {} & -\mathrm{i}\omega_{\boldsymbol{k}\nu}\xi_{\boldsymbol{k}\nu}(t) - \mathrm{i}\sum_{\nu'}\Sigma_{\nu\nu'}(\boldsymbol{k})\xi_{\boldsymbol{k}\nu'}(t) \\ & + (x_{\boldsymbol{k}\nu} - z_{\boldsymbol{k}\nu})\sum_{\boldsymbol{k}'}\sum_{\nu'}[\gamma(\boldsymbol{k}'\nu')\xi_{\boldsymbol{k}'\nu'}(t) - \gamma^*(\boldsymbol{k}'\nu')\xi^*_{-\boldsymbol{k}'\nu'}(t)]W(\boldsymbol{k}-\boldsymbol{k}', t) \\ & + \sum_j \Lambda(\boldsymbol{k}\nu, \boldsymbol{k}'_j)E^{\mathrm{c}}_j(t)\exp(-\mathrm{i}\omega_j t)\,. \end{aligned} \tag{4.13a}$$

Here, $\Sigma_{\nu\nu'}(\boldsymbol{k})$ is the phonon-induced polariton self-energy given in eq. (A.14b) and

$$\gamma(\boldsymbol{k}\nu) \equiv C_k(w^*_{\boldsymbol{k}\nu} + y^*_{\boldsymbol{k}\nu}) + \mathrm{i}D_k(x^*_{\boldsymbol{k}\nu} - z^*_{\boldsymbol{k}\nu})\,. \tag{4.13b}$$

Finally, the last term in eq. (4.13a) describes the above discussed generation of polaritons, where $E_j^e(t)$ is the (slowly varying) amplitude of the jth external electric field. The proportionality constant $\Lambda(k\nu, k_j')$ is nonzero only if the jth external field mode exactly matches the polariton $k\nu$; its magnitude is then a complicated function of geometry and frequency which we do not calculate here. Of course, this "source term" only makes sense for pulses which are long compared to an optical cycle.

As next step in the hierarchy, we need equations for the two-particle variables contained in $\langle \hat{W}(k - k', t)\rangle$. In section 3 we considered the exciton two-particle variables, $Q(k, p, t)$ [cf. eqs. (3.24)], but this choice is not useful here, because these variables couple to expectation values of products of exciton and radiation operators, which we cannot factor in the limit of strong polariton effects. Instead, it is more appropriate and more direct to consider polariton two-particle variables. From eq. (4.12), we see that four types of such variables are involved. However, as in general $|z_{k\nu}| \ll 1$ and, moreover, for the self-energy models to which we will confine ourselves later on, $|z_{k\nu}| \ll |x_{k\nu}|$, we will only maintain the first r.h.s. term in eq. (4.12), so that

$$W(k, t) \approx (2/N) \sum_p \sum_{\nu\nu'} x_{p-k/2,\nu'} x^*_{p+k/2,\nu} \Xi_{\nu\nu'}(k, p, t) , \tag{4.14}$$

$$\Xi_{\nu\nu'}(k, p, t) \equiv \langle \hat{\xi}^\dagger_{p-k/2,\nu'}(t) \hat{\xi}_{p+k/2,\nu}(t) \rangle . \tag{4.15}$$

The next step in the hierarchy now results in the equation of motion for the variables $\Xi_{\nu\nu'}(k, p, t)$, which reads

$$\begin{aligned}(\mathrm{d}/\mathrm{d}t)\Xi_{\nu\nu'}(k, p, t) = {} & \mathrm{i}(\omega_{p-k/2,\nu'} - \omega_{p+k/2,\nu})\Xi_{\nu\nu'}(k, p, t) - \mathrm{i} \sum_{p'} \sum_{\nu''\nu'''} \Sigma(k, \nu; p, p')\Xi_{\nu''\nu'''}(k, p', t) \\ & + \xi^*_{p-k/2,\nu'}(t) \sum_j \Lambda(p + k/2, \nu, k_j')E_j^e(t) \exp(-\mathrm{i}\omega_j t) \\ & + \xi_{p+k/2,\nu}(t) \sum_j \Lambda^*(p - k/2, \nu', k_j')E_j^{e*}(t) \exp(\mathrm{i}\omega_j t) . \end{aligned} \tag{4.16}$$

The first term in this equation reflects the linear coherent motion [first r.h.s. term in eq. (4.10)]. The nonlinear coherent motion is neglected on this level, because it couples to variables which are of fourth and higher orders in the external field amplitudes, which is beyond the leading order (3) for four-wave mixing processes. The second term in eq. 4.16) accounts for phonon scattering. The calculation of the self-energy kernel $\Sigma(k, \nu; p, p')$ $[\nu \equiv (\nu, \nu', \nu'', \nu''')]$ is addressed in appendix A (eq. A.16), and remarks similar to those following eq. (3.26) for the exciton self-energy apply here. In particular, we see again that the "center-of-mass" wave vector k is conserved in the scattering process. Finally, the last two contributions in eq. (4.16) account for creation of two-particle coherences from existing single-particle amplitudes and new polaritons generated by external fields [cf. the generation term in eq. (4.13a)].

4.3. Polariton dynamics probed by transient grating spectroscopy

We now apply the two-particle polariton hierarchy [eqs. (4.13a) and (4.16)] to the TG experiment in the limit of strong polariton effects. Two external pump fields $[(k_1', \omega_1)$ and $(k_2', \omega_2)]$ create polaritons, $k_1\nu_1$ and $k_2\nu_2$, resulting in a grating characterized by the wave vector $k_1 - k_2$. After a delay time τ, a probe pulse (k_3', ω_3) generates probe polaritons, $k_3\nu_3$, which interact nonlinearly with the grating and

give rise to signal polaritons with wave vector $\boldsymbol{k}_s \equiv \boldsymbol{k}_1 - \boldsymbol{k}_2 + \boldsymbol{k}_3$. The amplitude $\xi_{\boldsymbol{k}_s\nu_s}(t)$ determines the amplitude of the observable field at $\boldsymbol{k}'_s \equiv \boldsymbol{k}'_1 - \boldsymbol{k}'_2 + \boldsymbol{k}'_3$. From eq. (4.13) we observe that the nonlinear source term for the signal polaritons to third order in the external field amplitudes is given by

$$(x_{\boldsymbol{k}_s\nu_s} - z_{\boldsymbol{k}_s\nu_s})\gamma(\boldsymbol{k}_3\nu_3)\xi^{(1)}_{\boldsymbol{k}_3\nu_3}(t)W^{(2)}(\boldsymbol{k}_1 - \boldsymbol{k}_2, t)\,, \tag{4.17}$$

where superscripts in parentheses indicate the order in powers of the external field amplitudes. We will assume an off-resonance (square) probe pulse that is short compared to the typical time scale for population decay. On this time scale, the amplitude $\xi^{(1)}_{\boldsymbol{k}_3\nu_3}(t)$ then behaves as a delta function centered around $t = \tau$, so that the time-integrated signal intensity (to third order in the external field intensities) is given by

$$S(\tau) \propto \int_{\tau}^{\infty} \mathrm{d}t\, |\xi^{(3)}_{\boldsymbol{k}_s\nu_s}(t)|^2 \propto |W^{(2)}(\boldsymbol{k}_1 - \boldsymbol{k}_2, \tau)|^2 |E^{\mathrm{e}}_3|^2\,. \tag{4.18}$$

Thus, as in the exciton theory of section 3.4, the TG signal is determined by the *exciton* population at the grating wave vector $\boldsymbol{k}_{\mathrm{g}} \equiv \boldsymbol{k}_1 - \boldsymbol{k}_2$. This is a direct consequence of the fact that the exciton population operator is really the only nonlinearity in our system (cf. section 3.1; the photons are perfect bosons). The difference with the theory of section 3 is, of course, that now the evolution of the exciton population occurs within the complete polariton system [eqs. (4.14)–(4.16)] instead of the isolated exciton system. We thus take into account that, even though there are no external fields during the pump-probe delay, the (microscopic) radiation field still affects the material. *The TG signal is a probe for polariton dynamics during the delay period.* A second difference between the exciton and polariton approaches is the initial condition immediately following the pump pulses. In section 3, these were exciton amplitudes and coherences (eqs. 3.44), whereas in the present treatment polariton amplitudes and coherences are appropriate. Using eq. (4.13a) for square excitation pulses with amplitudes E^{e}_j and a duration τ_{e} that is short enough to neglect the self-energy ($\tau_{\mathrm{e}}|\Sigma_{\nu\nu'}| \ll 1$), we obtain

$$\xi^{(1)}_{\boldsymbol{k}_j\nu_j}(t) = \Lambda(\boldsymbol{k}_j\nu_j, \boldsymbol{k}'_j)tE^{\mathrm{e}}_j \exp(-\mathrm{i}\omega_j t)\,, \qquad j = 1, 2\,, \quad 0 < t < \tau_{\mathrm{e}}\,. \tag{4.19}$$

This leads in particular to the initial condition for the delay period

$$\xi^{(1)}_{\boldsymbol{k}_j\nu_j}(\tau_{\mathrm{e}}) = \Lambda(\boldsymbol{k}_j\nu_j, \boldsymbol{k}'_j)\tau_{\mathrm{e}}E^{\mathrm{e}}_j \exp(-\mathrm{i}\omega_j\tau_{\mathrm{e}})\,. \tag{4.20}$$

More directly relevant to the description of the TG, are the initial conditions for the two-particle variables $\Xi^{(2)}_{\nu\nu'}(\boldsymbol{k}_{\mathrm{g}}, \boldsymbol{p}, t)$. Using eq. (4.19) in eq. (4.16) and neglecting the self-energy contributions during the pulses, we obtain

$$\Xi^{(2)}_{\nu\nu'}(\boldsymbol{k}_{\mathrm{g}}, \boldsymbol{p}, \tau_{\mathrm{e}}) = \Lambda(\boldsymbol{k}_1\nu_1, \boldsymbol{k}'_1)\Lambda^*(\boldsymbol{k}_2\nu_2, \boldsymbol{k}'_2)E^{\mathrm{e}}_1E^{\mathrm{e}*}_2\tau^2_{\mathrm{e}} \exp[\mathrm{i}(\omega_2 - \omega_1)\tau_{\mathrm{e}}]\,\delta_{\boldsymbol{p}\boldsymbol{p}_{\mathrm{g}}}\,, \tag{4.21}$$

with $\boldsymbol{p}_{\mathrm{g}} \equiv (\boldsymbol{k}_1 + \boldsymbol{k}_2)/2$. Note that this result is consistent with the factorization $\langle \hat{\xi}^{\dagger}_{\boldsymbol{k}'\nu'}(t)\xi_{\boldsymbol{k}\nu}(t)\rangle^{(2)} = \langle \hat{\xi}^{\dagger}_{\boldsymbol{k}'\nu'}(t)\rangle^{(1)}\langle \xi_{\boldsymbol{k}\nu}(t)\rangle^{(1)}$ during the pulses, which results from the fact that phonon scattering can be neglected for these early times. An analogous factorization has been used in section 3.4 to determine the initial two-particle exciton variables.

In summary, the TG signal can, in principle, be calculated from eqs. (4.18) and (4.14) after solving the coupled equations of motion (4.16) for the two-particle variables $\Xi^{(2)}_{\nu\nu'}(\boldsymbol{k}_g, \boldsymbol{p}, t)$ (for all $\boldsymbol{p}$ and with $\boldsymbol{k}_g \equiv \boldsymbol{k}_1 - \boldsymbol{k}_2$ fixed) during the pump-probe delay period. During this period, the last two terms in eq. (4.16) are absent (no external fields) and the initial condition for this period is given by eq. (4.21). In practice, we have to restrict the treatment to simple models for the self-energy (or scattering) kernel to find analytic expressions for the signal. Before discussing such models, we give a general result. In the absence of scattering (low temperature), the TG signal does not decay. Namely, the solution of eq. (4.16) for $\boldsymbol{k} = \boldsymbol{k}_g$ is in this case trivially given by the initial condition (4.21) with an additional phase factor $\exp[i(\omega_2 - \omega_1)\tau]$. As this factor gives the only τ dependence of $W(\boldsymbol{k}_g, \tau)$, the signal does not depend on τ at all. It should be noted that this result does not rely on the approximation eq. (4.14), but also holds if the complete form eq. (4.12) for the exciton population is used. The physical explanation is, of course, that the initially created polariton coherence (eq. 4.21) is an eigenstate of the system in the absence of scattering.

We now discuss two specific models for the phonon-induced scattering kernel $\Sigma(\boldsymbol{k}, \nu; \boldsymbol{p}, \boldsymbol{p}')$ in eq. (4.16), for which analytic results can be obtained. In the exciton theory, we used the Haken–Strobl model. As discussed in section 3.5, this is a (high-temperature) strong-collision model that scatters all excitons into each other with equal rate $\hat{\Gamma}$, irrespective of their energies. Using the same model for polaritons would be very unrealistic. First, because these excitations span an enormous bandwidth. Second, it is only the exciton component of the polariton that couples directly to phonons, so that photon-like polaritons cannot be scattered very strongly. A simple model that takes these considerations into account, is a *restricted Haken–Strobl model*, which is defined as follows. All polaritons with exciton components $|x_{k\nu}|^2 > \frac{1}{2}$ scatter into each other with equal rate $\hat{\Gamma}_p$, whereas all other (photon-like) polaritons do not take part in the scattering process at all. This model boils down to the Haken–Strobl model for the restricted set of exciton-like polaritons, which (section 4.1) constitute the upper polariton branch for $|\boldsymbol{k}| < k_0$ and the lower branch for $|\boldsymbol{k}| > k_0$ ($k_0 \approx \Omega_0/c$ marks the photon–exciton band crossing). We thus consider only one effective branch (i.e., only one polariton per wave vector) with width f (fig. 7), so that branch labels can be dropped without ambiguity.

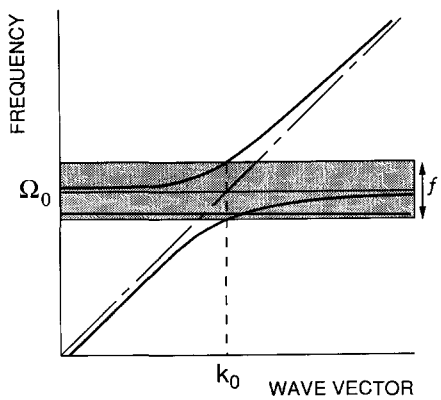

Fig. 7. Illustration of the restricted Haken–Strobl scattering model for polaritons. All polaritons within the shaded region of width f (eq. 4.6) have exciton components greater than $\frac{1}{2}$ (section 4.1) and are assumed to scatter into each other with equal rates. Ω_0 is the exciton frequency at zero (optical) wave vector and $k_0 = \Omega_0/c$ indicates the exciton–photon (dashed diagonal) band crossing. The polariton stopgap is not shown and exciton dispersion has been neglected.

In the Laplace domain, eq. (4.16) for $\boldsymbol{k} = \boldsymbol{k}_g$ now takes the form

$$s\Xi^{(2)}(\boldsymbol{k}_g, \boldsymbol{p}, s) = [\mathrm{i}\omega_{\boldsymbol{p}-\boldsymbol{k}_g/2} - \mathrm{i}\omega_{\boldsymbol{p}+\boldsymbol{k}_g/2} - (\hat{\Gamma}_p + \gamma_p)]\Xi^{(2)}(\boldsymbol{k}_g, \boldsymbol{p}, s) + (\hat{\Gamma}_p/N)\sum_{\boldsymbol{p}'}\Xi^{(2)}(\boldsymbol{k}_g, \boldsymbol{p}', s) + \Xi^{(2)}(\boldsymbol{k}_g, \boldsymbol{p}, t=0)\,, \tag{4.22a}$$

with the initial condition

$$\Xi^{(2)}(\boldsymbol{k}_g, \boldsymbol{p}, t=0) \propto E_1^e E_2^{e*}\delta_{\boldsymbol{p}\boldsymbol{p}_g}\,. \tag{4.22b}$$

Here we assumed that initially exciton-like polaritons are excited. In eq. (4.22a) we added an overall loss of polaritons with rate γ_p. The equation of motion is identical to eq. (3.43), except that the exciton dispersion and scattering rates are replaced by those for the polaritons. The solution for the $\Xi^{(2)}(\boldsymbol{k}_g, \boldsymbol{p}, s)$ is, therefore, easily obtained by analogy to the solution in section 3. In calculating the signal from this solution, we use one more approximation, namely we replace eq. (4.14) by

$$W^{(2)}(\boldsymbol{k}_g, s) \approx (2/N)\sum_{\boldsymbol{p}}\Xi^{(2)}(\boldsymbol{k}_g, \boldsymbol{p}, s)\,. \tag{4.23}$$

We thus approximate all polariton transformation coefficients $x_{k\nu}$ for the exciton-like polaritons by unity. Admittedly, this is a strong discretization of the exciton character, but in view of the very simple scattering model, it seems unnecessary to account in a more rigorous way for these coefficients. The solution for $W(\boldsymbol{k}_g, s)$ is now of the same form as eq. (3.46b), with $\hat{\Gamma} \to \hat{\Gamma}_p$, $\gamma \to \gamma_p$, and $\mathcal{J}(\boldsymbol{p}) \to \omega_{\boldsymbol{p}-\boldsymbol{k}_g/2} - \omega_{\boldsymbol{p}+\boldsymbol{k}_g/2}$. In the coherent limit ($\hat{\Gamma}_p = 0$), this yields for the signal

$$S(\tau) = \exp(-2\gamma_p\tau) \quad \text{(coherent)}\,, \tag{4.24}$$

which agrees with our general conclusion that in the absence of scattering the signal does not decay (apart from the trivial population loss with rate $2\gamma_p$). In the opposite limit of strong scattering ($\hat{\Gamma}_p \gg |\omega_{\boldsymbol{p}-\boldsymbol{k}_g/2} - \omega_{\boldsymbol{p}+\boldsymbol{k}_g/2}|, \gamma_p$) we obtain, in analogy to eq. (3.49),

$$S(\tau) = \exp[-2(\gamma_p + D_p|\boldsymbol{k}_1 - \boldsymbol{k}_2|^2)\tau] \quad \text{(incoherent)}\,, \tag{4.25}$$

with the polariton diffusion constant (tensor)

$$D_p \equiv \frac{1}{|\boldsymbol{k}_g|^2}\frac{1}{\hat{\Gamma}_p N}\sum_{\boldsymbol{p}}(\omega_{\boldsymbol{p}-\boldsymbol{k}_g/2} - \omega_{\boldsymbol{p}+\boldsymbol{k}_g/2})^2\,. \tag{4.26}$$

Here, we assumed that $\omega_{\boldsymbol{k}_1} = \omega_{\boldsymbol{k}_2}$, which holds under general symmetry conditions with respect to the experimental setup.

Equation (4.26) can be rewritten using the polariton group velocity $\boldsymbol{v}_p(\boldsymbol{p}) \equiv \nabla_{\boldsymbol{p}}\omega_{\boldsymbol{p}}$ [cf. eq. (3.38a)]. For an isotropic d-dimensional system, $\omega_{\boldsymbol{p}}$ is a function of $|\boldsymbol{p}|$ only and we have

$$D_p \approx \frac{1}{d\hat{\Gamma}_p}\frac{1}{N}\sum_{\boldsymbol{p}} v_p^2(\boldsymbol{p}) \equiv \frac{1}{d\hat{\Gamma}_p}\bar{v}_p^2\,, \tag{4.27}$$

with $\bar{v}_p$ an effective polariton group velocity. As polaritons have a photon component, it is clear that $\bar{v}_p$ is larger than the effective exciton group velocity $\bar{v}_e$ (eq. 3.38b) for the same system. Thus, ignoring possible differences in the exciton and polariton scattering rates, the general effect of polaritons on the TG will be to accelerate the decay. An estimate for $\bar{v}_p$ is calculated in appendix D, within the infinite effective exciton-mass approximation ($\bar{v}_e = 0$ then!) on a simple cubic lattice. We find

$$(\bar{v}_p/c)^2 \approx \pi(f/\Omega)(a/\lambda_0)^3 , \tag{4.28}$$

with a the lattice constant and $\lambda_0 = 2\pi c/\Omega$ the vacuum wavelength corresponding to the molecular transition.

Although, strictly speaking, our crystal model is oversimplified to fully represent aromatic molecular crystals, it is tempting to use eq. (4.28) also for this class of crystals by replacing a^3 by the volume of a unit cell. We then obtain $\bar{v}_p \approx 2 \times 10^5$ cm/s and $\bar{v}_p \approx 10^6$ cm/s for the lowest singlet a-transitions in naphthalene and anthracene, respectively. (For f and Ω, we used the values given in section 4.1; for a^3, we used 400 Å^3 for naphthalene and 600 Å^3 in the case of anthracene.) This result for anthracene is an order of magnitude larger than the estimate made by Agranovich et al. [51] for the relevant polariton group velocity (see below). In view of the simple model and the approximations used, it is not surprising to find such a large discrepancy.

The situation in anthracene is probably much better described by the second scattering model that we wish to discuss here: the *bottleneck model*. This model is inspired by the explanation by Agranovich et al. [51, 52] for the TG experiments on anthracene crystals carried out by Rose et al. [2b]. Let the experiment be such that the two pump pulses have frequencies just in the exciton band, so that they excite first-order polaritons with high wave vector and strong exciton character (fig. 8). Accounting for a positive effective exciton mass, it is reasonable to assume that at low temperature, polariton–phonon scattering will cause the initially created polaritons to relax rapidly to the bottleneck region, where the

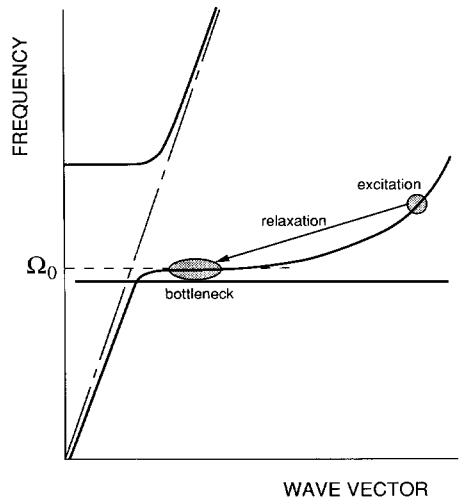

Fig. 8. Illustration of the bottleneck model for polariton scattering. Compared to fig. 7, a larger part of the Brillouin zone is shown and a finite (positive) effective exciton mass has been included. High wave-vector polaritons in the lower branch are excited by pulses with frequencies just above Ω_0 (the zero wave-vector exciton frequency) and rapidly relax to the polariton bottleneck, where the actual TG decay takes place.

density of states levels off. This classical (particle) picture translates into the following model for rapid initial relaxation of the polariton coherences $\Xi(\boldsymbol{k}, \boldsymbol{p}, t)$.

(i) The polariton center-of-mass wave vector $\boldsymbol{k}$ is conserved at its initial value $\boldsymbol{k}_g = \boldsymbol{k}_1 - \boldsymbol{k}_2$; we have obtained this previously as a general result for phonon-induced scattering processes. This is equivalent to the assumption in ref. [52] that during the rapid relaxation process, the spatial density of polaritons created by the interfering pump pulses is unchanged.

(ii) $\boldsymbol{p}$ relaxes rapidly to the bottleneck region. This is equivalent to the statement in ref. [52] that the polariton momentum (wave vector) relaxes rapidly. In general, $\boldsymbol{p}$ must be expected to be distributed over the entire bottleneck region after the relaxation, because many scattering steps involving many different phonons can take place during this process [52]. We note that the classical interpretation of $\boldsymbol{p}$ as the polariton momentum that relaxes to the bottleneck, only makes sense if $|\boldsymbol{k}_g/2|$ is small compared to the wave-vector width of the bottleneck region. Only then does the coherence $\Xi(\boldsymbol{k}_g, \boldsymbol{p}, t)$ involve two polaritons with wave vectors $\boldsymbol{p} \pm \boldsymbol{k}_g/2$ that also lie within the bottleneck region. For the experiments on anthracene, this is indeed the case, as these were carried out at very small cross angles Θ of the pump pulses, so that the grating wave number was always much less than optical wave numbers [2b].

If the initial relaxation is fast enough, the observed part of the TG decay now starts from a new initial condition for the coherences within the bottleneck. We will assume that within the bottleneck all polaritons scatter into each other with rate $\hat{\Gamma}_p$ and that there is an overall loss of polaritons with rate γ_p. Like the first scattering model that we discussed, this defines a restricted Haken–Strobl model, for which the equation of motion (4.16) can be solved analytically. To calculate the signal from this solution, we use eq. (4.23), which is a good approximation in the bottleneck, because the coefficients $|x_{k\nu}|$ are close to unity there. Nevertheless, the polariton group velocity may differ appreciably from the bare exciton group velocity [60]. Let v_b denote the typical group velocity in the bottleneck region. If $\hat{\Gamma}_p \gg |\boldsymbol{k}_g| v_b$, the polariton motion is diffusive on the length scale of the grating and we recover eq. (4.25) for the signal, with the diffusion constant eq. (4.27), except that the effective group velocity $\bar{v}_p$ is replaced by v_b.

This result is independent of the exact initial condition within the bottleneck; such an insensitivity to the initial condition was also noted in the strong scattering limit of the exciton theory (section 3.4). The present expression for the signal was also used by Agranovich et al. [51, 52]; our approach shows how to derive it microscopically. For anthracene, $v_b \approx 10^5$ cm/s; combining this with a scattering length $v_b/\hat{\Gamma}_p \approx 10^{-5}$ cm (estimated from absorption data), one arrives at $D_p \approx 1\ \mathrm{cm}^2/\mathrm{s}$ [51], which agrees with the observed values [2b].

We conclude the discussion of the bottleneck model by noting that in the limit of weak scattering, $\hat{\Gamma}_p \ll |\boldsymbol{k}_g| v_b$, the initial condition is in general important for the form of the TG signal. Decay will always occur, even if $\hat{\Gamma}_p = \gamma_p = 0$, because the initially populated coherences $\Xi(\boldsymbol{k}_g, \boldsymbol{p}, t)$ for different $\boldsymbol{p}$ values in the bottleneck will dephase with respect to each other.

4.4. *Polariton effects in frequency-domain four-wave mixing*

In this section we discuss the degenerate four-wave mixing experiment in terms of polaritons. Two cw external electric fields with wave vectors $\boldsymbol{k}'_j$, frequencies ω_j, and amplitudes E^e_j $(j = 1, 2)$ are incident on the crystal and we are interested in the signal with wave vector $\boldsymbol{k}'_s = 2\boldsymbol{k}'_1 - \boldsymbol{k}'_2$ and frequency $\omega_s = 2\omega_1 - \omega_2$. The amplitude of this signal is proportional to the amplitude of the polariton with wave vector $\boldsymbol{k}_s = 2\boldsymbol{k}_1 - \boldsymbol{k}_2$ that is generated nonlinearly in the crystal by the first-order polaritons with wave vectors $\boldsymbol{k}_1$ and $\boldsymbol{k}_2$. Our description is based on the temporal Fourier transforms of the two-particle

polariton hierarchy eqs. (4.13a) and (4.16). We will confine ourselves to the restricted Haken–Strobl model introduced in section 4.3, and, as in the exciton theory of section 3.3, we will only calculate contributions to the signal with possible resonances at $\omega_{12} \equiv \omega_1 - \omega_2 = 0$.

From the Fourier transform of eq. (4.13a) we find for the signal amplitude to third order in the field amplitudes

$$\xi^{(3)}_{k_s\nu_s}(\omega_s) \propto (x_{k_s\nu_s} - z_{k_s\nu_s})\gamma(k_1\nu_1)\xi^{(1)}_{k_1\nu_1}(\omega_1)\sum_p \Xi^{(2)}(k_g, p, \omega_{12}), \tag{4.29}$$

where we used eq. (4.23) and $k_g = k_1 - k_2$, as before. The two-particle variables for different momenta p obey coupled equations of motion that are obtained from eq. (4.16) with the restricted Haken–Strobl scattering model,

$$-i\omega_{12}\Xi^{(2)}(k_g, p, \omega_{12}) = [i(\omega_{p-k_g/2} - \omega_{p+k_g/2}) - (\hat{\Gamma}_p + \gamma_p)]\Xi^{(2)}(k_g, p, \omega_{12}) + \frac{\hat{\Gamma}_p}{N}\sum_{p'}\Xi^{(2)}(k_g, p', \omega_{12})$$
$$+ [\xi^{(1)*}_{k_2\nu_2}(\omega_2)\Lambda(k_1\nu_1, k_1')E_1^e + \xi^{(1)}_{k_1\nu_1}(\omega_1)\Lambda^*(k_2\nu_2, k_2')E_2^{e*}]\delta_{pp_g}, \tag{4.30}$$

$p_g \equiv (k_1 + k_2)/2$.

This equation is solved in the standard way (appendix B) and after substituting the first-order polariton amplitudes from the linear approximation to eq. (4.13a), we obtain

$$\xi^{(3)}_{k_s\nu_s}(\omega_s) \propto (x_{k_s\nu_s} - z_{k_s\nu_s})\frac{\gamma(k_1\nu_1)\Lambda^2(k_1\nu_1, k_1')\Lambda^*(k_2\nu_2, k_2')(E_1^e)^2E_2^{e*}}{-i\omega_{12} - i(\omega_{k_2} - \omega_{k_1}) + \hat{\Gamma}_p + \gamma_p}$$
$$\times\left(1 - \frac{\hat{\Gamma}_p}{N}\sum_p(-i\omega_{12} - i\omega_{p-k_g/2} + i\omega_{p+k_g/2} + \hat{\Gamma}_p + \gamma_p)^{-1}\right)^{-1}. \tag{4.31}$$

We will assume that the second factor on the r.h.s. has no sharp dependence on ω_{12}. For excitons, this was found as a result of cancellations between the source σ_R and the quantity $-i\omega_{12} - i[J(k_2) - J(k_1)] + \hat{\Gamma} + \gamma$ in eq. (3.32). In the present case, $i\sigma_R$ is replaced by the factor multiplying δ_{pp_g} in eq. (4.30), and a cancellation is not likely, even though we have no detailed form for $\Lambda(k\nu, k')$. Note, however, that $\omega_1 = \omega_{k_1}$ and $\omega_2 = \omega_{k_2}$, as the frequencies of the first-order polaritons have to equal the frequencies of the external fields. This is an essential difference with the exciton theory.

We thus conclude that the first denominator on the r.h.s. of eq. (4.31) does not depend on ω_{12} at all! Any ω_{12}-resonance must emerge from the last factor,

$$R(k_g, \omega_{12}) \equiv \left(1 - \frac{\hat{\Gamma}_p}{N}\sum_p(-i\omega_{12} - i\omega_{p-k_g/2} + i\omega_{p+k_g/2} + \hat{\Gamma}_p + \gamma_p)^{-1}\right)^{-1}. \tag{4.32}$$

For $\hat{\Gamma}_p = 0$, we have $R(k_g, \omega_{12}) = 1$, so that no ω_{12}-resonance is found. Conversely, in the limit of strong dephasing ($\hat{\Gamma}_p \gg \gamma_p$, $|\omega_{p-k_g/2} - \omega_{p+k_g/2}|$), we find (cf. appendix C),

$$R(k_g, \omega_{12}) = 1 + \hat{\Gamma}_p/(-i\omega_{12} + \gamma_p + D_p k_g^2), \tag{4.33}$$

with D_p the polariton diffusion constant as defined in eq. (4.26). The intensity of the D4WM signal, $\sim|\xi^{(3)}_{k_s\nu_s}|^2 \sim |R(\boldsymbol{k}_g, \omega_{12})|^2$, then exhibits a Lorentzian resonance analogous to the one in eq. (3.35) (replace $\hat{\Gamma} \to \hat{\Gamma}_p$, $\gamma \to \gamma_p$, $D_e \to D_p$). Comparing this with our results in section 4.3, we also conclude that, as in the exciton case, the amplitude of the D4WM signal is related to the amplitude of the TG signal by a single Fourier transform.

5. Concluding remarks

The calculation of the nonlinear optical response in condensed phases is a complicated many-body problem involving the material and the radiation-field degrees of freedom. Numerous approximate schemes have been developed over the years with various degrees of sophistication in order to calculate optical nonlinearities [19–23, 70, 71, 92]. The present review provides a unified theoretical description which clarifies the interrelationships among the different schemes and their range of validity. Figure 9 illustrates the systematic hierarchy of approximations. Starting with the multipolar Hamiltonian [73] which is fully retarded and contains no explicit intermolecular interactions, we can rigorously derive

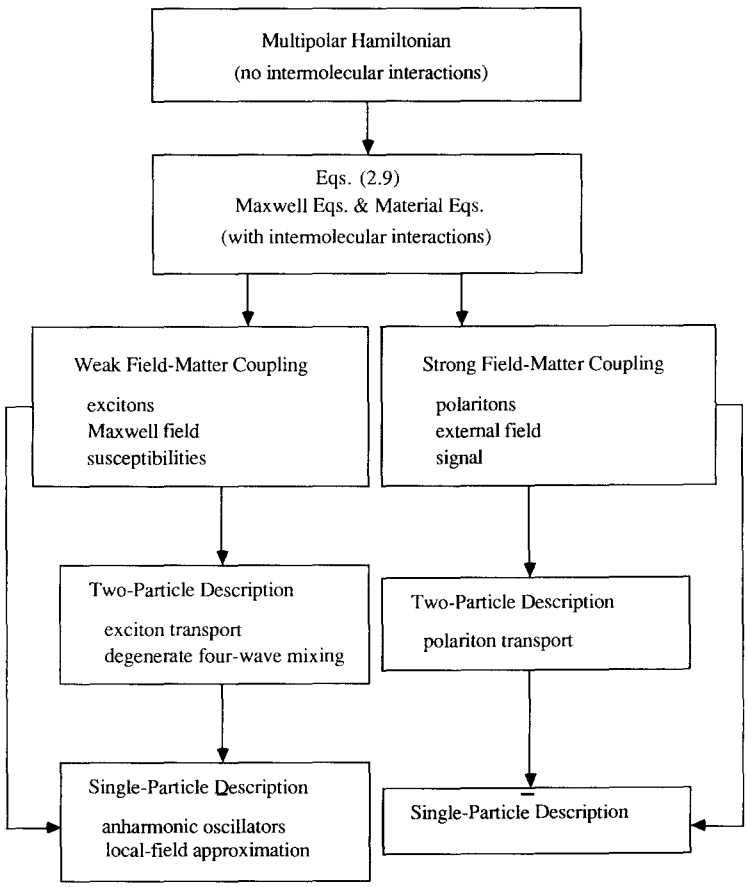

Fig. 9. Schematic diagram showing the hierarchy of approximations used in this paper.

Heisenberg equations of motion (eq. 2.9) in which intermolecular forces are explicitly included [76]. Equation (2.9), which applies to any material and field operator $\hat{Q}$, is the starting point for the present microscopic theory. For $\hat{Q} = \hat{E}$, we get the Maxwell equation (eq. 4.3b). In simple single-molecule theories of nonlinear response, one often uses the Schrödinger picture and solves for the density matrix [19–23]. This procedure is impractical for complex many-body systems, since the complete many-body density matrix is very complicated and contains too much information. The Heisenberg equations, on the other hand, allow the direct calculation of the relevant observables.

At this point, as shown in fig. 9, we should follow two separate routes, depending on the radiation–matter coupling strength (f). The key parameter is $f/\Gamma(\boldsymbol{k})$. The exciton dephasing rate $\Gamma(\boldsymbol{k})$ may be obtained from linear optical measurements [see eq. (3.12b)]. If it is sufficiently large [$\Gamma(\boldsymbol{k}) \gg f$], it destroys the coherence between the radiation and exciton modes, which then become weakly coupled. In this case, the material–radiation correlations can be neglected, and we may derive coupled equations for the field and the material degrees of freedom as illustrated in the left route in fig. 9 (section 3). The field satisfies the Maxwell equations whereas the material system (excitons) satisfies an infinite hierarchy of coupled equations in which the polarization $\langle \hat{P} \rangle$ is coupled to the expectation value of the Maxwell field and to higher variables such as $\langle \hat{P}\hat{W} \rangle$, which in turn couple successively to higher-order variables. By solving these equations perturbatively in the average Maxwell field $\boldsymbol{E}$, we obtain the optical susceptibilities $\chi^{(1)}$, $\chi^{(3)}$, etc.

The success of this method is based on the fact that the linear optical properties of the system depend only on single-particle states whereas weak nonlinearities, such as $\chi^{(3)}$ and $\chi^{(5)}$, depend only on a few particles. This situation, which is similar to the zero-temperature many-body theory [44, 81], allows us to truncate the hierarchy very early and still maintain the essential physics of the system. The simplest approximation is obtained by factorizing at the single-particle level (section 3.2). In this case, the only relevant material dynamical variables (by assumption) are the polarization variables. The nonlinear susceptibility $\chi^{(3)}$ can then be written in various equivalent forms. Within this factorization, the local-field approximation [eqs. (3.19) and (3.20)] holds, and the many-body problem reduces to essentially a single-body calculation. We further recover the coupled-oscillator expression (eq. 3.14a) with interaction-induced correction terms. At this level of description, the susceptibilities have resonances at the Frenkel exciton energies, exciton transport is not accounted for, and we cannot describe the TG or degenerate four-wave mixing experiments.

When the hierarchy is truncated at the binary (two-particle) level (sections 3.3 and 3.4), we obtain a good description of quantum transport and we can make the connection to the phenomenological macroscopic treatments of the grating experiment which use master equations, the Boltzmann equation, and the diffusion equation (section 3.5). The single Fourier-transform relation between the TG and its frequency-domain analogue (degenerate four-wave mixing) is demonstrated.

The two-particle description illustrates the limitations of Bloembergen's classical anharmonic oscillator picture [19]. When nonlinearities are important, new dynamical variables (other than the polarization P) become relevant. The oscillator model neglects the contributions of these additional variables and requires the factorization of every variable in terms of the polarization. In our equations we choose a particular two-body factorization in which $\hat{W}$ is the source of nonlinearity. This nonlinearity is local in space (intramolecular) and seems adequate for the calculation of the TG experiment, since the signal depends on $\hat{W}$. It should be emphasized, however, that alternative sources of nonlinear evolution may be important in other situations [47, 59] (cf. section 3.1). In particular, enhanced (cooperative) optical nonlinearities, which may be observed in molecular aggregates, have been shown to originate from intermolecular (nonlocal) nonlinearities [35]. The present hierarchy is

illustrated in fig. 9. The single-particle description can be obtained directly from eqs. (2.9) (as done in section 3.2), or by factorizing the two-particle variables into products of single-particle variables.

When the oscillator strength per unit volume is sufficiently large and dephasing processes, are slow [$f \gg \Gamma(\boldsymbol{k})$], the radiation and the exciton degrees of freedom are strongly coupled, and they should be treated as a single dynamical system. In this limit, the description of optical processes in terms of polariton models is most natural (section 4) and is illustrated in the route shown on the right side in fig. 9. Although it is formally possible to define nonlinear susceptibilities even in this limit [66, 67], they are complicated and not particularly useful. In section 4 we develop a polariton hierarchy [76] which allows us to expand the nonlinear signal directly in terms of the *external* fields (rather than the *Maxwell* fields) and to abandon the notion of susceptibilities. Note that this expansion then depends on the boundary conditions relating the external field to the polaritons.

Ovander [59] has incorporated polariton effects in nonlinear optics, by expressing his total Hamiltonian, which also contains cubic and quartic terms, in terms of the polariton creation and annihilation operators. The harmonic (quadratic) part then assumes, by definition, the simple form of a set of noninteracting harmonic oscillators (the bare polaritons). The anharmonic terms yield, even for the simplest approximations of the polariton transformation, a large number of interaction terms which are responsible for nonlinear processes, and Ovander treats them as perturbations to the harmonic Hamiltonian. The Fermi golden rule is used to evaluate polariton fusion and fission rates, which are related to, e.g., the sum harmonic intensity, the Raman scattering intensity, etc., depending on the specific perturbation term under consideration. This formulation has several limitations. The resulting Hamiltonian is very complicated, the Bose approximation used for the Pauli operators results in the neglect of intramolecular nonlinearities, and the Fermi golden rule does not suffice to treat nonlinear processes of order higher than three; higher-order perturbation theory has to be used to describe these.

Our polariton hierarchy does not suffer from these difficulties. In the strong-coupling regime analyzed in section 4, the TG probes the dynamics of polaritons. Like the exciton motion, polariton dynamics can be either coherent or incoherent (diffusive), depending on the magnitude of polariton dephasing. Two conditions have to be satisfied in order for the dynamics to show diffusive polariton motion, namely, $\Gamma(\boldsymbol{k}) \ll f$ and $\hat{\Gamma}_{\mathrm{p}} \gg |\omega_{\boldsymbol{p}-\boldsymbol{k}_{\mathrm{g}}/2} - \omega_{\boldsymbol{p}+\boldsymbol{k}_{\mathrm{g}}/2}|$ (section 4.3). The exciton dephasing rate has to be sufficiently small for the elementary excitations to be polaritons and the polariton dephasing should be sufficiently large to make the motion incoherent. Both conditions can be satisfied simultaneously. A two-particle and single-particle level of approximation exists for polaritons, in complete analogy with what we derived for excitons. Since our interest is in polariton transport, which is absent in the single-particle description, we considered only the two-particle level.

An important conclusion of the present analysis is that observation of coherent exciton motion for dipolar excitons is impossible, because, when exciton damping is small enough to give coherent exciton motion, the radiation modes are necessarily strongly coupled with the polarization, so that polariton effects become significant. Coherent exciton motion over distances greater than the optical wavelength is therefore an unrealistic and oversimplified model of elementary excitations in molecular crystals at low temperatures.

The present formulation and equations of motion can be directly used and extended to treat optical nonlinearities in other systems. There is currently a growing interest in the optical properties of nanostructures [108–113]. These are fabricated molecular assemblies with specific molecular-level order. Examples are clusters, monolayers and multilayers. Our equations of motion are ideally suited for the microscopic calculations of optical nonlinearities in these systems. Other interesting extensions of the present formulation involve the incorporation of short-range forces and static and dynamical

disorder [82]. This is important for calculating optical nonlinearities in doped glasses, polymers, solutions, and in mixed crystals.

Acknowledgements

J.K. acknowledges support by the Netherlands Organization for Scientific Research (NWO) through the award of a Huygens Fellowship. S.M. acknowledges the Camille and Henry Dreyfus Foundation. The support of the Air Force Office of Scientific Research, the National Science Foundation and the Petroleum Research Fund, administered by the American Chemical Society, is gratefully acknowledged. We wish to thank Professor V.M. Agranovich for useful comments. Finally, we thank Rose Marie Ferreri and Arlene Bristol for the careful typing of the manuscript.

Appendix A. Elimination of phonon degrees of freedom

In this appendix we discuss the elimination of phonon variables underlying the various self-energy and scattering kernels for excitons and polaritons given in sections 3 and 4, respectively. To this end, several approaches can be used, which do not differ essentially in their results [42, 68, 114]. Here we use the projection-operator technique which was also employed in ref. [68]. The relevant Hamiltonian for our problem reads

$$\hat{H} = \hat{H}_{\rm s} + \hat{H}_{\rm ph} + \hat{H}_{\rm sp} \,. \tag{A.1}$$

Here $\hat{H}_{\rm s}$ stands for the "system" Hamiltonian. To describe the scattering of excitons on phonons (section 3), we choose the exciton Hamiltonian for $\hat{H}_{\rm s}$,

$$\hat{H}_{\rm s} = \hbar \sum_{k} \Omega_k \hat{B}_k^{\dagger} \hat{B}_k \,. \tag{A.2a}$$

(We use the Heitler–London approximation in this appendix.) To describe polariton–phonon scattering (section 4), we choose

$$\hat{H}_{\rm s} = \hbar \sum_{k\nu} \omega_{k\nu} \hat{\xi}_{k\nu}^{\dagger} \hat{\xi}_{k\nu} \,, \tag{A.2b}$$

with $\omega_{k\nu}$ the polariton dispersion in the absence of exciton damping [$\Gamma(k) = 0$ in eq. (4.6)]. Both excitons and polaritons are treated as bosons in the calculation of the self-energies. The phonons constitute a "bath" and are described by the Hamiltonian $\hat{H}_{\rm ph}$ (eq. 2.13). Finally, $\hat{H}_{\rm sp}$ denotes the system–bath interaction (eq. 2.14). If we take the polaritons as the system, $\hat{H}_{\rm sp}$ has to be expressed in terms of polariton operators, which is done using the inverse polariton transformation eq. (4.9b); it is customary to make the approximation $z_{k\nu} = 0$ when doing this [60a, 68, 80].

We will work in the Schrödinger picture and define $\hat{\rho}(t)$ to be the total density operator of the system and the bath. We now define a projection onto a reduced density operator by [68, 115]

$$\hat{\sigma}(t) \equiv \hat{\rho}_{\rm ph}^{T} \, {\rm Tr}_{\rm ph} \hat{\rho}(t) \,, \tag{A.3}$$

where $\hat{\rho}_{\rm ph}^{T}$ is the density operator for phonons in thermal equilibrium at temperature T and $\mathrm{Tr}_{\rm ph}$ traces over the phonon degrees of freedom. The details of this projection can be found in ref. [68]. In particular, it can be shown that up to second order in $\hat{H}_{\rm sp}$, the contribution from the phonon bath to the evolution of the expectation value of an arbitrary system operator $\hat{O}_{\rm s}$, is given by

$$\left(\frac{\mathrm{d}}{\mathrm{d}t}\langle\hat{O}_{\rm s}(t)\rangle\right)_{\rm ph} = -\int_{-\infty}^{t}\mathrm{d}t'\,\mathrm{Tr}[\{L_{\rm sp}\exp[\mathrm{i}L_{\rm s}(t-t')]\,L_{\rm sp}\hat{O}^{\dagger}\}^{\dagger}\hat{\sigma}(t')]\,, \tag{A.4}$$

$$\hbar L_{\rm s}\hat{O} \equiv [\hat{H}_{\rm s}, \hat{O}]_{-}\,, \qquad \hbar L_{\rm sp}\hat{O} \equiv [\hat{H}_{\rm sp}, \hat{O}]_{-}\,, \tag{A.5a, b}$$

where Tr denotes the total trace.

We first consider the exciton case and calculate the effect of the phonon bath on the variables $\langle\hat{B}_{\boldsymbol{k}}(t)\rangle$ and $\langle\hat{B}^{\dagger}_{\boldsymbol{k}'}(t)\hat{B}_{\boldsymbol{k}}(t)\rangle$. For $\langle\hat{B}_{\boldsymbol{k}}(t)\rangle$, the result is readily obtained from the scattering contribution to $\langle\hat{\xi}_{\boldsymbol{k}\nu}(t)\rangle$ that was derived in appendix A of ref. [68]. To this end, we drop the branch-labels and -sums in that derivation, we replace the polariton dispersion by the exciton dispersion and we set all polariton transformation coefficients $x_{\boldsymbol{k}\nu}$ equal to unity. Without further derivation we give the result within the Markov approximation, keeping both the frequency shift and width,

$$[(\mathrm{d}/\mathrm{d}t)\langle\hat{B}_{\boldsymbol{k}}(t)\rangle]_{\rm ph} = -\mathrm{i}\Sigma(\boldsymbol{k})\langle\hat{B}_{\boldsymbol{k}}(t)\rangle\,, \tag{A.6a}$$

with the complex self-energy

$$\Sigma(\boldsymbol{k}) \equiv -\frac{1}{\hbar^2 N}\lim_{\eta\to 0^{+}}\sum_{\boldsymbol{q}s}|\tilde{F}_s(\boldsymbol{k},\boldsymbol{q})|^2\left(\frac{\langle n_{\boldsymbol{q}s}\rangle_{\rm T}}{\Omega_{\boldsymbol{k}+\boldsymbol{q}}-\Omega_{\boldsymbol{k}}-\bar{\Omega}_{\boldsymbol{q}s}-\mathrm{i}\eta}+\frac{\langle n_{-\boldsymbol{q}s}+1\rangle_{\rm T}}{\Omega_{\boldsymbol{k}+\boldsymbol{q}}-\Omega_{\boldsymbol{k}}+\bar{\Omega}_{-\boldsymbol{q}s}-\mathrm{i}\eta}\right),$$
$$\tilde{F}_s(\boldsymbol{k},\boldsymbol{q}) \equiv F_s(\boldsymbol{k},\boldsymbol{q})+\chi_s(\boldsymbol{q})\,. \tag{A.6b}$$

Here $\langle n_{\boldsymbol{q}s}\rangle_{\rm T}$ is the thermal (Bose–Einstein) occupation of phonons with wave number $\boldsymbol{q}$ in branch s. We note that this result can also be derived on the operator level [114], which we used in eq. (3.1). Taking the limit $\eta\to 0^{+}$ explicitly, we arrive at eqs. (3.3) for the phonon-induced frequency shift and damping rate of the exciton. Of course, $\langle\hat{B}^{\dagger}_{\boldsymbol{k}}(t)\rangle$ obeys eq. (A.6a) with $\Sigma(\boldsymbol{k})$ replaced by $-\Sigma^{*}(\boldsymbol{k})$ [$\Sigma^{*}(\boldsymbol{k})$ denotes the complex conjugate of $\Sigma(\boldsymbol{k})$].

We now briefly outline the derivation of the phonon contribution to the evolution of the exciton coherence $\langle\hat{B}^{\dagger}_{\boldsymbol{k}'}(t)\hat{B}_{\boldsymbol{k}}(t)\rangle$, which we need in section 3.3. We take $\hat{O}_{\rm s}=\hat{B}^{\dagger}_{\boldsymbol{k}'}\hat{B}_{\boldsymbol{k}}$ in eq. (A.4), and straightforward algebra leads to ($\tau\equiv t-t'$)

$$L_{\rm sp}\exp(\mathrm{i}L_{\rm s}\tau)\,L_{\rm sp}(\hat{B}^{\dagger}_{\boldsymbol{k}}\hat{B}_{\boldsymbol{k}'}) = \frac{1}{\hbar\sqrt{N}}\sum_{\boldsymbol{q},s}\tilde{F}_s(\boldsymbol{k},\boldsymbol{q})\exp[\mathrm{i}(\Omega_{\boldsymbol{k}+\boldsymbol{q}}-\Omega_{\boldsymbol{k}'})\tau]\,L_{\rm sp}[\hat{B}^{\dagger}_{\boldsymbol{k}+\boldsymbol{q}}\hat{B}_{\boldsymbol{k}'}\hat{X}_{\boldsymbol{q}s}(\tau)]$$
$$-\frac{1}{\hbar\sqrt{N}}\sum_{\boldsymbol{q},s}\tilde{F}_s(\boldsymbol{k}'-\boldsymbol{q},\boldsymbol{q})\exp[\mathrm{i}(\Omega_{\boldsymbol{k}}-\Omega_{\boldsymbol{k}'-\boldsymbol{q}})\tau]\,L_{\rm sp}[\hat{B}^{\dagger}_{\boldsymbol{k}}\hat{B}_{\boldsymbol{k}'-\boldsymbol{q}}\hat{X}_{\boldsymbol{q}s}(\tau)]\,, \tag{A.7a}$$

$$\hat{X}_{\boldsymbol{q}s}(\tau) \equiv \hat{b}_{\boldsymbol{q}s}\exp(-\mathrm{i}\bar{\Omega}_{\boldsymbol{q}s}\tau)+\hat{b}^{\dagger}_{-\boldsymbol{q}s}\exp(\mathrm{i}\bar{\Omega}_{-\boldsymbol{q}s}\tau)\,. \tag{A.7b}$$

For the commutators appearing in the r.h.s. of eq. (A.7a) we obtain

$$L_{\rm sp}[\hat{B}^{\dagger}_{k+q}\hat{B}_{k'}\hat{X}_{qs}(\tau)]$$
$$= \frac{1}{\hbar\sqrt{N}}\sum_{q',s'}[\tilde{F}_{s'}(k+q,q')\hat{B}^{\dagger}_{k+q+q'}\hat{B}_{k'} - \tilde{F}_{s'}(k'-q',q')\hat{B}^{\dagger}_{k+q}\hat{B}_{k'-q'}](\hat{b}_{q's'}+\hat{b}^{\dagger}_{-q's'})\hat{X}_{qs}(\tau)$$
$$+ \frac{1}{\hbar\sqrt{N}}\sum_{k''}\tilde{F}_{s}(k'',-q)\hat{B}^{\dagger}_{k+q}\hat{B}_{k'}\hat{B}^{\dagger}_{k''-q}\hat{B}_{k''}[\exp(\mathrm{i}\bar{\Omega}_{-qs}\tau)-\exp(-\mathrm{i}\bar{\Omega}_{qs}\tau)]\,, \tag{A.8a}$$

$$L_{\rm sp}[\hat{B}^{\dagger}_{k}\hat{B}_{k'-q}\hat{X}_{qs}(\tau)]$$
$$= \frac{1}{\hbar\sqrt{N}}\sum_{q',s'}[\tilde{F}_{s'}(k,q')\hat{B}^{\dagger}_{k+q'}\hat{B}_{k'-q} - \tilde{F}_{s'}(k'-q-q',q')\hat{B}^{\dagger}_{k}\hat{B}_{k'-q-q'}]\hat{X}_{qs}(\tau)(\hat{b}_{q's'}+\hat{b}^{\dagger}_{-q's'})$$
$$+ \frac{1}{\hbar\sqrt{N}}\sum_{k''}\tilde{F}_{s}(k'',-q)\hat{B}^{\dagger}_{k''-q}\hat{B}_{k''}\hat{B}^{\dagger}_{k}\hat{B}_{k'-q}[\exp(\mathrm{i}\bar{\Omega}_{-qs}\tau)-\exp(-\mathrm{i}\bar{\Omega}_{qs}\tau)]\,. \tag{A.8b}$$

We will neglect the last contributions (the k'' summations) in these equations, as they couple to a higher (quartic) exciton variable. We now combine eqs. (A.7) and (A.8), and after some straightforward algebra we obtain

$$\mathrm{Tr}[\{L_{\rm sp}\exp(\mathrm{i}L_{\rm s}\tau)\,L_{\rm sp}(\hat{B}^{\dagger}_{k}\hat{B}_{k'})\}^{\dagger}\hat{\sigma}(t')] = \frac{1}{\hbar^2 N}\sum_{qs}\tilde{F}^{*}_{s}(k,q)\exp[-\mathrm{i}(\Omega_{k+q}-\Omega_{k'})\tau]G(\tau)$$
$$\times[\tilde{F}^{*}_{s}(k+q,-q)\langle\hat{B}^{\dagger}_{k'}(t')\hat{B}_{k}(t')\rangle - \tilde{F}^{*}_{s}(k'+q,-q)\langle\hat{B}^{\dagger}_{k'+q}(t')\hat{B}_{k+q}(t')\rangle]$$
$$-\frac{1}{\hbar^2 N}\sum_{qs}\tilde{F}^{*}_{s}(k'+q,-q)\exp[-\mathrm{i}(\Omega_{k}-\Omega_{k'+q})\tau]G^{*}(\tau)$$
$$\times[\tilde{F}^{*}_{s}(k,q)\langle\hat{B}^{\dagger}_{k'+q}(t')\hat{B}_{k+q}(t')\rangle - \tilde{F}^{*}_{s}(k',q)\langle\hat{B}^{\dagger}_{k'}(t')\hat{B}_{k}(t')\rangle]\,, \tag{A.9}$$

$$G(\tau)\equiv\langle n_{qs}\rangle_{\rm T}\exp(\mathrm{i}\bar{\Omega}_{qs}\tau)+\langle n_{-qs}+1\rangle_{\rm T}\exp(-\mathrm{i}\bar{\Omega}_{-qs}\tau)\,. \tag{A.10}$$

Equation (A.9) combined with eq. (A.4) defines the phonon contribution to the equation of motion for $\langle\hat{B}^{\dagger}_{k'}(t)\hat{B}_{k}(t)\rangle$. This equation can be made time-local by applying a Markov approximation. To this end, we approximate [68]

$$\langle\hat{B}^{\dagger}_{k'}(t')\hat{B}_{k}(t')\rangle \approx \langle\hat{B}^{\dagger}_{k'}(t)\hat{B}_{k}(t)\rangle\exp[-\mathrm{i}(\Omega_{k'}-\Omega_{k})\tau]\,, \tag{A.11}$$

and we calculate the remaining time integrals by adding a convergence factor $\exp(-\eta\tau)$ $(\eta\to 0^{+})$. We then obtain

$$[(\mathrm{d}/\mathrm{d}t)\langle\hat{B}^{\dagger}_{k'}(t)\hat{B}_{k}(t)\rangle]_{\rm ph} = \mathrm{i}[\Sigma^{*}(k')-\Sigma(k)]\langle\hat{B}^{\dagger}_{k'}(t)\hat{B}_{k}(t)\rangle$$
$$+\mathrm{i}\sum_{q}[\tilde{\Sigma}^{*}(k',k,q)-\tilde{\Sigma}(k,k',q)]\langle\hat{B}^{\dagger}_{k'+q}(t)\hat{B}_{k+q}(t)\rangle\,, \tag{A.12}$$

with $\Sigma(\boldsymbol{k})$ as defined in eq. (A.6b) and

$$\tilde{\Sigma}(\boldsymbol{k}, \boldsymbol{k}', \boldsymbol{q}) \equiv \frac{1}{\hbar^2 N} \lim_{\eta \to 0^+} \sum_s \tilde{F}_s^*(\boldsymbol{k}, \boldsymbol{q}) \tilde{F}_s(\boldsymbol{k}', \boldsymbol{q}) \left(\frac{\langle n_{\boldsymbol{q}s} \rangle_T}{\Omega_{\boldsymbol{k}'+\boldsymbol{q}} - \Omega_{\boldsymbol{k}'} - \bar{\Omega}_{\boldsymbol{q}s} - \mathrm{i}\eta} + \frac{\langle n_{-\boldsymbol{q}s} + 1 \rangle_T}{\Omega_{\boldsymbol{k}'+\boldsymbol{q}} - \Omega_{\boldsymbol{k}'} + \bar{\Omega}_{-\boldsymbol{q}s} - \mathrm{i}\eta} \right). \tag{A.13}$$

The first r.h.s. term in eq. (A.12) simply contains the uncorrelated sum of the self-energies of $\langle \hat{B}_{\boldsymbol{k}'}^\dagger(t) \rangle$ and $\langle \hat{B}_{\boldsymbol{k}}(t) \rangle$, and is the "$T_1$"-contribution [22, 75] to the total self-energy of $\langle \hat{B}_{\boldsymbol{k}'}^\dagger(t) \hat{B}_{\boldsymbol{k}}(t) \rangle$. The second r.h.s. term in eq. (A.12) reflects correlated dynamics of the bra and the ket side of the density operator ("T_2^*" or pure dephasing contribution) [22, 75]. If we rewrite eq. (A.12) in terms of the variables $Q(\boldsymbol{k}, \boldsymbol{p}, t)$ introduced in section 3.3, we finally arrive at the phonon contributions in eq. (3.25) with the self-energy matrix eq. (3.26).

We conclude this appendix by considering the case that the polaritons constitute the system (eq. A.2b) and we give the phonon-induced self-energies for $\langle \hat{\xi}_{\boldsymbol{k}\nu}(t) \rangle$ and $\langle \hat{\xi}_{\boldsymbol{k}'\nu'}^\dagger(t) \hat{\xi}_{\boldsymbol{k}\nu}(t) \rangle$. In the approximation that the polariton transformation coefficients $z_{\boldsymbol{k}\nu} \approx 0$, the calculation is very analogous to the one for excitons, and we just give the final results,

$$\left[\frac{\mathrm{d}}{\mathrm{d}t} \langle \hat{\xi}_{\boldsymbol{k}\nu}(t) \rangle \right]_{\mathrm{ph}} = -\mathrm{i} \sum_{\nu'} \Sigma_{\nu\nu'}(\boldsymbol{k}) \langle \hat{\xi}_{\boldsymbol{k}\nu'}(t) \rangle , \tag{A.14a}$$

$$\Sigma_{\nu\nu'}(\boldsymbol{k}) \equiv -\frac{1}{\hbar^2 N} \lim_{\eta \to 0^+} \sum_{\boldsymbol{q}s} \sum_{\nu''} |F_s(\boldsymbol{k}, \boldsymbol{q})|^2 |x_{\boldsymbol{k}+\boldsymbol{q}\nu''}|^2 x_{\boldsymbol{k}\nu} x_{\boldsymbol{k}\nu'}^* \times \left(\frac{\langle n_{\boldsymbol{q}s} \rangle_T}{\omega_{\boldsymbol{k}+\boldsymbol{q}\nu''} - \omega_{\boldsymbol{k}\nu'} - \bar{\Omega}_{\boldsymbol{q}s} - \mathrm{i}\eta} + \frac{\langle n_{-\boldsymbol{q}s} + 1 \rangle_T}{\omega_{\boldsymbol{k}+\boldsymbol{q}\nu''} - \omega_{\boldsymbol{k}\nu'} + \bar{\Omega}_{-\boldsymbol{q}s} - \mathrm{i}\eta} \right); \tag{A.14b}$$

$$\left[\frac{\mathrm{d}}{\mathrm{d}t} \langle \hat{\xi}_{\boldsymbol{k}'\nu'}^\dagger(t) \hat{\xi}_{\boldsymbol{k}\nu}(t) \rangle \right]_{\mathrm{ph}} = \mathrm{i} \sum_{\nu''\nu'''} [\Sigma_{\nu'\nu'''}^*(\boldsymbol{k}') \delta_{\nu\nu''} - \Sigma_{\nu\nu''}(\boldsymbol{k}) \delta_{\nu'\nu'''}] \langle \hat{\xi}_{\boldsymbol{k}'\nu'''}^\dagger(t) \hat{\xi}_{\boldsymbol{k}\nu''}(t) \rangle + \mathrm{i} \sum_{\boldsymbol{q}} \sum_{\nu''\nu'''} [\tilde{\Sigma}_{\nu'\nu\nu'''\nu''}^*(\boldsymbol{k}', \boldsymbol{k}, \boldsymbol{q}) - \tilde{\Sigma}_{\nu\nu'\nu''\nu'''}(\boldsymbol{k}, \boldsymbol{k}', \boldsymbol{q})] \langle \hat{\xi}_{\boldsymbol{k}'+\boldsymbol{q}\nu'''}^\dagger(t) \hat{\xi}_{\boldsymbol{k}+\boldsymbol{q}\nu''}(t) \rangle , \tag{A.15a}$$

$$\tilde{\Sigma}_{\nu\nu'\nu''\nu'''}(\boldsymbol{k}, \boldsymbol{k}', \boldsymbol{q}) \equiv \frac{1}{\hbar^2 N} \lim_{\eta \to 0^+} \sum_s \tilde{F}_s^*(\boldsymbol{k}, \boldsymbol{q}) \tilde{F}_s(\boldsymbol{k}', \boldsymbol{q}) x_{\boldsymbol{k}\nu} x_{\boldsymbol{k}+\boldsymbol{q}\nu''}^* x_{\boldsymbol{k}'\nu'}^* x_{\boldsymbol{k}'+\boldsymbol{q}\nu'''} \times \left(\frac{\langle n_{\boldsymbol{q}s} \rangle_T}{\omega_{\boldsymbol{k}'+\boldsymbol{q}\nu'''} - \omega_{\boldsymbol{k}'\nu'} - \bar{\Omega}_{\boldsymbol{q}s} - \mathrm{i}\eta} + \frac{\langle n_{-\boldsymbol{q}s} + 1 \rangle_T}{\omega_{\boldsymbol{k}'+\boldsymbol{q}\nu'''} - \omega_{\boldsymbol{k}'\nu'} + \bar{\Omega}_{-\boldsymbol{q}s} - \mathrm{i}\eta} \right). \tag{A.15b}$$

Note that Eqs. (A.14b) and (A.15b) reduce to the exciton self-energies eqs. (A.6b) and (A.13), respectively, if all $x_{\boldsymbol{k}\nu}$ are set to unity, the (summations over) branch labels are dropped, and the polariton dispersion is replaced everywhere by the exciton dispersion. Equation (A.15a) for the two-particle polariton variables can be rewritten in terms of the variables $\Xi_{\nu\nu'}(\boldsymbol{k}, \boldsymbol{p}, t)$ introduced in section 4.2. This leads to the second term in eq. (4.16), with

$$\Sigma(\boldsymbol{k}, \boldsymbol{\nu}; \boldsymbol{p}, \boldsymbol{p}') \equiv [\delta_{\nu'\nu'''} \Sigma_{\nu\nu''}(\boldsymbol{p} + \boldsymbol{k}/2) - \delta_{\nu\nu''} \Sigma_{\nu'\nu'''}^*(\boldsymbol{p} - \boldsymbol{k}/2)] \delta_{\boldsymbol{p}\boldsymbol{p}'} + \tilde{\Sigma}_{\nu\nu'\nu''\nu'''}(\boldsymbol{p} + \boldsymbol{k}/2, \boldsymbol{p} - \boldsymbol{k}/2, \boldsymbol{p}' - \boldsymbol{p}) - \tilde{\Sigma}_{\nu'\nu\nu'''\nu''}^*(\boldsymbol{p} - \boldsymbol{k}/2, \boldsymbol{p} + \boldsymbol{k}/2, \boldsymbol{p}' - \boldsymbol{p}) , \tag{A.16}$$

where $\boldsymbol{\nu}$ is symbolic for $(\nu, \nu', \nu'', \nu''')$.

Appendix B. The two-particle Green function

In this appendix, we solve the equation of motion for two-particle coherences within the Haken–Strobl model. This equation is encountered in sections 3.3 (eq. 3.30), 3.4 (eq. 3.43), 4.3 (eq. 4.22) and 4.4 (eq. 4.30). For explicitness, we adhere to the problem of section 3.3; the other applications are readily translated to the notation used here. The equation of interest reads

$$-\mathrm{i}\omega Q(\boldsymbol{p},\omega) = [\mathrm{i}\mathcal{J}(\boldsymbol{p}) - (\hat{\Gamma}+\gamma)]Q(\boldsymbol{p},\omega) + (\hat{\Gamma}/N)\sum_{\boldsymbol{p}'} Q(\boldsymbol{p}',\omega) + f(\boldsymbol{p})\,, \tag{B.1}$$

where we defined

$$\mathcal{J}(\boldsymbol{p}) \equiv J(\boldsymbol{p}-\boldsymbol{k}_{\mathrm{g}}/2) - J(\boldsymbol{p}+\boldsymbol{k}_{\mathrm{g}}/2)\,. \tag{B.2}$$

The variable $\boldsymbol{k}_{\mathrm{g}}$ is suppressed in all quantities, as the equation of motion is trivial with respect to it ($\boldsymbol{k}_{\mathrm{g}}$ is conserved). The ω-dependence is indicated explicitly, as this variable is independent of $\boldsymbol{k}_{\mathrm{g}}$ in the time-resolved applications (sections 3.4 and 4.3). Finally, we assumed a general source $f(\boldsymbol{p})$.

For one-dimensional systems, eq. (B.1) has been solved by Haken and Strobl [88], Reineker [54], and Garrity and Skinner [55], using eigenvector analysis. In this appendix, we will solve eq. (B.1) using the Green function method of ref. [40]. The problem in the equation is the second right-hand side term, which results from pure dephasing processes ($\sim\hat{\Gamma}$). In the absence of this term, the equation is diagonal in $\boldsymbol{p}$ and trivial to solve:

$$Q^0(\boldsymbol{p},\omega) \equiv G^0_{\boldsymbol{p}}(\omega) f(\boldsymbol{p})\,, \quad G^0_{\boldsymbol{p}}(\omega) = [-\mathrm{i}\omega - \mathrm{i}\mathcal{J}(\boldsymbol{p}) + \hat{\Gamma} + \gamma]^{-1}\,, \tag{B.3a, b}$$

and expression (B.3b) is the unperturbed Green function.

As the perturbation in the full equation (B.1) couples to all momenta $\boldsymbol{p}'$ with *equal* strength, it represents a single impurity in the Fourier space conjugate to $\boldsymbol{p}$. Therefore, the full problem can be solved through a T-matrix analysis [116]. We use the following Fourier transforms:

$$Q(m,\omega) = (1/\sqrt{N})\sum_{\boldsymbol{p}} Q(\boldsymbol{p},\omega)\exp(-\mathrm{i}\boldsymbol{p}\cdot\boldsymbol{r}_m)\,, \tag{B.4a}$$

$$\mathcal{J}_{mn} = \frac{1}{N}\sum_{\boldsymbol{p}} \mathcal{J}(\boldsymbol{p})\exp[-\mathrm{i}\boldsymbol{p}\cdot(\boldsymbol{r}_m - \boldsymbol{r}_n)]\,, \qquad f(m) = \frac{1}{\sqrt{N}}\sum_{\boldsymbol{p}} f(\boldsymbol{p})\exp(-\mathrm{i}\boldsymbol{p}\cdot\boldsymbol{r}_m)\,. \tag{B.4b, c}$$

Equation (B.1) then translates into

$$\sum_n [-\mathrm{i}\omega\delta_{mn} - \mathrm{i}\mathcal{J}_{mn} + (\hat{\Gamma}+\gamma)\delta_{mn} - \hat{\Gamma}\delta_{mn}\delta_{m0}]Q(n,\omega) = f(m)\,. \tag{B.5}$$

The full Green function in coordinate representation is defined by

$$Q(m,\omega) \equiv \sum_n G_{mn}(\omega) f(n)\,, \tag{B.6}$$

and is now easily found to obey

$$\sum_{m'} [-\mathrm{i}\omega\delta_{mm'} - \mathrm{i}\mathcal{J}_{mm'} + (\hat{\Gamma}+\gamma)\delta_{mm'} - \hat{\Gamma}\delta_{mm'}\delta_{m0}]G_{m'n}(\omega) = \delta_{mn}\,. \tag{B.7}$$

Standard T-matrix analysis with $\hat{\Gamma}\delta_{mm'}\delta_{m0}$ as perturbing potential now yields [40]

$$G_{mn}(\omega) = G^0_{mn}(\omega) + G^0_{m0}(\omega)G^0_{0n}(\omega)\hat{\Gamma}/[1 - \hat{\Gamma}G^0_{00}(\omega)] . \tag{B.8}$$

Here, G^0_{mn} is the unperturbed Green function in coordinate representation

$$G^0_{mn}(\omega) = (1/N)\sum_{\boldsymbol{p}} G^0_{\boldsymbol{p}}(\omega)\exp[-\mathrm{i}\boldsymbol{p}\cdot(\boldsymbol{r}_m - \boldsymbol{r}_n)] \tag{B.9}$$

[cf. eq. (B.3b)]. The eventual quantity of interest is [see, e.g., eq. (3.29)] $\Sigma_{\boldsymbol{p}}Q(\boldsymbol{p}, \omega)$, which can be written as:

$$\sum_{\boldsymbol{p}} Q(\boldsymbol{p}, \omega) = \sqrt{N}Q(m = 0, \omega) = \sqrt{N}\Big(\sum_n G^0_{0n}(\omega)f(n)\Big)[1 - \hat{\Gamma}G^0_{00}(\omega)]^{-1} , \tag{B.10}$$

where in the last step we used eqs. (B.6) and (B.8). Using eqs. (B.3b), (B.4c), and (B.9), we finally arrive at

$$\sum_{\boldsymbol{p}} Q(\boldsymbol{p}, \omega) = \frac{\Sigma_{\boldsymbol{p}}[-\mathrm{i}\omega - \mathrm{i}\mathcal{J}(\boldsymbol{p}) + \hat{\Gamma} + \gamma]^{-1}f(\boldsymbol{p})}{1 - (\hat{\Gamma}/N)\Sigma_{\boldsymbol{p}'}[-\mathrm{i}\omega - \mathrm{i}\mathcal{J}(\boldsymbol{p}') + \hat{\Gamma} + \gamma]^{-1}} . \tag{B.11}$$

Appendix C. The diffusive limit of the D4WM intensity

In this appendix we derive eq. (3.35) for the D4WM intensity in the diffusive limit [$\hat{\Gamma} \gg |J(\boldsymbol{p} - \boldsymbol{k}_g/2) - J(\boldsymbol{p} + \boldsymbol{k}_g/2)|$ (for all $\boldsymbol{p}$) *and* $\hat{\Gamma} \gg \gamma$]. We start from

$$S(\boldsymbol{k}_s, \omega_s) \propto |R(\boldsymbol{k}_g, \omega_{12})|^2 , \tag{C.1}$$

$$R(\boldsymbol{k}_g, \omega_{12}) \equiv \Big(1 - \frac{\hat{\Gamma}}{N}\sum_{\boldsymbol{p}}[-\mathrm{i}\omega_{12} - \mathrm{i}\mathcal{J}(\boldsymbol{p}) + \hat{\Gamma} + \gamma]^{-1}\Big)^{-1} , \tag{C.2a}$$

where we used the shorthand notation

$$\mathcal{J}(\boldsymbol{p}) = J(\boldsymbol{p} - \boldsymbol{k}_g/2) - J(\boldsymbol{p} + \boldsymbol{k}_g/2) . \tag{C.2b}$$

Straightforward Taylor expansion yields

$$\sum_{\boldsymbol{p}}[-\mathrm{i}\omega_{12} - \mathrm{i}\mathcal{J}(\boldsymbol{p}) + \hat{\Gamma} + \gamma]^{-1} \approx \frac{1}{-\mathrm{i}\omega_{12} + \hat{\Gamma} + \gamma}\sum_{\boldsymbol{p}}\Big[1 + \frac{\mathrm{i}\mathcal{J}(\boldsymbol{p})}{-\mathrm{i}\omega_{12} + \hat{\Gamma} + \gamma} - \Big(\frac{\mathcal{J}(\boldsymbol{p})}{-\mathrm{i}\omega_{12} + \hat{\Gamma} + \gamma}\Big)^2\Big] . \tag{C.3}$$

The second term on the r.h.s. vanishes upon summation [$\Sigma_{\boldsymbol{p}}\mathcal{J}(\boldsymbol{p}) = 0$], because $\mathcal{J}(\boldsymbol{p})$ is the difference of two lattice Fourier transforms and $\boldsymbol{p}$ runs over an entire Brillouin zone. In the third term within the r.h.s. summation, we approximate $-\mathrm{i}\omega_{12} + \hat{\Gamma} + \gamma \approx \hat{\Gamma}$, assuming that over the frequency range of

interest $|\omega_{12}| \ll \hat{\Gamma}$. This will be verified a posteriori. Substituting eq. (C.3) into eq. (C.2a), we then arrive at

$$R(\boldsymbol{k}_g, \omega_{12}) = \frac{-i\omega_{12} + \hat{\Gamma} + \gamma}{-i\omega_{12} + \gamma + D_e \boldsymbol{k}_g^2} \approx 1 + \frac{\hat{\Gamma}}{-i\omega_{12} + \gamma + D_e \boldsymbol{k}_g^2}, \tag{C.4}$$

$$D_e \boldsymbol{k}_g^2 \equiv (1/\hat{\Gamma}N) \sum_{\boldsymbol{p}} [\mathcal{J}(\boldsymbol{p})]^2 . \tag{C.5}$$

At this point, it is useful to note that $R(\boldsymbol{k}, \omega)$ is essentially the Green function for the exciton population $W(\boldsymbol{k}, \omega)$ in momentum–frequency representation. This is seen by combining eqs. (3.24b), (3.32), and (C.2a). In the last form of eq. (C.4), the term 1 may be neglected relative to the second term, so that we recognize the Green function for a diffusing particle with diffusion constant D_e. Thus, D_e has the meaning of an exciton diffusion coefficient; in general, D_e depends on the wave vector $\boldsymbol{k}_g$. Combining eqs. (C.1) and (C.4) and using $D_e \boldsymbol{k}_g^2 \ll \hat{\Gamma}$ (because $|\mathcal{J}(\boldsymbol{p})| \ll \hat{\Gamma}$ for all $\boldsymbol{p}$), we finally obtain

$$S(\boldsymbol{k}_s, \omega_s) = 1 + \hat{\Gamma}(\hat{\Gamma} + 2\gamma)/[\omega_{12}^2 + (\gamma + D_e \boldsymbol{k}_g^2)^2] . \tag{C.6}$$

This signal has a Lorentzian resonance with width $\gamma + D_e \boldsymbol{k}_g^2 \ll \hat{\Gamma}$, which justifies a posteriori our assumption that $|\omega_{12}| \ll \hat{\Gamma}$ in the frequency region of interest.

Appendix D. Effective polariton group velocity in the restricted Haken–Strobl model

In this appendix, we calculate an estimate to the effective polariton group velocity defined through eq. (4.27) for the restricted Haken–Strobl model. Our system is not isotropic and the polariton frequency depends both on the direction and the magnitude of its wave vector. In order to obtain a simple analytical result, we will replace the dispersion relation eq. (4.6a) [with $\Gamma(\boldsymbol{k}) = 0$: strong polariton effects] by that of transverse polaritons in an isotropic (atomic) system with transition dipole μ. This dispersion relation reads (ω is the polariton frequency) [43, 48a, 57]

$$(kc)^2/\omega^2 = 1 + f^2/(\omega_\perp^2 - \omega^2) \equiv \varepsilon(\omega) , \tag{D.1}$$

with $f^2 \equiv 8\pi\rho\Omega\mu^2/\hbar$ [cf. eq. (4.6b)]. As mentioned in section 4.1, f is the frequency separation between the upper and lower polariton curves at the wave number k_0 where the exciton band and photon dispersion line cross. In practice, $f \ll \Omega$. In eq. (D.1) an infinite effective exciton mass is assumed and $\omega_\perp$ is the transverse dipolar exciton frequency at optical wave vectors ($\boldsymbol{k} \approx \boldsymbol{0}$) [48a],

$$\omega_\perp = (\Omega^2 - f^2/3)^{1/2} \approx \Omega - f^2/6\Omega . \tag{D.2}$$

We also define the longitudinal exciton frequency [48a],

$$\omega_\parallel = (\Omega^2 + 2f^2/3)^{1/2} \approx \Omega + f^2/3\Omega . \tag{D.3}$$

These expressions for $\omega_\perp$ and $\omega_\parallel$ are easily obtained from eq. (3.6) and the approximation to the dipole sum $J(\boldsymbol{k})$ given below (eq. 3.17). In the continuum limit for $\boldsymbol{k}$ ($N, V \to \infty$, $N/V = \rho$), we now have

$$\bar{v}_{\mathrm{p}}^{2} = \frac{1}{(2\pi)^{3}\rho} \int \mathrm{d}\boldsymbol{k}\, v_{\mathrm{p}}^{2}(k) = \frac{1}{2\pi^{2}\rho} \int \mathrm{d}k\, k^{2} v_{\mathrm{p}}^{2}(k) \,. \tag{D.4}$$

The integral has two contributions: one from the upper branch, extending from $k = 0$ to $k = k_0$, and one from the lower, ranging from $k = k_0$ to the edge of the Brillouin zone (fig. 7). It is convenient to transform to the frequency as variable,

$$\int \mathrm{d}k\, k^{2} v_{\mathrm{p}}^{2}(k) = \int \mathrm{d}\omega\, \varepsilon(\omega)(\omega/c)^{2} v_{\mathrm{p}}(\omega) \,. \tag{D.5}$$

$v_{\mathrm{p}}(\omega)$ can be found by taking differentials of both sides of the relation

$$\varepsilon(\omega)\omega^{2} = k^{2}c^{2} \,. \tag{D.6}$$

We then obtain

$$v_{\mathrm{p}}(\omega) = \frac{\mathrm{d}\omega}{\mathrm{d}k} = \frac{2c\omega\sqrt{\varepsilon(\omega)}}{\varepsilon'(\omega)\omega^{2} + 2\omega\varepsilon(\omega)} \,, \quad \varepsilon'(\omega) \equiv \mathrm{d}\varepsilon/\mathrm{d}\omega \,. \tag{D.7}$$

Using eq. (D.1), we arrive at

$$v_{\mathrm{p}}(\omega) = c\sqrt{\varepsilon(\omega)}\, \frac{(\omega_{\perp}^{2} - \omega^{2})^{2}}{(\omega_{\perp}^{2} - \omega^{2})^{2} + f^{2}\omega_{\perp}^{2}} \,. \tag{D.8}$$

The $\sqrt{\varepsilon(\omega)}$ poses no problem as the integration occurs outside the region where $\varepsilon(\omega) < 0$ (the polariton stopgap ranging from $\omega_{\perp}$ to $\omega_{\parallel}$).

Combining eqs. (D.1)–(D.5) and (D.8), we arrive at

$$\bar{v}_{\mathrm{p}}^{2} = I_{1} + I_{2} \,, \tag{D.9a}$$

$$I_{1} = \frac{1}{2\pi^{2}\rho c} \int_{\omega_{\parallel}}^{\omega_{\parallel} + f/2} \mathrm{d}\omega\, \frac{\omega^{2}(\omega^{2} - \omega_{\parallel}^{2})^{3/2}(\omega^{2} - \omega_{\perp}^{2})^{1/2}}{(\omega^{2} - \omega_{\perp}^{2})^{2} + f^{2}\omega_{\perp}^{2}} \,, \tag{D.9b}$$

$$I_{2} = \frac{1}{2\pi^{2}\rho c} \int_{\omega_{\perp} - f/2}^{\omega_{\perp}} \mathrm{d}\omega\, \frac{\omega^{2}(\omega_{\parallel}^{2} - \omega^{2})^{3/2}(\omega_{\perp}^{2} - \omega^{2})^{1/2}}{(\omega^{2} - \omega_{\perp}^{2})^{2} + f^{2}\omega_{\perp}^{2}} \,. \tag{D.9c}$$

Here we have used the fact that the upper branch has as lowest frequency $\omega_{\parallel}$ and the lower branch has highest frequency $\omega_{\perp}$. The other integration boundaries are determined by the polariton frequencies at $k = k_0$, $\omega = \omega_{\perp} \pm f/2$, where in eq. (D.9b) we approximated $\omega_{\perp} + f/2 \approx \omega_{\parallel} + f(1 - f/\Omega)/2 \approx \omega_{\parallel} + f/2$. (Use eqs. (D.2) and (D.3) and the fact that $f/\Omega \ll 1$.) As the integration domains are restricted to a region close to the transition frequency Ω, a resonance approximation can be applied to the integrands. After straightforward changes of variables, we arrive at

$$I_1 = \frac{f^2\Omega}{4\pi^2\rho c} \int_0^{\Omega/f} \mathrm{d}x \, \frac{x^{3/2}(1+x)^{1/2}}{(1+x)^2 + (\Omega/f)^2} , \tag{D.10a}$$

$$I_2 = \frac{f^2\Omega}{4\pi^2\rho c} \int_0^{\Omega/f} \mathrm{d}x \, \frac{(1+x)^{3/2}x^{1/2}}{x^2 + (\Omega/f)^2} . \tag{D.10b}$$

As $\Omega/f \gg 1$, a good estimate is obtained from

$$\bar{v}_p^2 = I_1 + I_2 \approx \frac{f^2\Omega}{2\pi^2\rho c} \int_0^{\Omega/f} \mathrm{d}x \, \frac{x^2}{x^2 + (\Omega/f)^2} = \frac{f\Omega^2}{2\pi^2\rho c} (1 - \pi/4) . \tag{D.11}$$

If we define $\lambda_0 = 2\pi c/\Omega$, the vacuum wavelength of the molecular transition, and a the lattice constant, we finally have $(1 - \pi/4 \approx 1/4)$,

$$(\bar{v}_p/c)^2 \approx \pi(f/\Omega)(a/\lambda_0)^3 . \tag{D.12}$$

References

[1] H.J. Eichler, P. Günter and D.W. Pohl, Laser-Induced Dynamic Gratings (Springer, Berlin, 1986).
[2] (a) J.R. Salcedo, A.E. Siegman, D.D. Dlott and M.D. Fayer, Phys. Rev. Lett. 41 (1978) 131;
(b) T.S. Rose, R. Righini and M.D. Fayer, Chem. Phys. Lett. 106 (1984) 13;
(c) T.S. Rose, V.J. Newell, J.S. Meth and M.D. Fayer, Chem. Phys. Lett. 145 (1988) 475.
[3] P.F. Liao, L. Humphrey, D.M. Bloom and S. Geschwind, Phys. Rev. B 20 (1979) 4145;
D.S. Hamilton, D. Heiman, I. Feinberg and R.W. Hellwarth, Opt. Lett. 4 (1979) 124.
[4] J.K. Tyminski, R.C. Powell and W.K. Zwicker, Phys. Rev. B 29 (1984) 6074.
[5] H.J. Eichler, Opt. Acta 24 (1977) 631;
A. Von Jena and H.E. Lessing, Opt. Quantum Electron. 11 (1979) 419;
H.J. Eichler, G. Salje and H. Stahl, J. Appl. Phys. 44 (1973) 5383;
H.J. Eichler, G. Enterlein, P. Glozback, J. Munschau and H. Stahl, Appl. Opt. 11 (1972) 372.
[6] D.W. Pohl, S.E. Schwarz and V. Irniger, Phys. Rev. Lett. 31 (1973) 32.
[7] M.D. Fayer, Annu. Rev. Phys. Chem. 33 (1982) 63.
[8] L.A. Gomez-Jahn, J.J. Kasinski and R.J. Dwayne Miller, Chem. Phys. Lett. 125 (1986) 500.
[9] (a) T. Kurihara, H. Kobayashi, K. Kubodera and T. Kaino, Chem. Phys. Lett. 165 (1990) 171;
(b) T. Hasegawa, K. Ishikawa, T. Kanetake, T. Koda, K. Takeda, H. Kobayashi and K. Kubodera, Chem. Phys. Lett. 171 (1990) 239.
[10] J.P. Woerdman and B. Boelger, Phys. Lett. A 30 (1969) 164;
J.P. Woerdman, Philips Res. Rep. Suppl. No. 7 (1971).
[11] D.W. Phillion, D.J. Kuizenga and A.E. Siegmann, Appl. Phys. Lett. 27 (1975) 85.
[12] K. Leo, T.C. Damen, J. Shah, E.O. Göbel and K. Köhler, Appl. Phys. Lett. 57 (1990) 19.
[13] C.A. Hoffman, K. Jarasiunas, H.T. Gerritsen and A.V. Nurmikko, Appl. Phys. Lett. 33 (1978) 536.
[14] K. Leo, M. Wegener, J. Shah, D.S. Chemla, E.O. Göbel, T.C. Damen, S. Schmitt-Rink and W. Schäfer, Phys. Rev. Lett. 65 (1990) 1340.
[15] J.J. Kasinski, L.A. Gomez-Jahn, K.J. Faran, S.M. Gracewski and R.J.D. Miller, J. Chem. Phys. 90 (1989) 1253.
[16] L. Genberg, Q. Bao, S. Gracewski and R.J.D. Miller, Chem. Phys, 131 (1989) 81.
[17] A. Yariv, Appl. Phys. Lett. 28 (1967) 88;
R.W. Hellwarth, J. Opt. Soc. Am. 67 (1977) 1.
[18] A.L. Smirl, G.C. Valley, K.M. Bohnert and T.F. Bogess, Jr, IEEE J. Quantum Electron. 24 (1988) 289.
[19] N. Bloembergen, Nonlinear Optics (Benjamin, New York, 1965).
[20] P.N. Butcher, Nonlinear Optical Phenomena (Ohio Univ. Press, Athens, Ohio, 1965).
[21] C. Flytzanis, in: Quantum Electronics, Vol. I, eds H. Rabin and C.L. Tang (Academic Press, New York, 1975) p. 1.
[22] Y.R. Shen, The Principles of Nonlinear Optics (Wiley, New York, 1984).

[23] S. Mukamel, Phys. Rep. 93 (1982) 1; Adv. Chem. Phys. 70 (1988) 165;
S. Mukamel and R.F. Loring, J. Opt. Soc. Am. B 3 (1986) 595;
S. Mukamel, Annu. Rev. Phys. Chem. 41 (1990) 647.
[24] B.I. Greene, J. Orenstein, R.R. Millard and L.R. Williams, Phys. Rev. Lett. 58 (1987) 2750;
B.I. Greene, J. Orenstein and S. Schmitt-Rink, Science 247 (1990) 679.
[25] M.K. Casstevens, M. Samoc, J. Pfleger and P.N. Prasad, J. Chem. Phys. 92 (1990) 2019.
[26] (a) Y.X. Yan, L.T. Cheng and K.A. Nelson, Advances in Nonlinear Spectroscopy, eds R.J.H. Clark and R.E. Hester (New York, Wiley, 1988) p. 299;
(b) K.A. Nelson and E.P. Ippen, Adv. Chem. Phys. 75 (1989) 1.
[27] (a) N.A. Kurnit, I.E. Abella and S.R. Hartmann, Phys. Rev. Lett. 13 (1964) 567;
(b) T.W. Mossberg, R. Kachru, S.R. Hartmann and A.M. Flusberg, Phys. Rev. A 20 (1979) 1976;
(c) W.H. Hesselink and D.A. Wiersma, in: Modern Problems in Condensed Matter Sciences, Vol. 4, eds V.M. Agranovich and A.A. Maradudin (North Holland, Amsterdam, 1983) p. 249.
[28] (a) S.D. Kramer and N. Bloembergen, Phys. Rev. B 14 (1976) 4654;
(b) N. Bloembergen, H. Lotem and R.T. Lynch, Indian J. Pure Appl. Phys. 16 (1978) 151.
[29] (a) T. Yajima and H. Souma, Phys. Rev. A 17 (1978) 309;
(b) T. Yajima, H. Souma and Y. Ishida, Phys. Rev. A 17 (1978) 324.
[30] J.J. Song, J.H. Lee and M.D. Levenson, Phys. Rev. A 17 (1978) 1439.
[31] (a) Y. Prior, A.R. Bogdan, M. Dagenais and N. Bloembergen, Phys. Rev. Lett. 46 (1981) 111;
(b) A.R. Bogdan, M.W. Downer and N. Bloembergen, Phys. Rev. A 24 (1981) 623;
(c) L.J. Rothberg and N. Bloembergen, Phys. Rev. A 30 (1984) 820;
(d) L. Rothberg, in: Progress in Optics, Vol. 24, ed. E. Wolf (North Holland, Amsterdam, 1987) p. 38.
[32] (a) J.R. Andrews, R.M. Hochstrasser and H.R. Trommsdorff, Chem. Phys. 62 (1981) 87;
(b) J.R. Andrews and R.M. Hochstrasser, Chem. Phys. Lett. 82 (1981) 381;
(c) R.M. Hochstrasser, G.R. Meredith and H.P. Trommsdorff, J. Chem. Phys. 73 (1980) 1009.
[33] R. Trebino and A.E. Siegman, J. Chem. Phys. 79 (1983) 3621.
[34] S. Mukamel, Phys. Rev. A 28 (1983) 3480;
R.W. Boyd and S. Mukamel, Phys. Rev. A 29 (1984) 1973;
V. Mizrahi, Y. Prior and S. Mukamel, Opt. Lett. 8 (1983) 145.
[35] F.C. Spano and S. Mukamel, Phys. Rev. A 40 (1989) 5783; J. Lumin 45 (1990) 412; Phys. Rev. Lett. 66 (1991) 1197.
[36] R.F. Loring and S. Mukamel, J. Chem. Phys. 84 (1986) 1228.
[37] J. Hegarty and M.D. Sturge, J. Opt. Soc. Am. B 2 (1985) 1143.
[38] R.M. Shelby and R.M. MacFarlane, Phys. Rev. Lett. 45 (1980) 1098.
[39] J. Klafter and J. Jortner, J. Chem. Phys. 71 (1979) 1961, 2210.
[40] R.F. Loring and S. Mukamel, J. Chem. Phys. 85 (1986) 1950.
[41] Th. Förster, Ann. Phys. (Leipzig) 2 (1948) 55;
D.L. Dexter, J. Chem. Phys. 21 (1953) 836.
[42] A.S. Davydov, Theory of Molecular Excitons (Plenum, New York, 1971).
[43] V.M. Agranovich and V.L. Ginzburg, Crystal Optics with Spatial Dispersion and Excitons (Springer, Berlin, 1984).
[44] D. Pines and P. Nozieres, The Theory of Quantum Liquids (Benjamin, New York, 1966).
[45] E.I. Rashba and M.D. Sturge, eds, Excitons (North Holland, Amsterdam, 1982).
[46] B. DiBartolo, Optical Interactions in Solids (Wiley, New York, 1968);
M. Pope and C.E. Swenberg, Electronic Processes in Organic Crystals (Clarendon Press, Oxford, 1982).
[47] V.M. Agranovich and M.D. Galanin, Electronic Excitation Energy Transfer in Condensed Matter, eds V.M. Agranovich and A.A. Maradudin (North Holland, Amsterdam, 1982).
[48] (a) R.S. Knox, Theory of Excitons (Academic Press, New York, 1963);
(b) V.L. Broude, E.I. Rashba and E.F. Sheka, Spectroscopy of Molecular Excitons (Springer, Berlin, 1985).
[49] R. Silbey, in: Modern Problems in Condensed Matter Sciences, Vol. 4, eds V.M. Agranovich and A.A. Maradudin (North-Holland, Amsterdam, 1983);
R. Silbey, Annu. Rev. Phys. Chem. 27 (1976) 203;
R. Kopelman, in: Topics in Applied Physics, Vol. 49, eds W.M. Yen and P.M. Selzer (Springer, Berlin, 1981) p. 241; in: Spectroscopy and Excitation Dynamics of Condensed Molecular Systems, eds V.M. Agranovich and R.M. Hochstrasser (North-Holland, Amsterdam, 1983) p. 139.
[50] D. Haarer and M.R. Philpott, in: Spectroscopy and Excitation Dynamics of Condensed Molecular Systems, eds V.M. Agranovich and R.M. Hochstrasser (North-Holland, Amsterdam, 1983) p. 27.
[51] V.M. Agranovich, A.M. Ratner and M. Salieva, Solid State Commun. 63 (1987) 329.
[52] V.M. Agranovich and T.A. Leskova, Solid State Commun. 68 (1988) 1029; in: Proc. US–USSR Condensed Matter Seminar (Irvine, 1989).

[53] V.M. Kenkre, in: Exciton Dynamics in Molecular Crystals and Aggregates, ed. G. Höhler (Springer, Berlin, 1982).
[54] P. Reineker, in: Exciton Dynamics in Molecular Crystals and Aggregates, ed. G. Höhler (Springer, Berlin, 1982).
[55] D.K. Garrity and J.L. Skinner, J. Chem. Phys. 82 (1985) 260.
[56] R.F. Loring and S. Mukamel, J. Chem. Phys. 83 (1985) 4353.
[57] J.J. Hopfield, Phys. Rev. 112 (1958) 1555.
[58] V.M. Agranovich, Zh. Eksp. Teor. Fiz. 37 (1959) 430 [Sov. Phys. – JETP 37 (1960) 307].
[59] L.N. Ovander, Usp. Fiz. Nauk 86 (1965) 3 [Sov. Phys. – Usp. 8 (1965) 337].
[60] (a) G.J. Small, in: Excited States, ed. E.C. Lim (Academic Press, New York, 1982);
(b) S.H. Stevenson, M.A. Connolly and G.J. Small, Chem. Phys. 128 (1988) 157.
[61] S.V. Tyablikov, Methods in the Quantum Theory of Magnetism (Plenum, New York, 1967).
[62] M. Orrit and P. Kottis, Adv. Chem. Phys. 74 (1988) 1.
[63] G.M. Gale, F. Vallée and C. Flytzanis, Phys. Rev. Lett. 57 (1986) 1867.
[64] D. Fröhlich, S. Kirchhoff, P. Köhler and W. Nieswand, Phys. Rev. B 40 (1989) 1976.
[65] V.N. Denisov, B.N. Mavrin and V.B. Podobedov, Phys. Rep. 151 (1987) 1.
[66] V.V. Obukhovskii and V.L. Strizhevskii, Zh. Eksp. Teor. Fiz. 50 (1966) 135 [Sov. Phys. – JETP 23 (1966) 91].
[67] V.M. Agranovich, L.N. Ovander and B.S. Toshich, Zh. Eksp. Teor. Fiz. 50 (1966) 1332 [Sov. Phys. – JETP 23 (1966) 885].
[68] J. Knoester and S. Mukamel, J. Chem. Phys. 91 (1989) 989.
[69] E. Hanamura, Phys. Rev. B 39 (1989) 1152.
[70] D. Bedeaux and N. Bloembergen, Physica 69 (1973) 67.
[71] J. Knoester and S. Mukamel, Phys. Rev. A 39 (1989) 1899;
J. Knoester and S. Mukamel, J. Opt. Soc. Am. B 6 (1989) 643.
[72] E.A. Power and S. Zienau, Philos. Trans. R. Soc. London, Ser. A 251 (1959) 427.
[73] D.P. Craig and T. Thirunamachandran, Molecular Quantum Electrodynamics (Academic Press, London, 1984).
[74] See, e.g., J. Fiutak, Can. J. Phys. 41 (1963) 12;
W.L. Peticolas, R. Norris and K.E. Rieckhoff, J. Chem. Phys. 42 (1965) 4164;
E.A. Power and T. Thirunamachandran, Phys. Rev. A 26 (1982) 1800;
W. Becker, Opt. Commun. 56 (1985) 107;
D.H. Kobe, Phys. Rev. Lett. 40 (1978) 538;
S.M. Golshan and D.H. Kobe, Phys. Rev. A 34 (1986) 4449.
[75] L. Allen and J.H. Eberly, Optical Resonance and Two-Level Atoms (Wiley, New York, 1975).
[76] J. Knoester and S. Mukamel, Phys. Rev. A 41 (1990) 3812.
[77] See, e.g., R.R. McLone and E.A. Power, Mathematika 11 (1964) 91.
[78] R.H. Lehmberg, Phys. Rev. A 2 (1970) 883.
[79] M. Born and K. Huang, Dynamical Theory of Crystal Lattices (Oxford Univ. Press, London, 1954).
[80] V.M. Agranovich and Yu.V. Konobeev, Sov. Phys. – Solid State 3 (1961) 260.
[81] S. Schmitt-Rink, D.A.B. Miller and D.S. Chemla, Phys. Rev. B 35 (1987) 8113;
S. Schmitt-Rink, D.S. Chemla and H. Haug, Phys. Rev. B 37 (1988) 941.
[82] S. Mukamel, Z. Deng and J. Grad, J. Opt. Soc. Am. B 5 (1988) 804.
[83] H.A. Lorentz, The Theory of Electrons (Dover Publ., New York, 1952).
[84] F.J. Belinfante, Physica 12 (1946) 1.
[85] W.R. Heller and A. Marcus, Phys. Rev. 84 (1951) 809.
[86] M.H. Cohen and F. Keffer, Phys. Rev. 99 (1955) 1128.
[87] G.R. Meredith, J. Chem. Phys. 75 (1981) 4317; 77 (1982) 5863.
[88] H. Haken and G. Strobl, Z. Phys. 262 (1973) 135.
[89] H. Sumi and Y. Toyozawa, J. Phys. Soc. Jpn 31 (1971) 342;
H. Sumi, J. Phys. Soc. Jpn 32 (1972) 616.
[90] H. Sumi, J. Chem. Phys. 67 (1977) 2943.
[91] A. Blumen and R. Silbey, J. Chem. Phys. 69 (1978) 3589.
[92] R.W. Hellwarth, Prog. Quantum Electron. 5 (1977) 1.
[93] Y.M. Wong and V.M. Kenkre, Phys. Rev. B 22 (1980) 3072.
[94] E. Wigner, Phys. Rev. 40 (1932) 749; M. Hillery, R.F. O'Connell, M.O. Scully and E.P. Wigner, Phys. Rep. 106 (1984) 121.
[95] R.F. Loring, D.S. Franchi and S. Mukamel, Phys. Rev. B 37 (1988) 1874;
S. Mukamel, D.S. Franchi and R.F. Loring, Chem. Phys. 128 (1988) 99.
[96] P.L. Bhatnagar, E.P. Gross and M. Krook, Phys. Rev. 94 (1954) 511.
[97] H. Risken, The Fokker–Planck Equation (Springer, Berlin, 1984).
[98] P. Reineker and R. Kühne, Z. Phys. B 22 (1975) 193.
[99] R. Kühne and P. Reineker, Z. Phys. B 22 (1975) 201.
[100] See, e.g., D.L. Huber, in: Laser Spectroscopy of Solids, eds W.M. Yen and P.M. Selzer (Springer, Berlin, 1981).

[101] V.M. Kenkre and R.S. Knox, Phys. Rev. Lett. 33 (1974) 803.
[102] J. Knoester and S. Mukamel, Phys. Rev. A 40 (1989) 7065.
[103] J.J. Hopfield, Phys. Rev. 182 (1969) 945.
[104] J.J. Hopfield and D.G. Thomas, Phys. Rev. 132 (1963) 563.
[105] S.I. Pekar, Zh. Eksp. Teor. Fiz. 33 (1957) 1022 [Sov. Phys. – JETP 6 (1958) 785].
[106] J.L. Birman, in: Excitons, eds E.I. Rashba and M.D. Sturge (North Holland, Amsterdam, 1982).
[107] F. Bassani, Helv. Phys. Acta 58 (1985) 244.
[108] A. Yariv and P. Yeh, Optical Waves in Crystals (Wiley, New York, 1984).
[109] H. Haug, ed., Optical Nonlinearities and Instabilities in Semiconductors (Academic Press, New York, 1988).
[110] D.S. Chemla and J. Zyss, Nonlinear Optical Properties of Organic Molecules and Crystals Vols. I and II (Academic Press, New York, 1987).
[111] D. Möbius and H. Kuhn, J. Appl. Phys. 64 (1988) 5138;
D. Möbius and H. Kuhn, Isr. J. Chem. 18 (1979) 375.
[112] M.L. Steigerwald and L.E. Brus, Acc. Chem. Res. 23 (1990) 183.
[113] F.F. So, S.R. Forrest, Y.Q. Shi and W.H. Steier, Appl. Phys. Lett. 56 (1990) 674.
[114] R. Kuklinski and S. Mukamel, Phys. Rev. B 42 (1990) 2959.
[115] T. Takagahara, Phys. Rev. B 31 (1985) 8171.
[116] E.N. Economou, Green's Functions in Quantum Physics (Springer, Berlin, 1983).
[117] L.A. Gomez-Jahn, Ph.D. Thesis, University of Rochester (1990).